Date: July 16, 2020

Proposal for JLab PAC48

Strange Hadron Spectroscopy with Secondary K_L Beam in Hall D

Experimental Support:

Shankar Adhikari[43], Moskov Amaryan (Contact Person, Spokesperson)[43], Arshak Asaturyan[1], Alexander Austregesilo[49], Marouen Baalouch[8], Mikhail Bashkanov (Spokesperson)[63], Vitaly Baturin[43], Vladimir Berdnikov[11,35], Olga Cortes Becerra[19], Timothy Black[60], Werner Boeglin[13], William Briscoe[19], William Brooks[54], Volker Burkert[49], Eugene Chudakov[49], Geraint Clash[63], Philip Cole[32], Volker Crede[14], Donal Day[61], Pavel Degtyarenko[49], Alexandre Deur[49], Sean Dobbs (Spokesperson)[14], Gail Dodge[43], Anatoly Dolgolenko[26], Simon Eidelman[6,41], Hovanes Egiyan (JLab Contact Person)[49], Denis Epifanov[6,41], Paul Eugenio[14], Stuart Fegan[63], Alessandra Filippi[25], Sergey Furletov[49], Liping Gan[60], Franco Garibaldi[24], Ashot Gasparian[39], Gagik Gavalian[49], Derek Glazier[18], Colin Gleason[22], Vladimir Goryachev[26], Lei Guo[14], David Hamilton[11], Avetik Hayrapetyan[17], Garth Huber[53], Andrew Hurley[56], Charles Hyde[43], Isabella Illari[19], David Ireland[18], Igal Jaegle[49], Kyungseon Joo[57], Vanik Kakoyan[1], Grzegorz Kalicy[11], Mahmoud Kamel[13], Christopher Keith[49], Chan Wook Kim[19], Eberhard Klemp[5], Geoffrey Krafft[49], Sebastian Kuhn[43], Sergey Kuleshov[2], Alexander Laptev[33], Ilya Larin[26,59], David Lawrence[49], Daniel Lersch[14], Wenliang Li[56], Kevin Luckas[28], Valery Lyubovitskij[50,51,52,54], David Mack[49], Michael McCaughan[49], Mark Manley[30], Hrachya Marukyan[1], Vladimir Matveev[26], Mihai Mocanu[63], Viktor Mokeev[49], Curtis Meyer[9], Bryan McKinnon[18], Frank Nerling[15,16], Matthew Nicol[63], Gabriel Niculescu[27], Alexander Ostrovidov[14], Zisis Papandreou[53], KiJun Park[49], Eugene Pasyuk[49], Lubomir Pentchev[49], William Phelps[10], John Price[7], Jörg Reinhold[13], James Ritman (Spokesperson)[28,68], Dimitri Romanov[26], Carlos Salgado[40], Todd Satogata[49], Susan Schadmand[28], Amy Schertz[56], Axel Schmidt[19], Daniel Sober[11], Alexander Somov[49], Sergei Somov[35], Justin Stevens (Spokesperson)[56], Igor Strakovsky (Spokesperson)[19], Victor Tarasov[26], Simon Taylor[49], Annika Thiel[5], Guido Maria Urciuoli[24], Holly Szumila-Vance[19], Daniel Watts[63], Lawrence Weinstein[43], Timothy Whitlatch[49], Nilanga Wickramaarachchi[43], Bogdan Wojtsekhowski[49], Nicholas Zachariou[63], Jonathan Zarling[53], Jixie Zhang[61]

Theoretical Support:

Alexey Anisovich[5,44], Alexei Bazavov[38], Rene Bellwied[21], Veronique Bernard[42], Gilberto Colangelo[3], Aleš Cieplý[46], Michael Döring[19], Ali Eskanderian[19], Jose Goity[20,49], Helmut Haberzettl[19], Mirza Hadžimehmedović[55], Robert Jaffe[36], Boris Kopeliovich[54], Heinrich Leutwyler[3], Maxim Mai[19], Terry Mart[65], Maxim Matveev[44], Ulf-G. Meißner[5,29], Colin Morningstar[9], Bachir Moussallam[42], Kanzo Nakayama[58], Wolfgang Ochs[37], Youngseok Oh[31], Rifat Omerovic[55], Hedim Osmanović[55], Eulogio Oset[62], Antimo Palano[64], Jose Peláez[34], Alessandro Pilloni[66,67], Maxim Polyakov[48], David Richards[49], Arkaitz Rodas[49,56], Dan-Olof Riska[12], Jacobo Ruiz de Elvira[3], Hui-Young Ryu[45], Elena Santopinto[23], Andrey Sarantsev[5,44], Jugoslav Stahov[55], Alfred Švarc[47], Adam Szczepaniak[22,49], Ronald Workman[19], Bing-Song Zou[4]

[1] A. I. Alikhanian National Science Laboratory (Yerevan Physics Institute (YerPhi))
[2] Departamento de Ciencias Fisicas, Universidad Andres Bello, Sazie 2212, Piso 7, Santiago, Chile
[3] University of Bern, CH-3012 Bern, Switzerland
[4] Institute of Theoretical Physics, CAS, Beijing 100190, People's Republic of China
[5] Helmholtz-Institut für Strahlen- und Kernphysik, Universität Bonn, Bonn 53115, Germany
[6] Budker Institute of Nuclear Physics SB RAS, Novosibirsk 630090, Russia
[7] California State University, Dominguez Hills, Carson, CA 90747, USA
[8] C.E.A. L'energie Atomique Et Aux Energies Alternatives, 91190 Saclay, France
[9] Carnegie Mellon University (CMU), Pittsburgh, PA 15213, USA
[10] Christopher Newport University (CNU), Newport News, VA 23606, USA
[11] The Catholic University of America (CUA), Washington, DC 20064, USA
[12] Finnish Society of Science and Letters, Helsinki 00130, Finland
[13] Florida International University (FIU), Miami, FL 33199, USA
[14] Florida State University (FSU), Tallahassee, FL 32306, USA
[15] Göthe University Frankfurt, Frankfurt 60323, Germany
[16] GSI Helmholtzzentrum für Schwerionenforschung GmbH, Darmstadt 64291, Germany
[17] Justus Liebig-University of Gießen, Gießen 35392, Germany
[18] University of Glasgow, Glasgow G12 8QQ, UK
[19] The George Washington University (GW), Washington, DC 20052, USA
[20] Hampton University, Hampton, VA 23668, USA
[21] University of Houston, Houston, TX 77204, USA
[22] Indiana University (IU), Bloomington, IN 47403, USA
[23] I.N.F.N. Sezione di Genova, Genova 16146, Italy
[24] I.N.F.N. Sezione di Roma, Roma 00185, Italy
[25] I.N.F.N. Sezione di Torino, Torino 10125, Italy
[26] National Rsearch Centre "Kurchatov Institute", Institute for Theoretical and Experimental Physics (ITEP), Moscow 117218, Russia
[27] James Madison University (JMU), Harrisonburg, VA 22807, USA
[28] Institute für Kernphysik & Jülich Center für Hadron Physics, Jülich 52425, Germany
[29] Institut für Advanced Simulation, Institut für Kernphysik and Jülich Center für Hadron Physics, Jülich 52425, Germany
[30] Kent State University (KSU), Kent, OH 44242, USA
[31] Kyungpook National University, Daegu 41566, Republic of Korea
[32] Lamar University, Beaumont, TX 77710, USA
[33] Los Alamos National Laboratory (LANL), Los Alamos, NM 87545, USA
[34] Universidad Complutense de Madrid, 28040 Madrid, Spain
[35] National Research Nuclear University Moscow Engineering Physics Institute (MEPhI), Moscow 115409, Russia
[36] Massachusetts Institute of Technology (MIT), Cambridge, MA 02139, USA
[37] Max-Planck-Institut für Physik, München D-80805, Germany
[38] Michigan State University (MSU), East Lansing, MI 48824, USA
[39] North Carolina A&T State University (N.C.A&T), Greensboro, NC 27411, USA
[40] Norfolk State University (NSU), Norfolk, VA 23504, USA
[41] Novosibirsk State University, Novosibirsk 630090, Russia
[42] Universite Paris-Sud 11, 91400 Orsay, France

[43] Old Dominion University (ODU), Norfolk, VA 23529, USA
[44] National Research Centre “Kurchatov Institute", Petersburg Nuclear Physics Institute (PNPI), Gatchina 188300, Russia
[45] Pusan National University, Busan 46241, Republic of Korea
[46] Nuclear Physics Institute, Rez 250 68, Czech Republic
[47] Rudjer Bošković Institute, Zagreb 10002, Croatia
[48] Institut für Theoretische Physik II - Ruhr-Universität, D-44780 Bochum, Germany
[49] Thomas Jefferson National Accelerator Facility (JLab), Newport News, VA 23606, USA
[50] Tomsk State University, Tomsk 634050, Russia
[51] Tomsk Polytechnic University, Tomsk 634050, Russia
[52] Institut für Theoretische Physics, Tübingen Universität, Tübingen 72076, Germany
[53] University of Regina (UR), Regina, SA S4S 0A2, Canada
[54] Universidad Técnica Federico Santa María, Casilla 110-V Valparaíso, Chile
[55] University of Tuzla, Tuzla 75000, Bosnia and Herzegovina
[56] College of William and Mary (W&M), Williamsburg, VA 23185, USA
[57] University of Connecticut (UConn), Storrs, CO 06269, USA
[58] University of Georgia (UGA), Athens, GA 30602, USA
[59] University of Massachusetts (UMASS Amherst), Amherst, MA 01003, USA
[60] University of North Carolina at Wilmington (UNCW), Wilmington, NC 28403, USA
[61] University of Virginia (UVa), Charlottesville, VA 22904, USA
[62] Centro Mixto Universidad de Valencia-CSIC, 46071 Valencia, Spain
[63] University of York (UoY), Heslington, York YO10 5DD, UK
[64] INFN Sezione di Bari, 70125 Bari, Italy
[65] FMIPA, Universitas Indonesia, Depok 16424, Indonesia
[66] European Centre for Theoretical Studies in Nuclear Physics and related Areas (ECT*) and Fondazione Bruno Kessler, Villazzano (Trento), I-38123, Italy
[67] INFN Sezione di Genova, Genova, I-16146, Italy
[68] Institut für Experimentalphysik I - Ruhr-Universität, Bochum 44780, Germany

(The KLF Collaboration)

Abstract

We propose to create a secondary beam of neutral kaons in Hall D at Jefferson Lab to be used with the GlueX experimental setup for strange hadron spectroscopy. The superior CEBAF electron beam will enable a flux on the order of $1 \times 10^4\ K_L/sec$, which exceeds the flux of that previously attained at SLAC by three orders of magnitude. It will allow a broad range of measurements that will correspondingly improve the statistics of earlier data obtained on a hydrogen target likewise by three orders of magnitude. The use of a deuteron target will provide first measurements ever with neutral kaons on neutrons.

The experiment will measure both differential cross sections and self-analyzed polarizations of the produced Λ, Σ, Ξ, and Ω hyperons using the GlueX detector at the Jefferson Lab Hall D. The measurements will span CM $\cos\theta$ from -0.95 to 0.95 in the range W = 1490 MeV to 2500 MeV. The new data will significantly constrain the partial wave analyses and reduce model-dependent uncertainties in the extraction of the properties and pole positions of the strange hyperon resonances, and establish the orbitally excited multiplets in the spectra of the Ξ and Ω hyperons. Comparison with the corresponding multiplets in the spectra of the charm and bottom hyperons will provide insight into he accuracy of QCD-based calculations over a large range of masses.

The proposed facility will have a defining impact in the strange meson sector through measurements of the final state $K\pi$ system up to 2 GeV invariant mass. This will allow the determination of pole positions and widths of all relevant $K^*(K\pi)$ S-,P-,D-,F-, and G-wave resonances, settle the question of the existence or nonexistence of scalar meson $\kappa/K_0^*(700)$ and improve the constrains on their pole parameters. Subsequently improving our knowledge of the low-lying scalar nonet in general.

Contents

1 Preamble

This proposal is an update to the conditionally approved K-Long Facility in Jefferson Lab Hall D proposal [C2–19–001] and in particular intended to address several specific questions raised by the PAC47 in 2019. Detailed simulations of several hyperon production channels and their inclusion into a global Partial Wave Analysis have been studied in order to determine the full systematic uncertainties associated with the experiment to extract the hyperon pole parameters. One important conclusion of these studies is that measurements with a neutral kaon beam are essential in order to resolve ambiguities in charged kaon beam measurements of hyperon resonance parameters.

We have also developed a method for measuring the $K\pi$ final system without reconstructing the recoil nucleon, allowing access to $|t|$ values for strange meson spectroscopy all the way down to threshold, and have extended these studies to $K\pi$ production off the Δ^{++}, allowing for the separation of the different isospin amplitudes. Conceptual designs for the components of the new K_L beamline are progressing well, and we have done detailed simulations of the neutron flux on the GlueX spectrometer, and how this could contribute to the reconstruction of K_L and neutron-induced reactions. These studies will be described in detail.

The KLF project proposes to establish a secondary K_L beamline at JLab Hall D for scattering experiments on both proton and neutron targets in order to determine the differential cross sections and the self-polarization of strange hyperons with the GlueX detector. These data will allow for precise PWA for the determination of all resonances up to 2500 MeV in the spectra of the Λ, Σ, Ξ, and Ω hyperons, the knowledge of which is very poor compared to the nucleon. The firm establishment of the lowest hyperon multiplets will allow for tests of models of hyperon structure, and comparison to future Lattice QCD calculations. Together with the progress made in understanding the spectrum of baryons containing charm and beauty quarks by experiments such as LHCb and Belle II, these hyperon measurements will provide new insight into the implications of QCD over a wide range of mass scales. In addition, this facility provides a unique environment to study strange meson spectroscopy through the $K\pi$ interaction, to locate the pole positions in S-, P-,D-,F- and G-waves, particularly for the low-lying S-wave strange scalar meson $\kappa/K_0^*(700)$.

The K_L beam will be generated by directing a high energy, high intensity photon beam onto a Be-target upstream of the GlueX detector. The flux of the K_L beam will be $\sim 1\times10^4$ K_L/sec on a liquid hydrogen/deuterium cryogenic target within the GlueX detector, which has a large acceptance with coverage of both charged and neutral particles. This flux will allow statistics in the case of the hydrogen target to exceed that of earlier experiments by almost three orders of magnitude. The main components of the experimental setup related to the K_L beamline are the Compact Photon Source, the Kaon Production Target, the sweeping magnet, and the Kaon Flux Monitor.

At the first stage, the KLF program will focus on two-body and quasi-two-body reactions: elastic $K_Lp \to K_Sp$ and charge-exchange $K_Lp \to K^+n$ reactions, then on two-body reactions producing $S=-1$ ($S=-2$) hyperons as $K_Lp \to \pi^+\Lambda$, $K_Lp \to \pi^+\Sigma^0(\pi^0\Sigma^+)$, and $K_Lp \to K^+\Xi^0$, as well as three body $K_Lp \to K^+K^+\Omega^-$. The differential cross section and self-polarization measurements of these reactions will be used as PWA inputs to determine the resonance pole parameters of the states described above.

2 Scope of the Proposal

The nature of QCD confinement continues to provide a challenge to our understanding of soft QCD. Experimental investigation of the baryon spectrum provides the obvious avenue to understand QCD in this region, since the location and properties of the excited states depend on the confining interaction and the relevant hadronic degrees of freedom.

Through analyses of decades worth of data, from both hadronic and electromagnetic scattering experiments, numerous baryon resonances have been observed, and many of which have had their masses, widths, and quantum numbers fully determined. There are 109 baryons in the PDG2018 listings, but only 58 of them with 4^* or 3^* quality [1]. Many more states are predicted by quark models (QMs). For example, in the case of $SU(6)_F \times O(3)$ symmetry, 434 resonances would be required, if all partly revealed multiplets were completed (three 70-plets and four 56-plets).

The light and strange quarks can be arranged in six baryonic families, N^*, Δ^*, Λ^*, Σ^*, Ξ^*, and Ω^*. The possible number of members in a family is not arbitrary [2]. Under the $SU(3)_F$ symmetry these are the octet: N^*, Λ^*, and Σ^*, and the decuplet: Δ^*, Σ^*, Ξ^*, and Ω^*. The number of experimentally identified resonances in each baryon family in PDG2018 summary tables is 17 N^*, 24 Δ^*, 14 Λ^*, 12 Σ^*, 7 Ξ^*, and 2 Ω^*. Constituent QMs, for instance, predict the existence of no fewer than 64 N^* and 22 Δ^* states with masses less than 3 GeV. The "missing-states" problem [3] is obvious from these numbers. To complete $SU(3)_F$ multiplets, one needs no fewer than 17 Λ^*s, 41 Σ^*s, 41 Ξ^*s, and 24 Ω^*s.

If these "missing resonances" exist, they have either eluded detection or have produced only weak signals in the existing data sets. The search for those resonances provides a most natural motivation for future measurements at Jefferson Lab. As stated in the *2015 Long Range Plan for Nuclear Science* [4]: *The new capabilities of the 12-GeV era facilitate a detailed study of baryons containing two and three strange quarks. Knowledge of the spectrum of these states will further enhance our understanding of the manifestation of QCD in the three-quark arena.*

The JLab 12 GeV energy upgrade, with the new Hall D, provides an ideal tool for extensive studies of both non-strange and, specifically, strange baryon resonances [5, 6]. Our plan is to take advantage of the existing high-quality photon beamline and the experimental area in the Hall D complex at Jefferson Lab to deliver a beam of K_L particles onto a LH_2/LD_2 target within the GlueX detector. The recently constructed GlueX detector is a large-acceptance spectrometer with good coverage for both charged and neutral particles that can be adapted to this purpose. Obviously, a K_L beam facility with good momentum resolution is crucial for providing the data needed to identify and characterize the properties of hyperon resonances.

The masses and widths of the lowest Λ and Σ baryons were determined mainly with kaon beam experiments in the 1970s [1]. The first determinations of the pole position in the complex-energy plane for a hyperon, for instance, for the $\Lambda(1520)3/2^-$, have been made only recently [7]. An intense K_L beam would open a new window of opportunity, not only to locate "missing resonances", but also to establish their properties by studying different decay channels systematically.

A recent white paper, dedicated to the physics with meson beams and endorsed by a broad physics community, summarized unresolved issues in hadron physics, and outlined the vast opportunities

and advances that only become possible with a "secondary beam facility" [8]. The Hall D K-long Facility (KLF) measurements will allow studies of very poorly known multiplets of Λ^*, Σ^*, Ξ^*, and even Ω^* hyperons with unprecedented statistical precision. These measurements also have the potential to observe dozens of predicted (but heretofore unobserved) states and to establish the quantum numbers of already observed hyperon resonances listed in PDG2018 [1]. Interesting puzzles exist for PDG-listed excited hyperons that do not fit into any of the low-lying excited multiplets, and these need to be further revisited and investigated. Excited Ξs, for instance, are very poorly known. Establishing and discovering new states is important, in particular, for determination of the multiplet structure of excited baryons.

Additionally, the proposed facility will also have great impact in the strange meson sector by measurements of the final-state $K\pi$ system from threshold up to 2 GeV in invariant mass to establish and improve on pole positions and widths of all $K^*(K\pi)$ P-wave states and the S-wave scalar meson κ or $K_0^*(700)$. In particular, the $\kappa/K_0^*(700)$ meson has been under discussion for decades and still remains to be unequivocally confirmed with corresponding quantum numbers by detailed phase-shift analysis with high statistics data [9, 11].

We have organized four Workshops: *Physics with Neutral Kaon Beam at JLab* (KL2016) (February 2016) [12], *Excited Hyperons in QCD Thermodynamics at Freeze-Out* (YSTAR2016) (November 2016) [13], *New Opportunities with High-Intensity Photon Sources* (HIPS2017) (February 2017) [14], and *Pion-Kaon Interactions* (PKI2018) (February 2018) [15]. They were dedicated to the physics of hyperons produced by the neutral kaon beam. The KL2016 Workshop [16] followed our LoI–12–15–001 [17] to help address the comments made by PAC43 and to prepare the full proposal for PAC45 [18]. The proposed KLF program is complementary, for instance, to the CLAS12 baryon spectroscopy experiments [19, 20] and would operate at Hall D for several years. The YSTAR2016 Workshop [21] was a successor to the recent KL2016 Workshop and considered the influence of possible "missing" hyperon resonances on QCD thermodynamics, on freeze-out in heavy ion collisions and in the early universe, and in spectroscopy. Then, the HIPS2017 Workshop [22] aimed at producing an optimized photon source concept with potential increase of scientific output at Jefferson Lab, and at refining the science for hadron physics experiments benefitting from such a high-intensity photon source. Finally, the PKI2018 Workshop is dedicated to the physics of strange mesons produced by the neutral kaon beam [23].

The proposal is organized in the following manner. The motivations for hyperon and kaon spectroscopy are reviewed in Sec. 3, with summaries of the high-impact measurements possible with the KLF given in Sec. 3.1 for hyperon spectroscopy, and in Sec. 3.2 for kaon spectroscopy. In Sec. 4, we give results of detailed simulation studies of key reaction channels. Full detector simulations, including background studies, of several hyperon production channels are described in Sec. 4.1, along with PWA studies showing the impact of these measurements on the hyperon spectrum. In Sec. 4.2, we describe the current status of our studies of the $K\pi$ system, including reactions with missing protons, and how they will impact our knowledge of the resonance parameters of the $\kappa/K_0^*(700)$. In Sec. 4.3, we give additional details of our studies of neutron-induced reactions. Our proposed K_L beam facility is described in Sec. 5 including: K_L production and properties of the secondary K_L beam, measurements of K_L flux, and cryogenic target. Further details of the organizational status and planning are given in Sec. 6 while summary and a beam time request is given in Sec. 7. The Appendices contain many technical details for our proposal.

3 Physics Highlights

3.1 Hyperon Spectroscopy

Lattice QCD and quark model calculations predict a rich spectrum of Λ^* and Σ^* states, many of which have large widths that can be studied at KLF but are not easily accessible in other reactions. As a typical example in Fig. 1 we demonstrate a complete PWA extraction of a fairly low lying but already broad Σ^* resonance in the reaction $K_L p \to \Xi^0 K^+$ assuming 20 (100) days of running shown in green (yellow), see Sec. 4.1 for details. A clean discrimination of broad excited states on top of many overlapping resonances with various different quantum numbers is a key feature of the KLF, unmatched by comparable experiments. The precision of KLF data clearly allows for the identification of these excited states in a mass range not accessible with previous measurements, and determination of their quantum numbers and pole positions, which can be then compared with calculations from Lattice QCD [24].

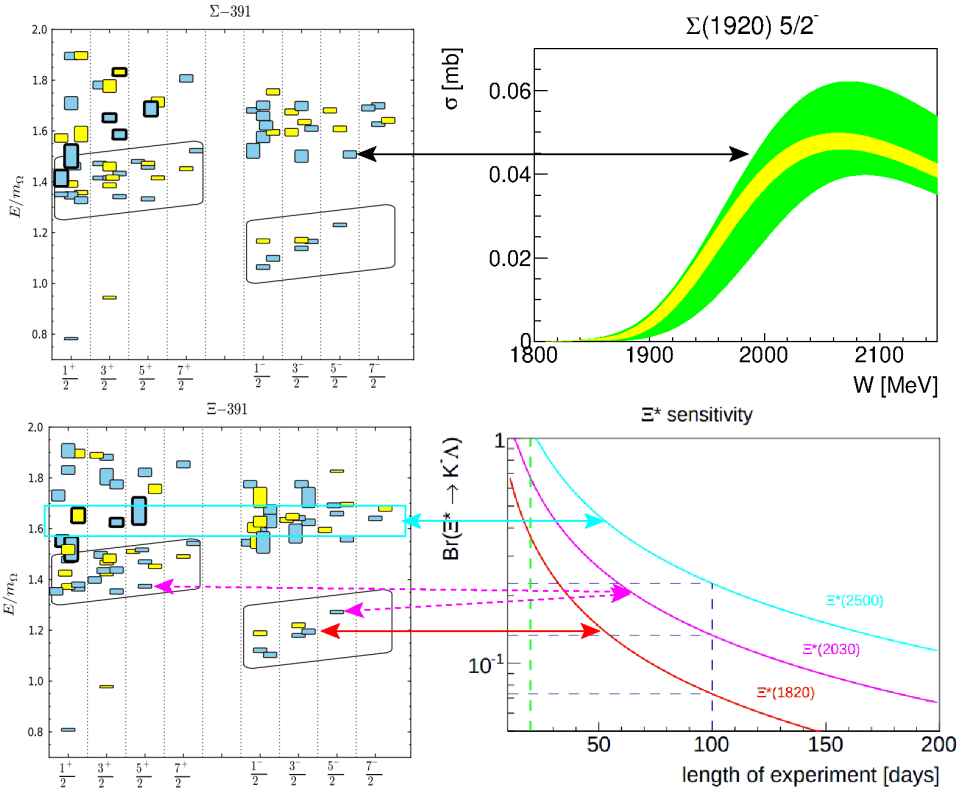

Figure 1: Example of comparison between expected KLF measurements (right) and Lattice QCD predictions for the hyperon spectrum [24] (left), see Section 4.1, Appendix A.3 and Ref. [25] of the text for details.

An additional power of KLF data is the ability to distinguish between different isospin exchanges, which helps identify new hyperon resonances and resolves ambiguities of fits to existing data. As

discussed in Sec. 4.1.2, we consider model of Σ hyperons which describes existing $\pi\Lambda/\pi\Sigma$ data well even with the addition of three Σ^* hyperons based on quark model expectations. However, the additional Σ^* lead to drastic differences in the expected differential cross sections and polarization observables, up to two orders of magnitude depending on if these expected, but unidentified states are included or not. This example shows the essential nature of K_L beam data in the global PWA analysis of hyperons.

The spectrum of Ξ hyperons also clearly has significant discovery potential with implications for heavy quark symmetry and relationships to mass splittings in charm and beauty hyperons. The bottom panel of Fig. 1 demonstrates the branching ratio sensitivity for several excited $\Xi^* \to \Lambda K$ as a function of running days for the experiment (see Appendix A.3 and Ref. [25] for details). These states are expected to be narrow and can be directly compared to the spectrum predicted by Lattice QCD [24].

In summary, this proposal aims to address many of the key open questions in strange hyperon spectroscopy. The detailed studies described in the following sections demonstrate the ability to determine the pole positions and decay modes of many resonances using rigorous PWA methods, beyond naive "bump hunting" assignments listed by in the Particle Data Group [1]. With these ability to perform these PWAs, the KLF experiment will settle the spectrum of $\Lambda^*, \Sigma^*, \Xi^*$ and even Ω^* spectra in the mass range up to 2500 MeV. More details about the theoretical and experimental techniques to be employed in KLF experiments can be found in following sections and supplementary materials.

3.2 Kaon Spectroscopy

One of the most controversial states in light meson spectroscopy is the elusive $\kappa/K^*(700)$. This broad resonance "still needs confirmation" according to the PDG2018 [1]. The reason for the importance of this state is twofold. First of all, the unambiguous determination of its existence would complete the lightest scalar meson nonet, together with the already observed $a_0(980)$, $f_0(980)$, and $\sigma/f_0(500)$ mesons. Secondly, the precise determination of the resonance parameters of the $\kappa/K^*(700)$ is necessary to distinguish between different models of its internal structure, which also will provide insight into its lighter cousin, the $\sigma/f_0(500)$. In addition to this state, there are several other strange-quark resonances belonging to heavier nonets which decay to $K\pi$ with sizeable branching ratios. Unfortunately most of the resonance parameters of these states have not been extracted with high accuracy due statistical limitations or uncontrolled systematic effects due to the simple models used to describe their lineshapes.

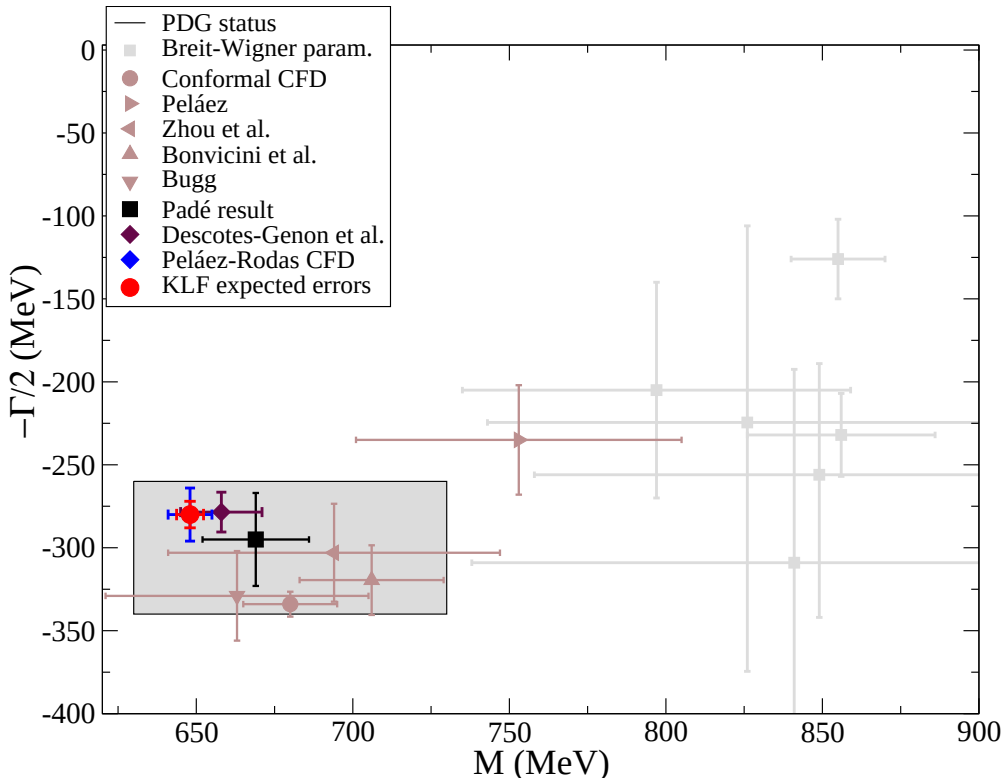

Figure 2: Expected precision on the $\kappa/K_0^*(700)$ pole parameters for 100 days of running time. The uncertainties of KLF prediction are presented in a red color within the blue error bars obtained without KLF data. The shadowed rectangle stands for PDG2018 uncertainties. (see Section 4.2 and Appendix A.4 for details).

The best way to unravel these states and improve the current knowledge on them is to study the $I = 1/2$ partial waves of $K\pi$ scattering, particularly in the elastic region. In order to have access to this scattering process we have to perform an analysis of production experiments like $KN \to K\pi N$ or $KN \to K\pi\Delta$, where the total transferred momentum to the final state baryon t (Mandelstam variable) is small. In this region, the interaction between the kaon and nucleon on the initial state

can be approximated by a one pion exchange. Provided the systematic effects of this approximation are under control, $K\pi$ scattering can be determined with high precision from the aforementioned production experiments. In the past, charged kaon beams were used for this purpose [26–31].

In order to directly measure S-wave phase-shift for isospin $I = 1/2$, as opposed to the sum of $I = 1/2$ plus $I = 3/2$ which was measured at LASS, in this proposal we simulated data in $K_L p \rightarrow K^- \pi^0 \Delta^{++}$ and $K_L p \rightarrow K_L \pi^- \Delta{+}{+}$ with different linear combinations of Clebsch-Gordan coefficients for $I = 1/2$ and $I = 3/2$. Measuring both of these channels allows us to isolate the contribution of the isospin $I = 1/2$ amplitude, as discussed in more detail in Sec. 4.2.

Measurements of $K\pi$ scattering in the $S-$wave will allow the K_L-Facility to contribute to our understanding of the elusive κ meson, as described in Section 4.2 and Appendix A.4. Figure 2 shows the expected improvement in the determination of the mass and width of the κ that can be reached with 100 days of running time. A phase-shift analysis of this scattering data will allow for a decisive determination of its properties by using above mentioned reactions with recoiling Δ^{++} in final state.

4 Simulations of Physics Reactions

Several simulations on various channels were performed to obtain an insight on the expected results and the beam time requirements for precision measurements. The simulations results that follow are based on a 100 days of beam time with a 1×10^4 K_L/sec impinged on a 40 cm long target. Generated events assuming standard beam/target conditions listed in Tables 4 and 5 are processed through a full Geant3-based Monte Carlo (MC) simulation of the GlueX detector [32]. Below we provide a summary of studies performed on various channels for Hyperon spectroscopy (more details can be found in Ref. [25]).

4.1 Hyperon Production Reactions

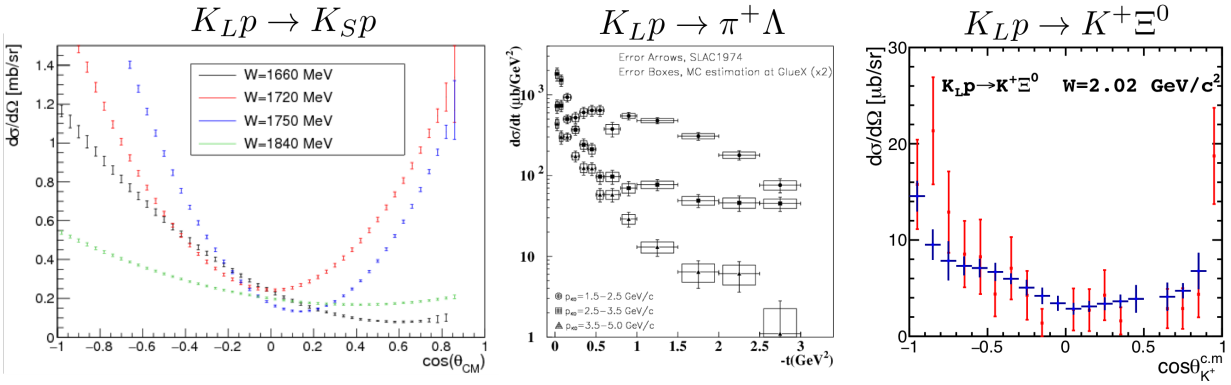

Figure 3: Differential cross sections for reactions (1), (2), and (3) exclusively reconstructed illustrating the statistical uncertainties after 100 days of running. Left: Cross sections of $K_Lp \to K_Sp$ binned in various W bins as a function of the center of mass angle (one can compare to existing data from Ref. [33]. Middle: Differential cross section for various kaon momentum bins as a function of t for $K_Lp \to \pi^+\Lambda$. The boxed errors indicate the statistical uncertainty increased by a factor of 2 after 100 days of running as compared to existing uncertainties [34]. Right: Cross section of $K_Lp \to K^+\Xi^0$ reconstructed exclusively for a specific W bin as a function of the kaon production angle. The uncertainties after 100 days of running are shown with blue error bars and are compared to the existing results (red error bars) [35].

For the case of hyperon spectroscopy, a number of channels that are key to studying hyperon resonances were simulated and studied in detail. Specifically, a summary of the simulation results on the following two-body reactions:

$$K_Lp \to K_Sp, \quad (1)$$
$$K_Lp \to \pi^+\Lambda, \quad (2)$$
$$K_Lp \to K^+\Xi^0, \quad (3)$$
$$K_Ld \to K^+\Xi^- p_{spectator}, \quad (4)$$
$$K_Lp \to K^+n. \quad (5)$$

are presented here (Fig. 3). An analog to the $N\pi$ reactions for the N^* spectra is the $\pi^+\Lambda$ (and $\pi^+\Sigma^0$, not shown here) and can provide crucial information on the excited spectrum of hyperons. The study of cascade data allows us to place stringent constraints on dynamical coupled-channel models and identify resonances that do not couple strongly to the $\pi\Lambda$ but decay preferably to a $K\Xi$ channel; analogous to N^* resonances that do not couple strongly to πN but are cleanly seen in $K\Lambda$ and $K\Sigma$ channels. In addition, cascade data on proton and neutron targets provides us with long-sought information on missing excited Ξ states, which can be easily identified and isolated using missing-mass and invariant-mass techniques, and the possibility to measure the quantum numbers of the already established $\Xi(1690)$ and $\Xi(1820)$ from a double-moment analysis. Finally, non-resonant contributions that could interfere with hyperon production amplitudes and distort hyperon signals can also be studied. This is because due to strangeness conservation, formation of intermediate resonances is forbidden in the $K_Lp \to K^+n$ reaction. Therefore, a detailed study of this reaction provides a clean and controlled way to study and eliminate nonresonant contributions.

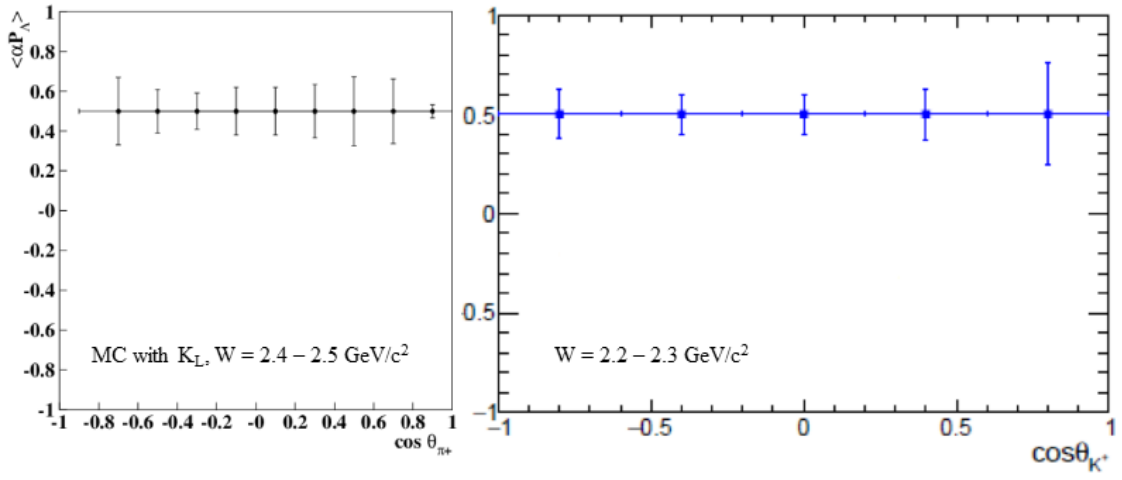

Figure 4: Two-fold differential results on the induced polarization of Λ (left) and Ξ^0 (right) from $K_Lp \to \pi^+\Lambda$ and $K_Lp \to K^+\Xi^0$ after 100 days of running.

The statistical uncertainties obtained after 100 days of running for the differential cross sections of reactions $K_Lp \to K_Sp$, $K_Lp \to \pi^+\Lambda$, and $K_Lp \to K^+\Xi^0$ are shown in Fig. 4. The proposed experiment will allow us to reconstruct about 2.7M K_Sp events in the $K_S \to \pi^+\pi^-$ channel, allowing an unprecedented and detailed investigation of the cross section ambiguities evident in existing results. Furthermore, the proposed experiment will significantly improve measurements of $K_Lp \to \pi^+\Lambda$ and $K_Lp \to K^+\Xi^0$ as illustrated by the uncertainties in Fig. 4.

Utilizing the large self-analyticity of hyperons through their parity violating weak decay, one can easily determine the hyperon induced polarization by studying the angular distribution of the hyperon decay products. Such measurements place further stringent constraints on the underlying dynamics and are shown to be an invaluable tool in identifying PWA amplitudes. Figure 4 shows the two-fold differential induced polarisation and the statistical uncertainties obtained after 100 days of running for $K_Lp \to \pi^+\Lambda$ (left) and $K_Lp \to K^+\Xi^0$ (right). The proposed experiment will increase

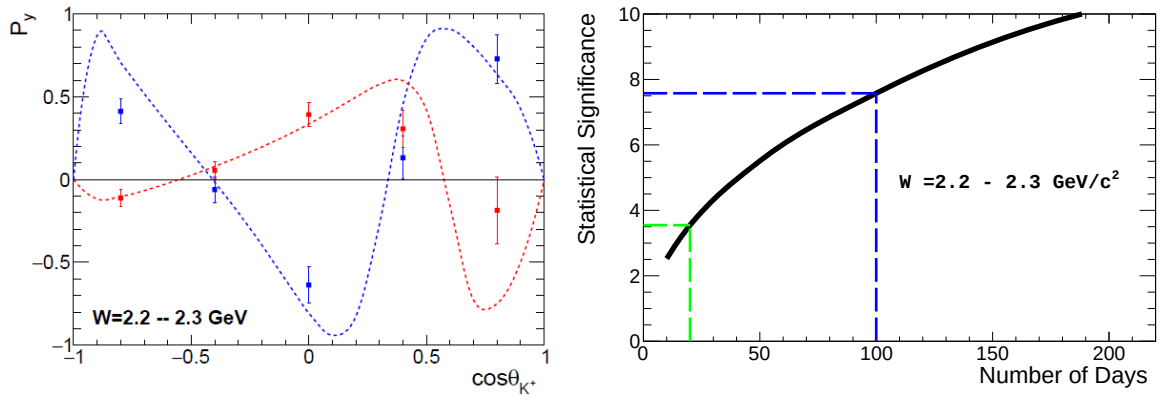

Figure 5: Left: Estimated statistical uncertainties of the induced polarization of the Ξ^- in a $K_L n \to K^+\Xi^-$ reaction as a function of CM $\cos\theta_{K^+}$ (two-fold differential). The curves show the theoretical predictions based on two solutions as described in Appendix A.3.12. Right: Expected statistical significance, in units of σs, to distinguish two models as a function of the running time. Two benchmark cases of 20 and 100 days are highlighted by the dashed green and blue curves, respectively.

significantly the kinematic coverage of available results and provide a statistical improvement by at least of factor of 2 on existing measurements.

The so-called coupled-channel Chiral Unitary approaches (UChPT) implement unitarity exactly via a re-summation of a chiral potential to a certain chiral order. They successfully describe all available anti-kaon-nucleon scattering data. In the most advanced formulation, such a UChPT approach relies on a chiral amplitude for meson-baryon scattering up to next-to-leading chiral order. The unitarity constraint is imposed via the Bethe-Salpeter equation either in the full off-shell formulation [36, 37] or in the so-called on-shell approximation [38, 39]. It was found there that various models, which typically have many free parameters, adjusted to the same experimental data, predict very different behavior of the scattering amplitude on and off the real energy-axis. This ambiguity can be traced back to the fact that the experimental data used to fix the parameters of the models is rather old and imprecise. In particular, there are missing good quality data filtering the isoscalar and isovector parts of the antikaon-nucleon amplitude. In this respect, the proposed measurement of the $K_L^0 p$ reactions to the $\pi\Lambda$, $\pi\Sigma$ and $K\Xi$ states will provide valuable constraints on the isovector sector of the $\bar{K}N$ interactions.

The K_L beam can be scattered on a neutron target, while measuring the strangeness $S = -1$ final meson-baryon states. In such a setup, the proposed experiment will become a new and very strongly desired source of experimental data to pinpoint the properties of the antikaon-nucleon scattering amplitude. To make this statement more quantitative, we compare predictions of both solutions of the model from Ref. [38]. These solutions agree with all scattering, threshold as well as the photoproduction data for the $\Sigma\pi$ line shapes by the CLAS Collaboration [40].

An analysis of generated polarization data from the reaction $K_L n \to K^+\Xi^-$ using models described in Appendix A.3.12 indicate than with 100 days of beamtime the expected statistical uncertainties allow a clear identification between the two available models, which give very different predictions. The left panel in Fig. 5 illustrates the expected two-fold differential results on the

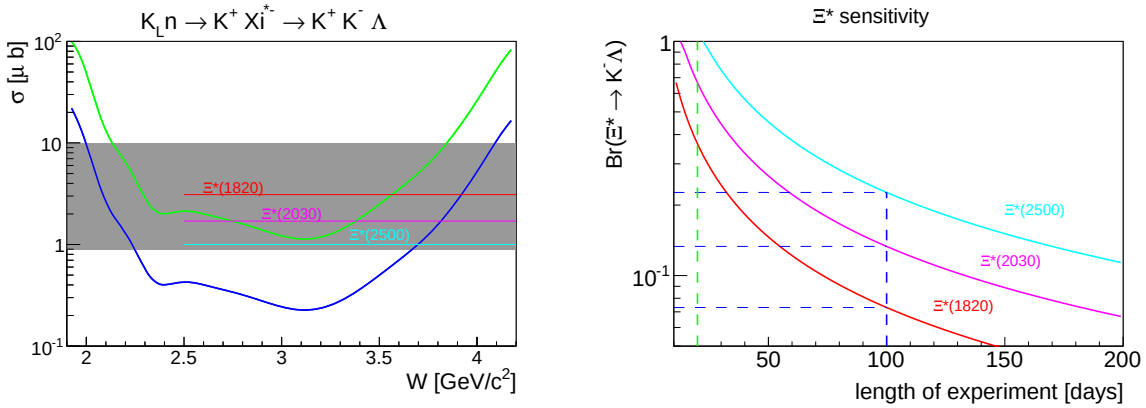

Figure 6: Left: Ξ^* discovery potential achievable at KLF during the 100 (blue) and 20 (green) day experiment, under assumption of 10 % statistical accuracy and $Br(\Xi^* \to \bar{K}\Lambda) = 1$. The gray band corresponds to typical Ξ^* cross sections and horizontal lines are few examples of BNL cross sections from Ref. [41]. Right: Estimation of lowest measurable $\Xi^* \to \bar{K}\Lambda$ branching fraction at KLF as a function of experiment duration at W$\sim$3.1$\pm$0.025 GeV. Two benchmark cases of 100 (20) days are highlighted by dashed blue (green) curves.

induced cascade polarization (Ξ^-) after 100 days of running using generated data from the two model predictions. The expected statistical significance for the model separation at the same W-bin as a function of experiment duration is shown in the right panel. The right panel indicates that a 100 days experiment would reach a decisive level of 7.6 σ separation power, compared to only a 3.5 σ separation after 20 days.

The spectrum of excited cascades is barely known and practically nothing is known about their quantum numbers. Detailed studies utilizing generated data were performed to investigate the discovery potential achievable at KLF including measurements on the neutron. The left panel of Fig. 6 shows the production cross sections that will be measurable at KLF with 100 days (blue) and 20 days (green) of running considering a 10 % statistical uncertainty and a branching ratio [1] $Br(\Xi^* \to \bar{K}\Lambda) = 1$. The right panel shows the lowest measurable $\Xi^* \to \bar{K}\Lambda$ branching fraction at KLF as a function of experiment duration indicating the lowest measurable branching ratios at 20 and 100 days. 100 days of running allows us to study the several Ξ^* states even with somewhat suppressed $\Xi^* \to \bar{K}\Lambda$ decay of heavy Ξ^*'s [2]. A W-variation of the Ξ^* production cross-section provide and important information on $\Xi^* \to \bar{K}\Lambda^*$ and $\Xi^* \to \bar{K}\Sigma^*$ couplings as an inverse process allowing further insight into Ξ^* internal structure.

Finally, the nonresonant reaction $K_L p \to K^+ n$, can be studied in a clean and controlled way and one can use this to identify nonresonant contributions to the hyperon production amplitudes. In 100 days of beamtime, we expect to detect $\sim$ 60M events significantly improving the statistical significance of existing measurements [42, 43] and provide precision measurements in the energy range 2 < W < 3.5 GeV where there are no data on this reaction at all.

[1] From BNL measurements given in Ref. [41] the Ξ^{*-} production cross section should be on the order of $1 - 10\ \mu b$ and the higher Ξ^* mass the lower the cross section, from $3.7 \mu b$ for the $\Xi^*(1820)$ to $1 \mu b$ for the $\Xi^*(2500)$.

[2] The $\Xi^* \to \bar{K}\Lambda$ is "dominant" for many Ξ^* states according to PDG2018 [1]

4.1.1 Expectations for Λ^* and Σ^* Spectroscopy via $K^+\Xi$ PWA:

The observation of Λ^* and Σ^* hyperons at KLF will require a coupled-channel PWA using the measured differential cross sections and recoil observables, which have been simulated as described in in Appendix A.3. The resonance poles in the complex energy plane will be used to confirm previously observed states and identify new Λ^* and Σ^* resonances in the hyperon spectrum.

The existing K_Lp database is so poor that PWAs of individual K_Lp-induced reactions may not be possible based on currently available data (Appendix A.3). In particular, there are no $K_Lp \to K^+\Xi^0$ polarization data available and there is only one energy for the $K_Lp \to \pi^+\Lambda$ reaction with both $d\sigma/d\Omega$ and polarization data. Our proposal does not consider the use of a polarized target at this stage and, for that reason, we will be able to measure polarization data for recoil observables only. Overall, one certainly cannot perform a reliable PWA for reactions in which only $d\sigma/d\Omega$ data are available. The existing K_Ln database is nonexistent.

Resonance	20 days: M, Γ	100 days: M, Γ	PDG2018: M, Γ	LQCD: M
$\Sigma(1920)5/2^-$	1977±21±25 327±25±25	1923±10±10 321±10±10		2027 2487 2659 2781
$\Sigma(2030)7/2^+$	1981±30±30 350±80	1930±20±30 400±40	2030±10 180±30	2686 2709 2793 2806

Table 1: Comparison of masses and widths (in MeV units) of simulated values with the results of PDG2018 [1] and LQCD [24] predictions.

To estimate the impact that new K_L measurements will have on fits, we have carried out a study $K_Lp \to K^+\Xi$ reaction. Using the recent BnGa solution [44, 45], we generated pseudo-data for the $K_Lp \to K^+\Xi$ reaction, which were subsequently passed through the Geant-simulated detector setup and analysed the same way as usual data. The $d\sigma/d\Omega$ and recoil polarization P with associated statistical errors were extracted for the PWA within BnGa framework. The pseudo-data were generated for our worse case of statistics for a $K_Lp \to K^+\Xi^0$ binning of 20 MeV in CM energy W and θ = 5 (10) 175° for $d\sigma/d\Omega$ and $\cos\theta$ = -0.8 (0.4) 0.8 for P. A series of global fits were obtained using settings associated with 20 and 100 days of running time within BnGa framework.

The simulated solution was obtained from the fit of the $K^-p \to K\Xi$ data using the K-matrix fit which included all 3 and 4 star Λ and Σ-hyperons [1] and an additional Σ state needed to fit the data. The quantum numbers of this state were found to be $5/2^-$ and its mass is located just above 1900 MeV. This fit also showed a notable deviation for the pole position of the $\Sigma(2030)7/2+$ state from the PDG2018 value (Table 1). The data from the K_Lp collision where only Σ hyperons are produced can provide a crucial information which can confirm or reject this solution.

The data simulated assuming 20 and 100 days of the data taken were fitted as a sum of the Breit-Wigner (BW) states. Although 20 day data set allowed us to reproduce the quantum numbers of the all contributions from the simulated solution the properties of the $\Sigma(1920)5/2^-$ and $\Sigma(2030)7/2^+$ hyperons were defined with large uncertainties. The mass of the $\Sigma(1920)5/2^-$ state was found to

be notably higher than that used in the simulation (Table 1). The fit of the 100-day data sets solve all the above-mentioned problems. The masses and the widths of the simulated states were fond to be much closer to those simulated in the solution and with much smaller errors. The fit of the 100 day data sets allowed us to define with much larger accuracy the couplings of the fitted states into $K\Xi$ channel.

An example of the fit results for $d\sigma/d\Omega$ and P for 20 and 100 days settings together with 100 days pseudo-data are shown on Fig. 7. To illustrate the effect for 20 (100) days data taking on resonance parameters, we plot the total cross section for two prominent Σ^* states: $\Sigma(1920)5/2^-$ and $\Sigma(2030)7/2^+$, see Fig. 8.

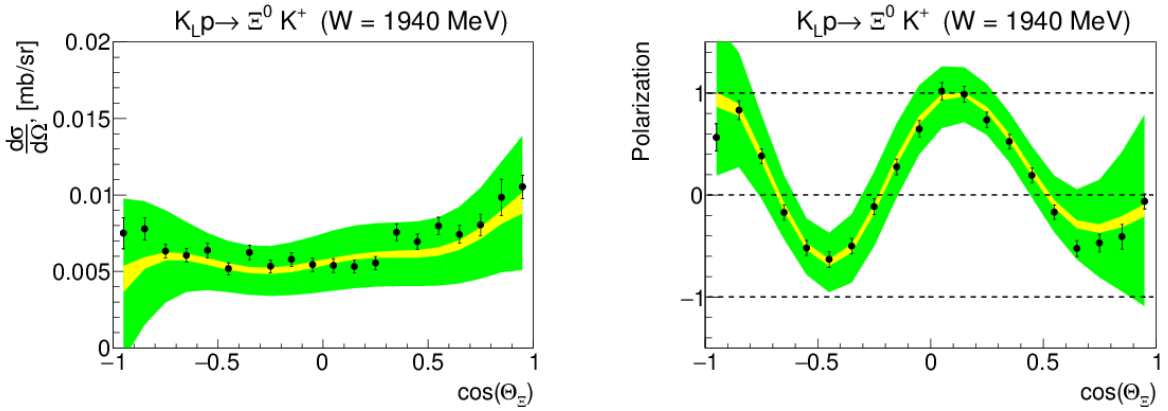

Figure 7: Two examples (W = 1940 MeV) showing the impact of the proposed data on the BnGa solutions. The green (yellow) hatched band indicates the present uncertainties for 20 (100) days of running time. The solid black points corresponds to the quasi-data expected for 100 days of experiment. $d\sigma/d\Omega$ on the left and P on the right panels.

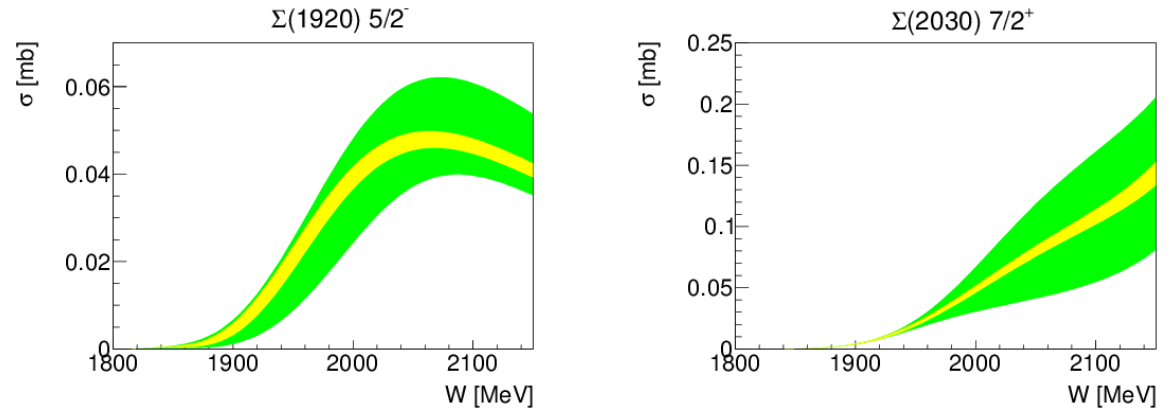

Figure 8: Resulting effect of 20 (green) and 100 (yellow) days of running time on two Σ^* resonances within BnGa PWA solution. $\Sigma^*(1920)5/2^-$ (left) and $\Sigma^*(2030)7/2^+$ (right).

The new measurements, specifically the 100 days of running time case will significantly reduce the uncertainties of the observables. The total angular resolution will therefore be greatly improved,

which will enhance the possibility of determining the number of amplitudes that are involved. With this greater understanding of these observables, effects of higher-spin resonances can be investigated.

To summarize: With 100 days of running time, we can provide a reliable solution for all the resonances having elastic branching ratios larger than 4 %, at least up to $l = 4$. With 20 days of beamtime, we could only carry out simple "bump-hunting" - an identification of well-defined and well-separated resonances with regular shapes. All irregular cases (e.g., molecular states with skewed shapes and complex energy-dependent-widths, threshold-effects, multiple interferences, etc.) and all the exotic states that are predicted to populate the hyperon spectrum will require high-precision polarization observables on the order of 0.1 or better to be identified. From our $K^+\Xi$ PWA study, we can infer that the precision of resonance parameters extracted from PWA of KLF data for the higher-mass Λ^* and Σ^* states we propose to measure will deteriorate without sufficient running time. The spectrum of excited Λ^* and Σ^* states is expected to be densely populated with typical mass differences of about 100 MeV for states with the same quantum numbers [1]. Therefore to disentangle the spectrum of observed hyperon states, we require sufficient precision for the extracted mass and width parameters, provided by the proposed 100 days of running time. With this 100 days of running time we could reach a precision level in the hyperon spectrum comparable to modern results of the SAID πN PWA [46].

4.1.2 Expectations for Σ^* Spectroscopy via a $\pi^+\Lambda$ and $\pi\Sigma$ PWA:

Another effect of the measurement of K_L-induced reactions on our knowledge of the hyperon spectrum was not fully understood until recently. Σ-baryons are both members of octet and decuplet of baryons, hence for each discovered N^* or Δ^* resonance we should find a complimentary Σ baryon. Having 17 N^* states and 10 Δ states we should expect no less than 27 Σ's instead of the 12 currently known [1].

It was long believed that large data sets accumulated with charged kaon beams in the simplest $\pi\Lambda/\pi\Sigma$ production reactions would be sufficient to identify all missing hyperon states, but these reactions themselves were found to not provide the sensitivity necessary to extract the missing states. However, the effect of neutral kaon beams was overlooked in these evaluations.

Let's consider the possible Σ-production channels with various kaon beams and nucleon target. The dynamics for the $K^-p \to \Sigma\pi$ reaction can be described with two isospin amplitudes A_1 and A_0, see Eq. (6).

$$\begin{aligned}
|A(\Sigma^+\pi^-)|^2 &= |\frac{1}{\sqrt{2}}A_1 + \frac{1}{\sqrt{3}}A_0|^2 = \frac{1}{6}(3|A_1|^2 + 2|A_0|^2 + 2\sqrt{6}Re(A_1^* \cdot A_0)) \\
|A(\Sigma^-\pi^+)|^2 &= |-\frac{1}{\sqrt{2}}A_1 + \frac{1}{\sqrt{3}}A_0|^2 = \frac{1}{6}(3|A_1|^2 + 2|A_0|^2 - 2\sqrt{6}Re(A_1^* \cdot A_0)) \\
|A(\Sigma^+\pi^0)|^2 &= |A(\Sigma^0\pi^+)|^2 = \frac{1}{2}|A_1|^2. \qquad (6)
\end{aligned}$$

The most abundant K^- reactions on proton contain both A_1 (Σ^*- channel), A_0 (Λ^*-channel) and their interference. The K^0 reactions on neutron contain the same amplitudes but with the different sign in the interference term, which is extremely helpful for separation of interference effects. Finally, the K^0 reactions on proton contain only the A_1 amplitude, with no ambiguities, Eq.(6).

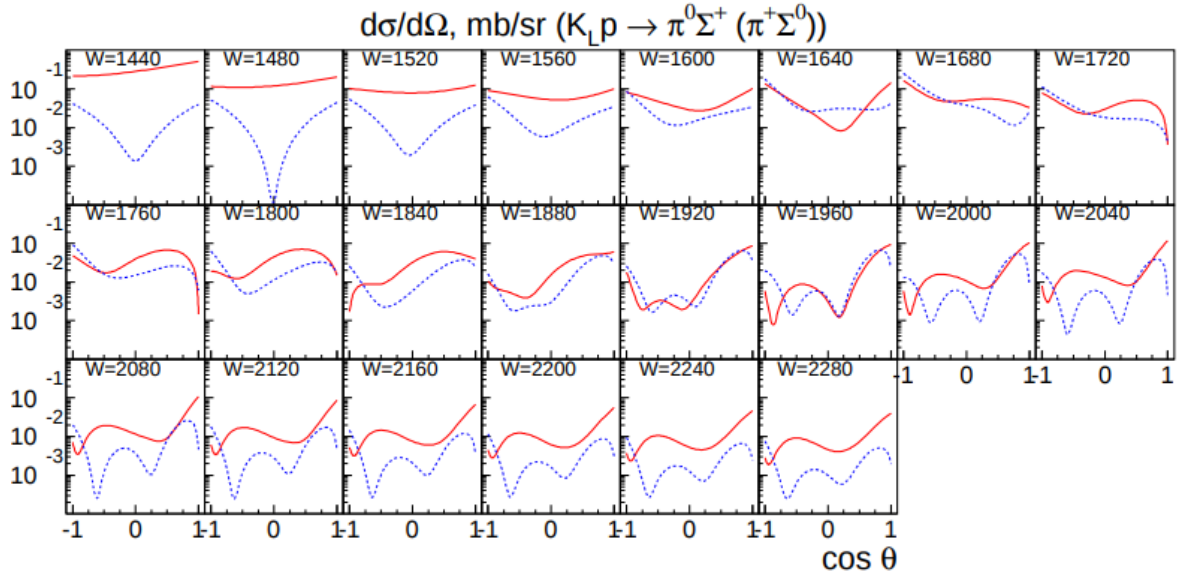

Figure 9: Resulting effect of K_Lp data on three new Σ^* resonances within BnGa PWA solution on differential observables in $K_Lp \to \pi\Sigma$ reactions [47], note the semi-log scale.

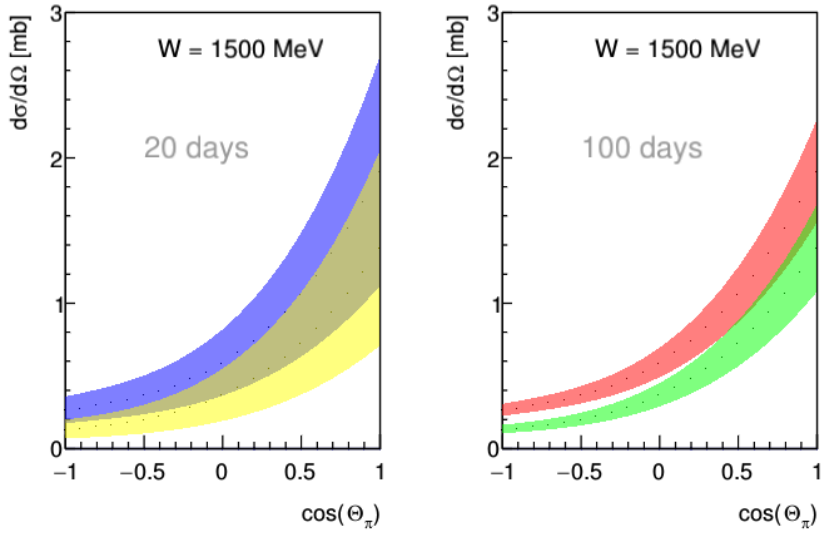

Figure 10: Resulting effect of K_Lp data on three new Σ^* resonances within BnGa PWA solution on the differential cross section for the $K_Lp \to \pi\Lambda$ reaction [47] for the 20 days (left) and 100 days (right) beamtime.

To quantify the effect of including K^0-induced $\pi\Sigma$ data on the possible Σ^* resonances we performed a dedicated study, where we fit existing $\pi\Lambda/\pi\Sigma$ data under two assumptions. In the first case we assumed known Σ resonances only, in the second one we have added three extra Σ states expected from baryon multiplet correspondence. Both models reproduce existing data very well. The marginal improvement of the fit results when including the additional Σ states can only be seen from the χ^2/dof and can hardly be differentiated from experimental plots. However the

predictions we get from these two fits differs drastically in K^0-induced reaction, as seen in Fig. 9.

The predictions of these two fits differs by nearly two orders of magnitude even in the simplest differential cross sections distributions. Both models also show very different behaviour in polarization observables.

A similar, but somewhat smaller effect is expected in $\Lambda\pi$ channel, see Fig. 10 (same models as in Fig. 9 or Ref. [47]). The difference in sensitivity is expected to originate from the difference in coupling constants of $\Sigma^* \to \Sigma\pi$ or $\Sigma^* \to \Lambda\pi$ decay branches.

Our study shows that the missing Σ states not seen in the simplest possible $\pi\Lambda/\pi\Sigma$ reactions originate not from a low sensitivity of theses reactions to the various Σ^*-excited states, but rather it shows the inability of theoretical extraction of these states in the absence of K^0 data.

4.2 $K\pi$ Spectroscopy

The simplest hadronic reaction that involves strange quarks is $K\pi$ scattering, therefore its experimental study plays a crucial role for our understanding of QCD in the non-perturbative domain. Theoretically the $K\pi$ scattering amplitude can be calculated based on Chiral Perturbation Theory at one loop [48, 49] and at two loops [50]. There are also LQCD calculations of $K\pi$ scattering from the first principles treatment of QCD [51–60].

The $K\pi$ scattering has two possible isospin channels, $I = 1/2$ and $I = 3/2$. For S-wave scattering, both are significant below 2 GeV, whereas for P-wave scattering, $I = 3/2$ is almost negligible. Below 1 GeV, the P-wave is basically a narrow elastic wave peaking at 892 MeV, interpreted as the $K^*(892)$ resonance. A second P-wave resonance, the $K_1^*(1410)$, exists above 1 GeV, although its properties are less precisely known. The $I = 3/2$ S-wave is elastic and repulsive up to 1.7 GeV and contains no known resonances. The P-wave $I = 3/2$ has been measured in Ref. [26] and is also repulsive but very small. However, the $I = 1/2$ S-wave has a peaking broad resonance above 1350 MeV, interpreted as $K_0^*(1430)$.

Most of the experimental studies of the $K\pi$ system have been performed by experiments scattering a kaon beam off of nucleons, where the single pion exchange process at low $|t| \leq 0.2$ GeV^2 provides access to the $K\pi$ scattering dynamics. At KLF there are a total of 9 possible production processes (listed in Eq. (7)) to study the $K\pi$ system that could be accessed through a K_L beam, proton target and recoiling proton, neutron or Δ^{++}.

$$\begin{aligned}
&K_L p \to K_L \pi^0 p,\\
&K_L p \to K^{\pm}\pi^{\mp} p,\\
&K_L p \to K_{(L,S)}\pi^+ n,\\
&K_L p \to K^+\pi^0 n,\\
&K_L p \to K^-\pi^0\Delta^{++},\\
&K_L p \to K_{(L,S)}\pi^-\Delta^{++}.
\end{aligned} \tag{7}$$

These reactions are proportional to different combinations of the $I = 1/2$ and $I = 3/2$ $K\pi$ scattering amplitudes, as explained in Appendix A.4. Isospin separation requires studying multiple

reactions with linearly independent isospin combinations, which in this case requires measuring a reaction with and without a K_L in the final state. We have selected three complementary reactions to simulate and demonstrate the precision of the proposed measurements which are summarized in this section and described in detail in Ref. [78].

The first reaction, $K_L p \to K^{\pm}\pi^{\mp}p$, provides access to the $K\pi$ scattering amplitudes via neutral pion exchange. Simulations of this reaction have demonstrated that it can be measured by a) not detecting the proton, providing acceptance down to t_{min} or b) detecting the complete final state, providing excellent resolution W and $|t|$ resolution but limiting the acceptance to $|t| > 0.01$ GeV^2.

The remaining two simulated reactions proceed via charge exchange resulting in a Δ^{++} recoil: $K_L p \to K^-\pi^0\Delta^{++}$ and $K_L p \to K_L\pi^-\Delta^{++}$. The charge exchange process has the advantage that it has been studied extensively by the LASS Collaboration and Estabrooks *et al.* and is known to be dominated by single pion exchange at low $|t|$. The energy available in the Δ^{++} decay also reduces the minimum accessible $|t|$ when the proton is reconstructed. However, kinematically t_{min} does increase significantly with $M_{K\pi}$ as pointed out in Ref. [26].

The extraction of the $K\pi$ scattering amplitude requires isolating the pion exchange contribution from other possible production mechanisms. The pion exchange contribution is expected to dominate at low $|t|$, and the simulation studies demonstrate the acceptance in this critical regime. However, significant theoretical modeling of the $|t|$ dependence of the production model will be required to extract the $K\pi$ scattering amplitudes. Systematic uncertainties due to this theoretical modeling are very difficult to estimate and thus were not taken into account in previous measurements.

While the simulations described in this proposal have focused on the proton target data, similar reactions will be analyzed with the 100 days of deuterium target running. This data will complement the proton target data and provide essential systematic checks on the extraction of the charged pion exchange contribution. In addition, the opportunity to study both proton and neutron target reactions at low t-Mandelstam will provide unprecedented access to all four isospin partners of $K_0^*(700)$ in a single experiment at KLF.

4.2.1 Impact on P-Wave Phase-Shift Study:

The pion exchange in the hadro-production mechanism of $K^{*0}(892)$ occurs mostly at low $-t$, therefore allowing access to the scattering amplitude of $K^0\pi^0 \to K^+\pi^-$, as illustrated in Fig. 11. Using the resolutions and efficiencies from our simulations, we can estimate the improvement that can be made on the scattering amplitude analysis of $K\pi \to K\pi$. The range of $-t$ that will be used in this comparison will be [0.14, 0.2] GeV^2 to ensure that the t efficiency is uniform. The efficiency of this t range selection is $\epsilon_\pi = 17.85\ \%$. The expected number of events in this case is 2×10^6 based on 100 days of running time.

The precise and robust determination of the P-wave elastic phase-shift is crucial for many process involving strangeness, particularly in that it is the dominant contribution to the $K\pi$ form factor. There exist several different alternative studies to the production experiments like the extraction of the vector form factor $f_\pm(t)$ by Ref. [75], where t is the four-momentum transfer. The vector form factor, at the optical point $f_+(0)$, has an impact on the measurement of the CKM matrix element V_{us} [75, 76], where the precision on this measurement plays an important role on probing the physics beyond the Standard Model. The phenomenological studies [75, 76] analyzed the $K\pi$

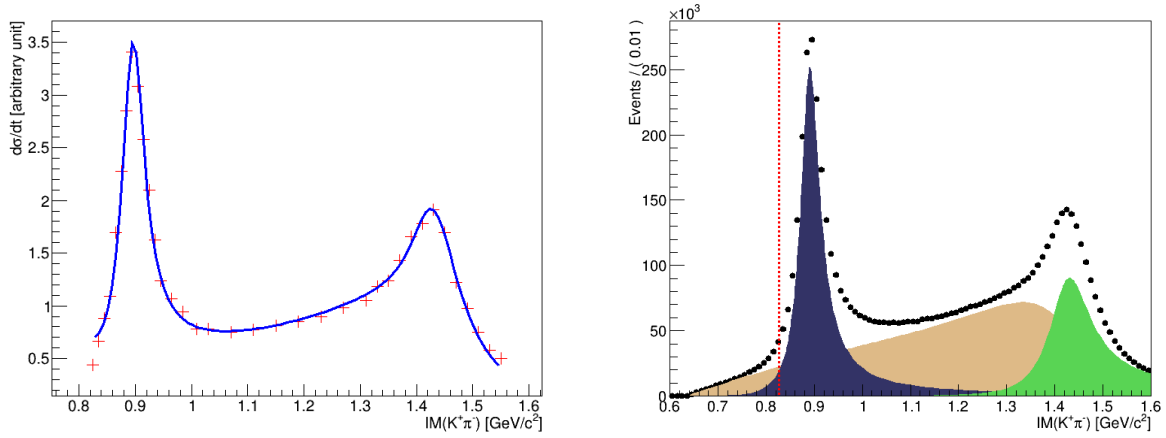

Figure 11: Left: Cross section of $K^- p \to K^+ \pi^- n$ as a function of the invariant mass from LASS results [27]. The blue line is the fit to the cross section using composite model containing two RBWs, spin-1 and spin-2, and S-wave LASS parameterization. Right: Expected distribution of the $K^+\pi^-$ invariant mass below 1.6 GeV from KLF after 100 days of running. The dark blue function represents the $K^+\pi^-$ P-wave, light brown the S-wave and green the D-wave. The dashed line represents the threshold of $K\pi$ invariant mass in LASS results [27].

P-wave phase-shift produced by the Belle Experiment [77] using the decay $\tau \to K\pi\nu_\tau$ and LASS data [26, 27] using the scattering reaction $K^- p \to K^+\pi^- n$. A major concern from these studies is that as explained in [75] the phase-shift extraction by the LASS experiment [26, 27] could be affected by a systematic effect. Furthermore, there is a clear tension regarding the parameters of the $K^*(892)$ between the modern τ decay experiments and the older LASS experiments.

A new, high-statistics measurement of this amplitude at the KLF could resolve these systematic effects and provide a new precision measurement of the $K^*(892)$ resonance parameters. We can evaluate the improvement that can be performed by KLF in these type of studies. A comparison between the projected KLF results and the LASS results [27], which perform a similar scattering reaction study with a charged kaon beam, is presented in Fig. 11 (left). The resulting model from the fit to LASS amplitude is used to simulate the distribution of the invariant mass of $K^+\pi^-$ in a P-wave with KLF.

4.2.2 S-wave and D-wave Production in $K_L p \to K^+\pi^- p$:

The $K\pi$ scattering S-wave has two possible isospin channels. Of those the isospin $I = 1/2$ S-wave contains two resonances, κ and $K_0^*(1430)$, both of which are not well defined. The isospin $I = 3/2$ S-wave is a repulsive interaction, and thus no resonances are seen with just a smooth linearly decreasing phase-shift instead. So far, the available data used to study the dynamics of the S-wave for both isospins are LASS data [26, 27]. The $K\pi$ P-wave and D-wave are better understood. The former has one elastic vector-meson resonance $K^*(892)$ which dominates the description of the partial wave, and two inelastic resonances with small branching ratios to $K\pi$ below 2 GeV, whereas the latter has one inelastic tensor meson resonance, the $K_2^*(1430)$. The simulation of the reaction $K_L p \to K^{*0}(892)p \to K^+\pi^- p$ in KLF can be used to estimate the total production rate of the different $K\pi$ waves. Fig. 11 (left) shows the fit to the cross section of LASS results.

After 100 days of KLF running, we expect 3.5×10^6 events for S-wave production and 1.2×10^6 event in the D-wave. The total 100 days production statistics for the $K^+\pi^-$ system is expected to be $\approx 7 \times 10^6$ events for the S, P, and D-waves combined. This production includes isospin $I = 1/2$ and $I = 3/2$ and represent about 50 times the dataset collected by LASS experiment [27]. Figure 11 (right) shows the expected $K^+\pi^-$ invariant mass distribution produced by the reaction $K_L p \to K^{*0}(892)p \to K^+\pi^- p$ in KLF.

It is important to note that especially in the region below 0.75 GeV we expect this new data to provide a dramatic improvement in these scattering amplitude determinations not only due to the very high statistics, but also because LASS did not provide any data below 0.75 GeV. These data are therefore very relevant for the extraction of the scalar-meson scattering lengths that will test the predictions and convergence of SU(3) Chiral Perturbation Theory. Moreover, the rigorous variable for analytic continuation to the complex plane is s, and due to the large width of the κ, the real part of the κ pole position in the s-plane, $\mathrm{Re}(M_\kappa - i\Gamma/2)^2 \simeq (M_\kappa^2 - \Gamma^2/4) \simeq 0.39\,\mathrm{GeV}^2$, is much closer to threshold $s_{th} \simeq 0.40\ \mathrm{GeV}^2$ than to its nominal mass $M_\kappa^2 \simeq 0.465\ \mathrm{GeV}^2$, which makes the determination of the pole especially sensitive to the threshold region. The KLF low-mass results are therefore of even greater relevance.

4.2.3 Kappa Investigation:

Reference	Pole Position (MeV) $\sqrt{s_\kappa} \equiv M - i\Gamma/2$	Comment
Bonvicini [82]	706.0±24.6-i 319.4±22.4	T-matrix pole model from CLEO
Bugg [83]	663±42-i 342±60	Model with LO Chiral symmetry
Peláez [84]	753±52-i 235±33	Unitarized ChPT up to NLO
Conformal CFD [79]	680±15-i 334±8	Conformal parameterization from dispersive fit
Padé [85]	670±18-i 295±28	Analytic local extraction from dispersive fit
Zhou *et al.* [71]	694±53-i 303±30	partial-wave dispersion relation. Cutoff on left cut.
Descotes-Genon *et al.* [11]	658±13-i 279±12	Roy-Steiner prediction. No S-wave data used below 1 GeV.
Pelaez-Rodas HDR [23, 80, 81]	648±7-i 280±16	Roy-Steiner analysis of scattering data
KLF expected errors	**648±4-i 280±8**	**As previous line but with KLF expected errors**

Table 2: Illustrative values of $\kappa/K_0^*(700)$-pole determinations from models (Lines 2 to 7). Line 8 is a model independent prediction from a dispersive analysis without using S-wave data below 1 GeV. We also compare in the last two lines the model independent extraction using present data versus the extraction using the expected KLF data.

The κ or $K_0^*(700)$ meson is a 0^+ resonance with strangeness. The pole of this resonance is found in the $K\pi$ S-wave with isospin $I = 1/2$. In case of neutral kaon scattering off the proton producing a $K\pi$ system with neutral or charged exchange, the S-wave final state is composed of the two isospin components $I = 1/2$ and $I = 3/2$. Therefore if possible, a separate determination of the two components to study the pole of the κ meson would be very important. It should be noted that this separation was not performed in the last LASS experiment [27]. Actually, the existing $I = 3/2$ data are older than the LASS experiment and are of much lower precision, which produces a large source of uncertainty that contaminates the extraction of the $I = 1/2$ amplitude and thus the $\kappa/K_0^*(700)$ or other strange resonance poles. Simulations of the two reactions $K_L p \to K^-\pi^0\Delta^{++}$ and $K_L p \to K_L\pi^-\Delta^{++}$ for 100 days of running provide estimates of the precision that will be obtained for the isospin separate phase-shifts, as presented in Appendix A.4 and an Analysis Note [78], and shown in Fig 12. **Note:** these phase shifts assume that the pion exchange

contribution to the scattering amplitude will be obtained through a model dependent fit to the $|t|$ dependence of the amplitudes as performed by the LASS Collaboration and Estabrooks *et al.*, however theoretical uncertainties due to this extraction were not included in these studies.

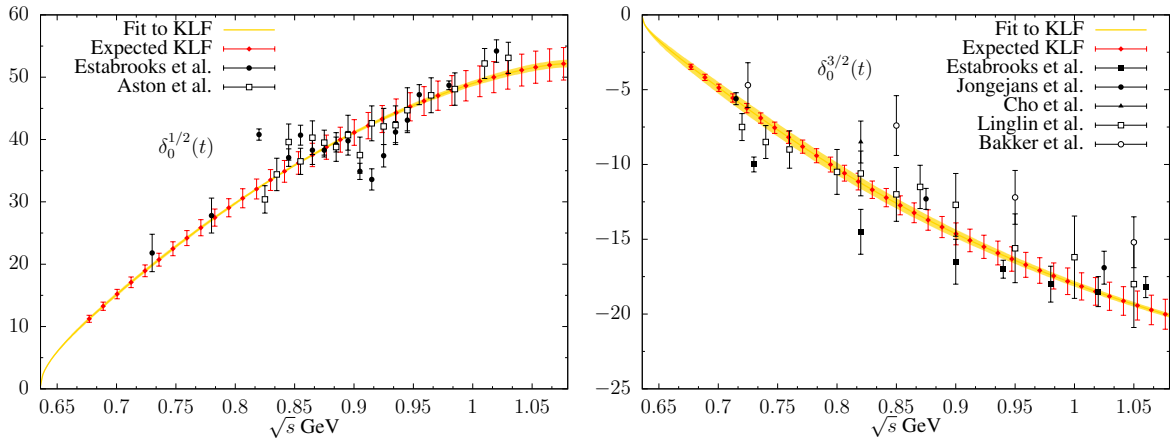

Figure 12: Left: The S-wave phase-shift for isospin $I = 1/2$ and Right: isospin $I = 3/2$ (in degrees) as a function of $\sqrt{s}$, invariant mass of $K\pi$ system (see text for details). The yellow band corresponds to the uncertainty of the fit to the world data without KLF data, whereas the red diamonds are KLF expected measurements with statistical and experimental systematic uncertainties added in quadrature. The projected KLF data correspond to 100 days of running.

In Figure 12, we present S-wave phase-shift for an isospin $I = 1/2$ and $I = 3/2$, which includes all world data on production experiments. The yellow band corresponds to the uncertainties of the fit to previous data. The red points with error bars are projected KLF data for 100 days of running with statistical and experimental systematic uncertainties added in quadrature.

There are many *models* describing the $\kappa/K_0^*(700)$ and its associated pole (see the PDG2018 [1] for an exhaustive compilation). For illustration we show some representative results in Fig. 13. Note that many of them still use BW parameterizations, which unfortunately are not applicable in this case because they violate chiral symmetry and do not have the left and circular cuts that are numerically relevant for precise determinations of the $\kappa/K_0^*(700)$ pole.

The other analyses we list in Table 2 are: a model of a T-matrix pole [82] and more sophisticated models including some implementation of chiral symmetry [83, 84], but still with some model dependence that is not included in their uncertainties. We also show a dispersive evaluation [71], where the difficult left and circular cut contributions have been approximated with some assumptions (like a cut-off), but with very conservative systematic uncertainties. In addition, we show two extractions of the pole, one exploiting the analyticity in the whole complex plane by means of a conformal expansion [79] and another one using Padé approximants to extract the pole parameters from local information of the amplitude near the pole without assuming a specific parameterization [85]. Both of them use as input a fit to data constrained with Forward Dispersion Relations and their uncertainties include an estimate of systematic effects. Other determinations in the literature, not shown here, are usually based on models and often quote uncertainties that do not include systematic effects.

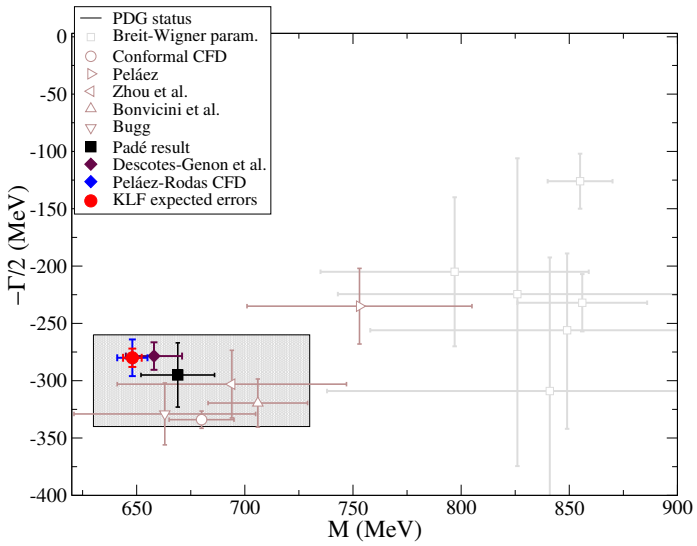

Figure 13: Present situation of the determinations of the $\kappa/K_0^*(700)$ pole. The figure is from Refs. [23, 80, 81] but we have added as a red point with uncertainties, the simulation of the pole position that would be obtained by means of a Roy-Steiner analysis by using simulated data from KLF experiment after 100 days of run, note that the blue error bars are for parameters obtained without KLF data and the tiny red error bars within the blue ones are obtained with KLF data. These calculations also include estimates of systematic effects. Note that the other points are either predictions [11] or illustrative models that may have additional systematic uncertainties due to their model dependence, like BW determinations. Shadowed rectangle stands for PDG2018 uncertainties.

Finally, as already commented, the most rigorous determination of the $\kappa/K_0^*(700)$ pole with a realistic estimate of both statistical and systematic uncertainties, can be made by means of Roy-Steiner Dispersion Relations. There is actually such an estimate of the pole [11], although it does not use data on the scalar wave below 1 GeV. Actually, the scalar partial waves in that region are obtained as solutions of the Roy-Steiner equations with input from other waves and higher energies. In this sense, the κ pole and the whole low-energy region in Ref. [11] are a prediction, not a determination from data.

Thus, in order to estimate the effect of the proposed KLF experiment, we have recalculated the pole obtained by using a Roy-Steiner analysis either using all the existing data [23, 80, 81] or with the LASS data rescaled to the expected accuracy of the KLF experiment. In the first case, without KLF, Peláez *et al.* [80, 81] finds $M_\kappa \simeq (648 \pm 7)$ MeV and $\Gamma_\kappa = (580 \pm 32)$ MeV, whereas by using the expected KLF data the uncertainties are divided by slightly more than a factor of two for the mass, so that we find: $M_\kappa \simeq (648 \pm 4)$ MeV; and by more than a factor of three for the width, finding: $\Gamma_\kappa = (580 \pm 16)$ MeV. With this assumed precision for the KLF measurement, a significant improvement on the $\kappa/K_0^*(700)$ search can be performed, especially by improving the elastic region of the $K\pi$ invariant mass. Fig. 13 shows as pole positions in the complex plane, the different determinations of the κ mass and width, that we have just described, including the determination with the expected amplitude and phase-space that will be produced by KLF. The expected result for the kappa pole is $\sqrt{s_\kappa} \equiv M - i\Gamma/2$ = (648±4 - i 280±8) MeV (the error coming from πK scattering is less than 1 MeV, the rest comes basically from the high energy Regge input and the crossed channel $\pi\pi \to K\bar{K}$ input to the dispersive integrals).

To summarize: The KLF experiment will provide the first measurement of the $K\pi$ scattering pro-

cess in more than 30 years, utilizing modern experimental techniques which will provide unprecedented statistical precision and access to much lower $K\pi$ masses than previous measurements. Of particular interest is the expected impact on the $I = 1/2$ channel where it will help to lower the tension between phenomenological dispersive determinations of scattering lengths from data versus those from Chiral Perturbation Theory and lattice QCD. Finally, it will significantly reduce the uncertainty in the mass and width determination of the controversial κ or $K_0^*(700)$.

4.3 Neutron-induced Reactions

Since all charged particles from the KPT will be wiped out from the beam by the sweeping magnet and the photon flux is also expected to be low, the only background which requires special considerations is due to neutron-induced reactions. The neutron flux on the cryogenic target is expected to be moderate, $6.6 \times 10^5\ n/sec$ [86], and moreover the neutron flux drops exponentially with energy (see Fig. 23 (left) for details), so generally the high-energy neutron flux is tiny. We have studied possible neutron-induced background thoroughly and found all neutron-related reaction to contribute at the level of 10^{-3} or lower. The highest (10^{-3} level) neutron background contribution is expected for inclusive reactions, while for exclusive reactions the neutron induced reactions can be completely eliminated due to their very different event topology and kinematics.

There are several neutron energy ranges which requires separate treatments:
1) $E_n > 1.6$ GeV, strangeness production threshold ($np \to K^+n\Lambda$ reaction is allowed), $\sim 1\%$ of the neutron flux;
2) $1.6 > E_n > 0.3$ GeV, single pion production threshold ($np \to \pi^+nn$ reaction is allowed; $np \to pn$ reaction has sufficient energy to be measured), $\sim 5\%$ of the neutron flux;
3) $E_n < 0.3\ GeV$, $\sim 94\%$ of the neutron flux - do not contribute at all.

We have identified three major sources of physical background: $np \to K^+n\Lambda$ (the next most probable reaction with strangeness, $np \to K^+n\Sigma$, has an order of magnitude smaller cross-section) and $np \to \pi^+nn$ with π^+ misidentifed as K^+.

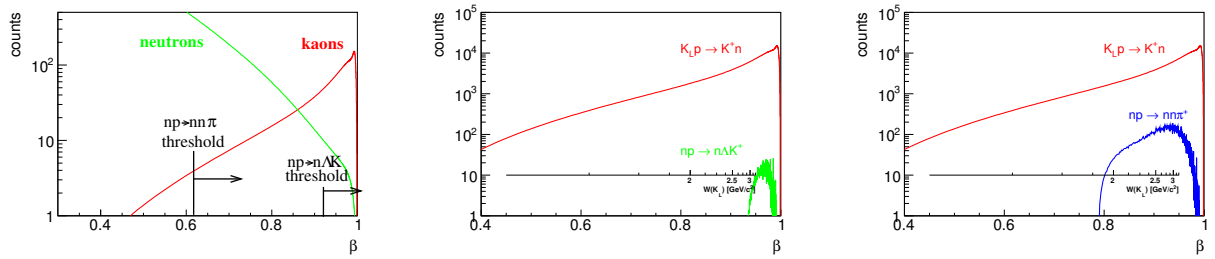

Figure 14: Left: Neutron and K_L fluxes as a function of velocity β. Middle: K^+ flux as a function of projectile velocity β for neutron-induced (green) and kaon-induced (red) reactions. Right: Same but for $np \to \pi^+nn$ (blue) and $K_Lp \to K^+n$ (red) reactions. Pion misidentification efficiency for the neutron-induced reaction is extracted from the full MC Geant simulation. Secondary axis showed corresponding W value under assumption of $K_Lp \to K^+n$ reaction.

As mentioned above, neutron flux drops exponentially with energy and generally the high-energy neutron flux is small, but nonvanishing. If neutrons and K_Ls have the same velocity, they cannot be separated by time-of-flight. However if K_L and neutrons have the same velocities they have very different energies, hence very different reaction kinematics. Moreover neutron-induced reactions always have extra particle in a final state compare to K_L-induced reactions (2-body final state for $K_Lp \to K^+n/K_Lp \to K^+\Xi$ vs 3-body $np \to K^+\Lambda n$).

Neutron-induced reactions have high cross sections, which is why one needs to consider them as a possible source of background. In Fig. 14 (left), one can see a comparison of kaon and neutron fluxes, similar to Fig. 23 (left) but in terms of β. Particles with the same β cannot be separated by time-of-flight. At $\beta = 0.86$ neutron and kaon fluxes become equal. This velocity corresponds to a neutron momentum of p_n = 1.6 GeV/c and kaon momentum of p_K = 0.8 GeV/c.

To evaluate the amount of background, we need to fold this flux with production cross section and reconstruction efficiency. The cross-section for the $np \to K^+\Lambda n$ reaction can be extracted using data from Ref. [87] and isospin factors. The cross-section for another background reaction, $np \to \pi^+nn$, can be taken from Ref. [88] ($np \to \pi^-pp$) using isospin coefficients as well. The result of folding of these cross-sections with the flux and detector reconstruction efficiency can be seen on Fig. 14 (middle and right).

As one can see, both reactions contribute at a very low level, Fig. 14, and in a very narrow range of energies. One can further suppress this type of backgrounds by exclusivity cuts. Altogether one can easily suppress these types of background below 10^{-4}.

One can make a more general statement: due to their high production threshold the $np \to K^+X$ reactions cannot serve as a background channel to any of kaon-induced hyperon production channels, neither for the s-channel Σ-production nor for the associated Ξ^*-production. The only inclusive reaction planned to be measured at KLF so far is $K_Lp \to K^+n$. Here the $np \to \pi^+nn$ reaction can play a role of a possible background at a sub-percent level. However it does not contribute to any higher multiplicity reactions due to exclusivity conditions. Indeed, to mimic the simplest $K_Lp \to \pi^+\Lambda$ reaction by the neutron induced process, one should have:

(i) $np \to \pi^+nn$ with pion rescattering within detector volume to adjust pion momentum-angle relation of a 3-body process to two-body $\Lambda\pi$

(ii) have secondary rescattering of ejected neutron on supporting structures with the reaction $nn \to \pi^-pn$ to produce $p\pi^-$ pair

(iii) have both p and π^- rescatter to tune their angle-energy to mimic Λ.

A combination of such low probability events make neutron induced background, absolutely impossible for the reactions we have considered so far in our proposal.

Neutron induced events can become a sizable background only to a very rare kaon-induced reactions with tiny cross-sections where the final state would be reconstructed inclusively/semi-exclusively. Neither of such reactions are considered in this proposal so far or planned to be investigated at the first stage of analysis.

4.3.1 Useful Neutron-induced Reactions:

Nucleon-nucleon interactions is a central piece of nuclear physics studies since the discovery of nuclei. Nuclear forces can be decomposed into an isospin $I = 1$ part accessible by proton-proton scattering which has been studied with reasonable accuracy in a wide range of energies, and an isospin $I = 0$ part which requires a neutron beam or target. In Fig. 15 (left), one can see the currently available data for the $I = 0$ channel. In a view of the upcoming Electron-Ion Collider (EIC) [89, 90] which enables a strong program in nucleon short-range correlations (SRC) [91, 92], where np-correlations comprise 90% of all events, our pure knowledge of nuclear potential and np-elastic scattering at energies as low as 1 GeV is truly deplorable.

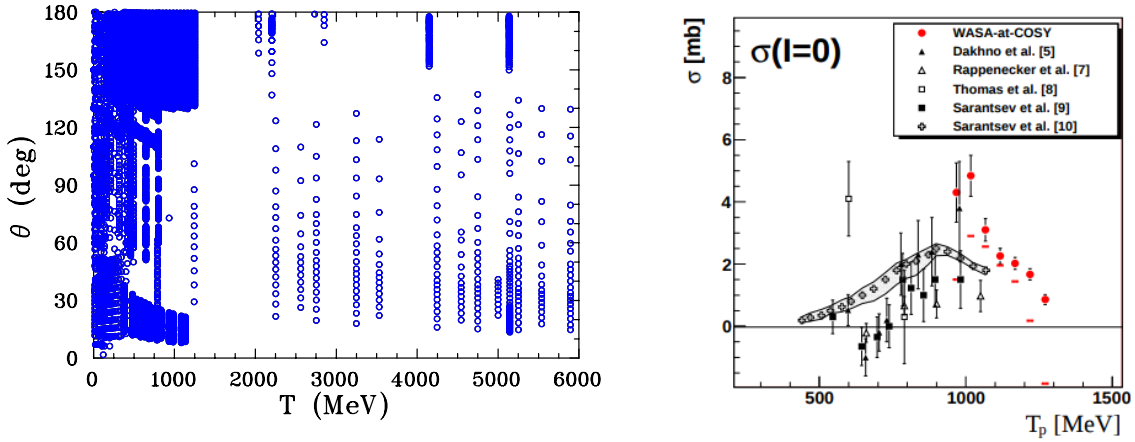

Figure 15: Left: Differential cross section data available for $np \to np$ reactions as a function of neutron kinetic energy [93]. Right: Total cross section in dependence of incident nucleon energy for the isoscalar single pion production from Ref. [88].

Neutrons are massive particles with lower velocities compare to K_L's, so excellent time-of-flight resolution available at KLF would allow for even more precise momentum measurements for the neutron beams. A very high np-elastic cross section and a good detection efficiency of a GlueX setup for a single proton track events, make this channel a golden by-product of a KLF program.

Keeping in mind that even the reaction with the highest cross-section, np-elastic scattering, is so poorly known one can immediately guess that all other less abundant reactions have fewer measurements. The next best examples here is a single pion production in an isoscaler channel. As can be seen from Fig. 15 (right), the data exist only for very narrow range of energies and agreement between various data sets is extremely pure. This is particularly unfortunate since the HADES Collaboration recently showed particularly clean non-interfering N^*'s and Δ^*'s excitations in high energy NN-collisions [94]. This topic might be a second strong by-product of a KLF program.

To summarize: One can expect more than 100M neutron induced single pion production events to be detected within 100 days of KLF beamtime, and an even larger number for np-elastic scattering events. Several other reactions with two- and three-pion production, and η-production, are also feasible.

5 Proposed KL Beam Facility

The GlueX spectrometer in Hall D at Jefferson Lab, shown in Figure 16, is a powerful tool employed by the GlueX Collaboration to investigate a wide range of topics in meson and baryon spectroscopy and structure, particularly the search for mesons with excited gluonic content, using the recently upgraded 12 GeV electron beam of CEBAF accelerator. The spectrometer is carefully designed [95] to measure the complete electromagnetic response for nucleons and nuclei across the kinematic plane: elastic, resonance, quasi-elastic, and deep inelastic reactions with almost 4π acceptance for all final state particles.

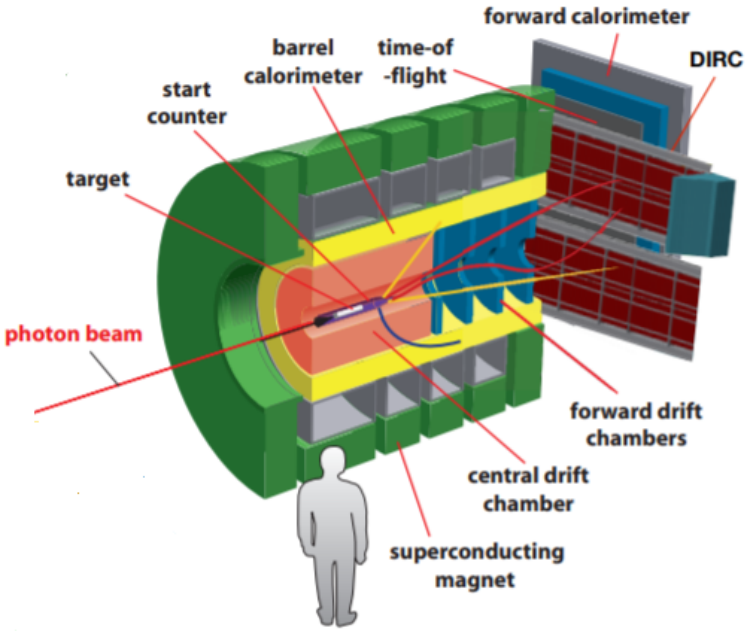

Figure 16: The GlueX spectrometer.

5.1 Beamline Delivery for Secondary K_L Beam

The proposed secondary K_L experiment requires time-of-flight measurements, which in turn requires substantially lower bunch repetition rates in CEBAF than the nominal 249.5 MHz or 499 MHz. Gun laser hardware lends itself to powers of two reductions in repetition rates, so this proposal includes beam delivery at either the 32nd (15.59 MHz) or 64th (7.80 MHz) harmonic of the nominal 499 MHz.

An average dump power limit of 30 kW to 60 kW for 12 GeV electrons in the CPS translates to average beam currents of 2.5 μA to 5.0 μA. Combining these beam requirements leads to individual bunch charges shown in Table 3.

Operations with 0.16 pC to 0.32 pC bunch charge has been demonstrated but shown to be challeng-

Current (μA)	Repetition Rate (MHz)	Harmonic of 499 MHz	Bunch Charge (pC)	Equivalent 499 MHz Current (μA)
2.5	15.59	32nd	0.16	80
2.5	7.80	64th	0.32	160
5.0	15.59	32nd	0.32	160
5.0	7.80	64th	0.64	320

Table 3: CEBAF injector bunch currents and repetition rates for Secondary K_L experiment.

ing in the 12 GeV era. Injector setup time of up to a week is required to limit bunch tails that cause beam trips and background, and intervention on the order of every few days is currently required to maintain a reasonable accelerator availability. The G0 experiment [96] ran 1.6 pC/bunch, but only at 3 GeV with the 6 GeV machine and in a dedicated configuration that required substantial interception to trim beam tails [97].

These concerns may be mitigated somewhat by completion of the injector upgrade program, including operations of a 200 keV gun, in the 2021 timeframe. The HV gun was installed in summer 2018, and some initial tests with modest gun voltages occurred in FY19, but the full injector upgrade for potential high bunch charge availability will not be available for study until FY21 [98].

Low frequency, high power amplifier use has been attempted at CEBAF in recent years, resulting in substantial damage and high amplifier failure rates even near 30 MHz because of high peak power required as repetition rate is lowered. The low bunch repetition rate with high bunch charge therefore also requires considerable investment.

With the existing and planned gun confirmation, laser development is required to achieve any of the planned bunch repetition rates. This requires construction of a pulse picker that would pass a sub-harmonic of the 249.5 MHz system (for example, 15.6 MHz) to avoid major impact to the existing 249.5/499 MHz laser systems. Amplification is then required before doubling to the proper wavelength to achieve useful power, even for 10 μA beam. Additional power amplification is necessary for the higher beam currents required here.

To build up a beamline delivery system for the secondary K_L beam requires the pulse picking system and the laser amplifier. The lead time on amplifiers can be long so ideally a year of advance funding would be necessary to design, build and demonstrate the system performance [97].

The G0 experiment [96] used a commercial Ti:Al_2SO_3 laser with a very long ($\sim$5 m) optical cavity that was very difficult to keep on and locked to the accelerator RF. This solution is not practical for the 12 GeV era.

5.1.1 Raster for K_L Beam

KLF requires a large electron beam incident on the CPS to minimize power density, and convergence of a projected photon beam on the target and collimator $\approx$65 m downstream of the CPS.

One option to address these requirements is installation of a beam raster, similar to rasters used in other CEBAF high-current halls. However, a raster intrinsically enlarges the beam divergence to achieve a larger beam size. This is inconsistent with the convergence requirements of the pro-

jected photon beam. We have instead considered adjustments to the existing Hall D final focus optics to maximize the beam size at the CPS while maintaining required projected photon beam convergence.

Reference [99] evaluates the existing Hall D final focus optics and quadrupole apertures for three conditions: 95% full width horizontal beam sizes of 1.0 cm, 1.4 cm, and 1.7 cm. A 95% full width vertical beam size of $\mathcal{O}(1$ cm) is expected at the CPS; it cannot be smaller than this to maintain reasonable projected photon beam convergence.

The 95% full width horizontal 1.0 cm beam size case is quite similar to existing optics for GlueX. Under these conditions, KLF should expect similar beam size stability to that observed during GlueX-II operations.

The 1.4 cm case requires more aggressive focusing that results in a maximum beam size in the existing final focus quadrupoles that is ≈65% of the existing aperture. At these beam sizes chromatic and nonlinear effects start contributing substantially to beam quality. It may be feasible to run KLF with this beam size at the CPS face, but beam size stability and sensitivity of tune may be problematic.

The 1.7 cm case requires substantially more aggressive focusing. The maximum beam size in the existing final focus quadrupoles in this condition would be at least 75% of the existing aperture. Here chromatic conditions and sensitivity of tune to energy fluctuations starts to dominate, and there is very little room for orbit and beam size variation.

For 95% full width horizontal beam sizes on the CPS dump face above 1.5 cm, new final focus quadrupoles would likely be required with larger apertures of 20–30 mm radius compared to the existing radii of 16 mm.

5.2 K_L Beam Overview

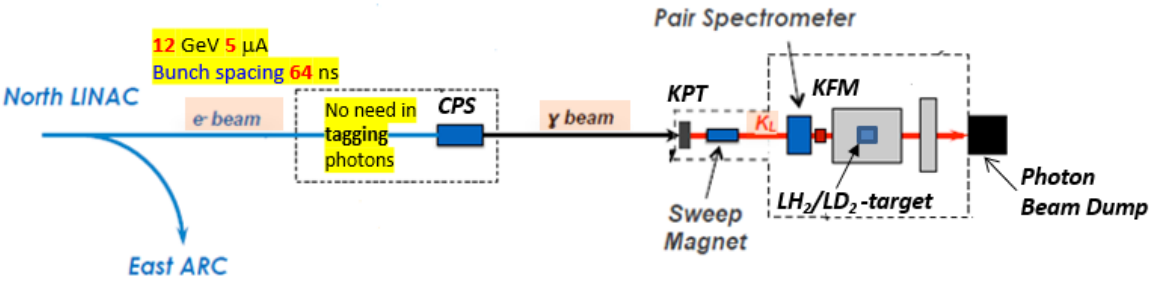

Figure 17: Schematic view of Hall D beam line with the production chain $e \to \gamma \to K_L$. The main components are the CPS, KPT, sweep magnet, and KFM (see text for details). We do not need in pair spectrometer [112]. Beam goes from left to right.

We propose to create a secondary beam of neutral kaons at Hall D at Jefferson Lab to be used with the GlueX experimental setup for strange hadron spectroscopy. The superior CEBAF electron beam will enable a flux on the order of $1 \times 10^4 K_L/sec$, which exceeds the kaon flux previously

attained at SLAC [34] by three orders of magnitude. Using a deuterium target in addition to the standard liquid hydrogen target will provide the first measurements ever with neutral kaons interacting with neutrons. The ability of the GlueX spectrometer to measure reaction fragments over wide ranges in polar θ and azimuthal ϕ angles with good coverage for both charged and neutral particles (see, for instance, Refs. [6, 100, 101]), together with the K_L energy information from the K_L time-of-flight, provides an ideal environment for these measurements.

A schematic view of the Hall D beam line showing the production chain $e \rightarrow \gamma \rightarrow K_L$ is given in Fig. 17. Tables 4 and 5 summarize beam properties and dimensions of targets, respectively.

Property	Value
Electron beam current (μA)	5
Electron flux at CPS (s^{-1})	3.1×10^{13}
Photon flux at Be-target $E_\gamma > 1500$ MeV (s^{-1})	4.7×10^{12}
K_L beam flux at cryogenic target (s^{-1})	1×10^4
K_L beam σ_p/p @ 1 GeV/c (%)	$\sim$1.5
K_L beam σ_p/p @ 2 GeV/c (%)	$\sim$5
K_L beam nonuniformity (%)	< 2
K_L beam divergence ($^\circ$)	< 0.15
$K^0/\overline{K^0}$ ratio at Be-target	2:1
Background neutron flux at cryogenic target (s^{-1})	6.6×10^5
Background γ flux at cryogenic target (s^{-1}), $E_\gamma > 100$ MeV	6.5×10^5

Table 4: Expected electron/photon/kaon beam conditions at the K_L experiment.

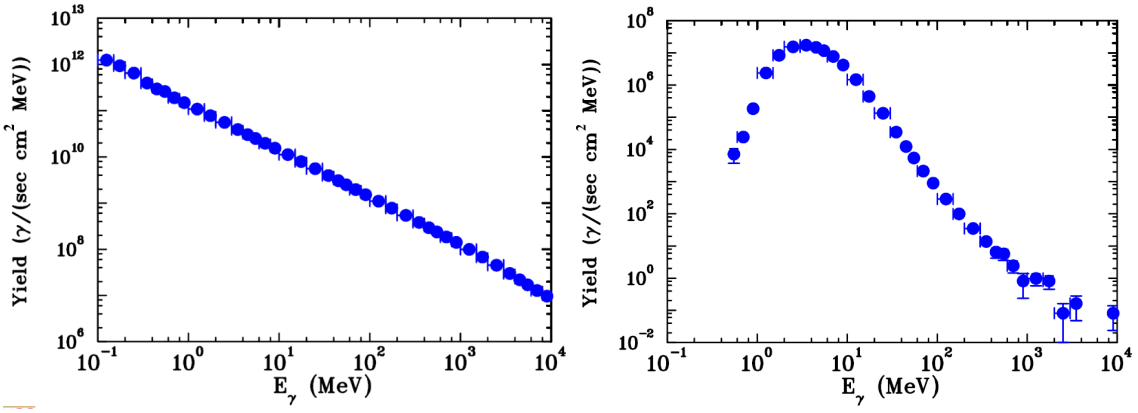

Figure 18: Energy spectrum of bremsstrahlung photons on the face of the Be-target (left) and on the face of the cryogenic target (right). Calculations were performed using the MCNP radiation transport code [103].

At the first stage, 12-GeV electrons (3.1×10^{13} e/sec) will scatter in the radiator inside the CPS [102], generating an intense beam of untagged bremsstrahlung photons with intensity (4.7×10^{12} γ/sec, for E_γ >1.5 GeV) impinging on the face of the Be-target. The main source of K_L production from the target is the ϕ-meson decay, whose photoproduction threshold is E_γ $\sim$1.58 GeV.

Property	Value
Copper radiator in CPS (%R.L.)	10
∅Be-target (m)	0.06
Be-target length (m)	0.40
∅LH_2/LD_2 cryogenic target (m)	0.06
LH_2/LD_2 cryogenic target length (m)	0.40
Photon beamline length (m)	67
Kaon beamline length (m)	24

Table 5: Expected targets properties at the K_L experiment.

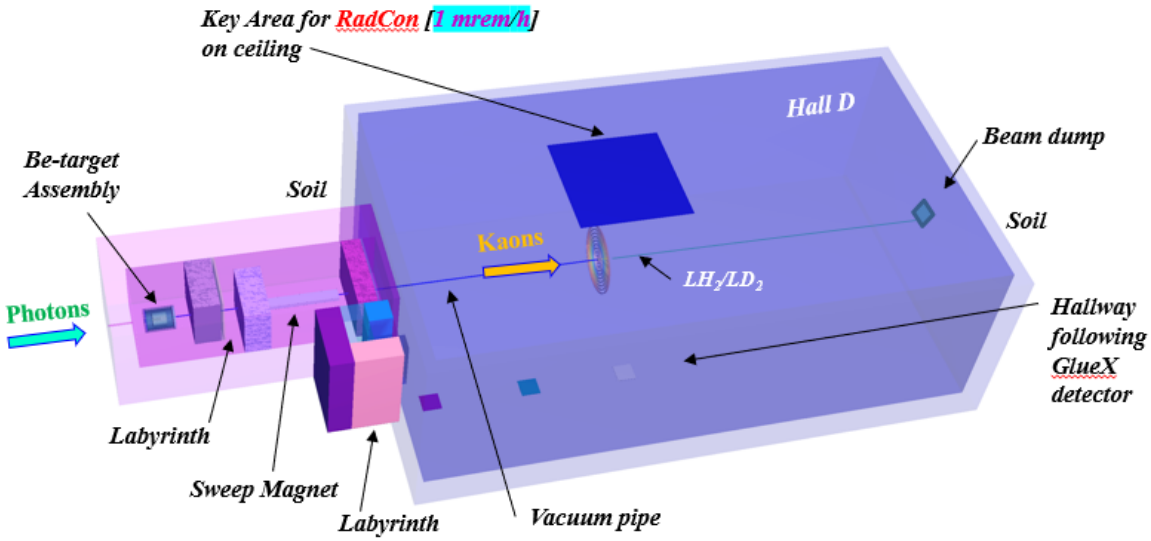

Figure 19: Schematic view of Hall D setting for the MCNP radiation transport code [103] calculations. The model is presented as semi-transparent for demonstration purposes. Beam goes from left to right.

The full energy spectrum of photons on the face of the Be-target is shown in Fig. 18 (left).

The energy spectrum of secondary photons on the face of the cryogenic target is shown on Fig. 18 (right). The flux is not sufficient to provide any significant background in the case of γp or γd interactions in the cryogenic target.

The CPS contains a copper radiator (10% X_0) that is capable of handling the power deposited in it by the 12-GeV, 60 kW electron beam, which will be fully absorbed inside the CPS dump. The CPS will be located downstream of the Hall-D tagger magnet. The Hall D tagger magnet and detectors will not be used.

At the second stage, the bremsstrahlung photons will hit the Be target (KPT) [86] located at the beginning of the collimator alcove (Fig. 19) in 67 m from CPS, and produce neutral kaons (1×10^4 K_L/sec), along with neutrons (6.6×10^5 n/sec), photons, and charged particles.

The vacuum beam pipe has a ∅0.07 m and prevents neutron rescattering in air. Finally, K_L mesons

will reach the LH_2/LD_2 cryogenic target located inside the GlueX spectrometer. The distance between the primary Be and cryogenic targets is 24 m.

5.3 Compact Photon Source for K_L

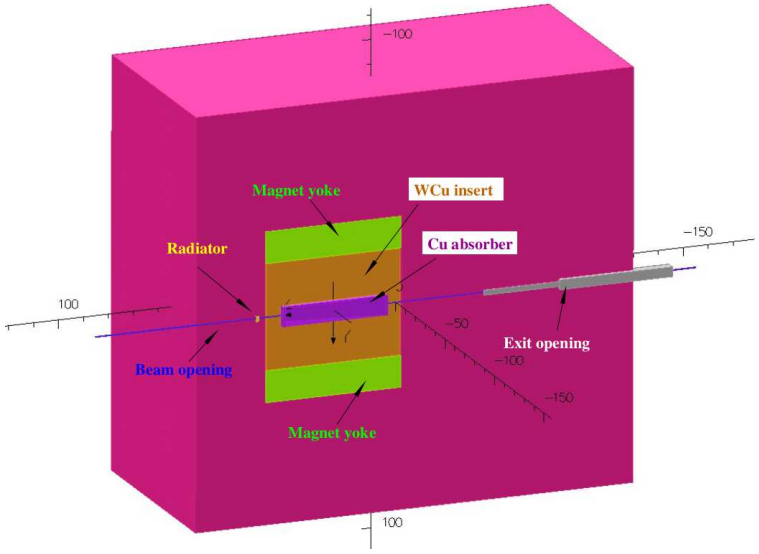

Figure 20: A cut-out diagram view of the CPS. Deflected electrons strike a copper absorber, surrounded by a W-Cu insert inside the magnet yoke. The outer rectangular region in this view is the shielding. In Hall D, this will consist primarily of lead. From Ref. [102].

An intense photon beam is needed to produce the flux of K_L mesons required for this experiment, with a photon flux several orders of magnitude larger than that used for current GlueX operations. At this very high flux, the current GlueX beam line would require substantial additional shielding and other modifications to protect against radiation damage. Instead, we propose to generate the photon beam using a device based on the novel Compact Photon Source (CPS), currently being developed for use in Hall C, which combines the photon beam radiator and dump in one properly shielded enclosure. The conceptual design of the CPS is well advanced and has been published earlier this year [102]. To briefly summarize the CPS design (illustrated in Fig. 20): immediately downstream of a 10% R.L. copper radiator lies the electron dump, which consists of a copper absorber, a tungsten/copper insert to provide additional shielding, and a radiation-hard magnet. The magnet bends the electrons that have passed the radiator into the absorber, in which all of their energy is dissapated, and only the photons continue through to pass through the collimated aperture (see Fig. 21). This dump is surrounded by additional shielding, primarily lead, to reduce both the prompt photon radiation and the activation dose. Outside of this main mass of shielding lies a 10 cm layer of borated polyethylene and an additional 5 cm of lead, the combination of which were found to dramatically decrease the radiation dose due to neutrons.

This design is well matched to the requirements of the KLF photon beam, with a only a few modifications required, and can easily fit in the area of the Hall D Tagger Hall, downstream of the current tagging spectrometer. The KLF electron beam power is expected to be twice that delivered

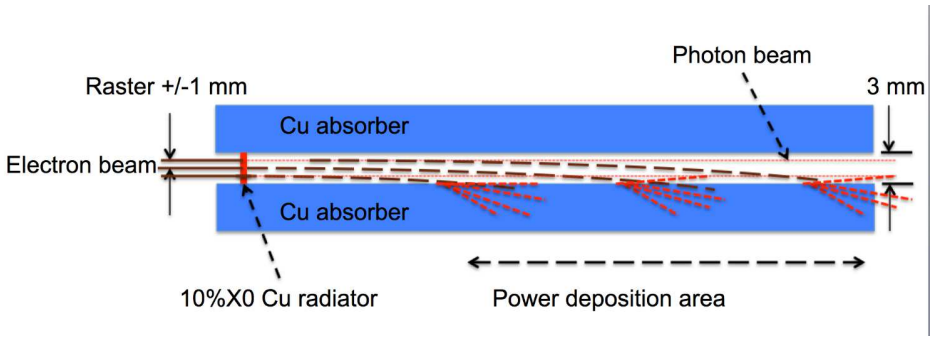

Figure 21: The scheme of beam deflection in the magnetic field to the absorber/dump. From Ref. [102]. In the Hall D design, the opening will be 1.5 cm vertically and horizontally.

to the Hall C CPS (60 kW compared to 30 kW), so the size of the absorber and the magnet must be increased to accommodate the extra beam power. Additionally, while the polarized target is just downstream of the CPS in the Hall C configuration, for KLF the photon beam must travel 67 m between the tagger and main experimental halls and kept aimed at the KPT. As described in the previous section, an electron beam of width ~ 1.5 cm in both the horizontal and vertical directions is possible with the current Hall D beam line, with an acceptable focus on the KPT. Finally, the design should be kept roughly within the weight limit of 150 t.

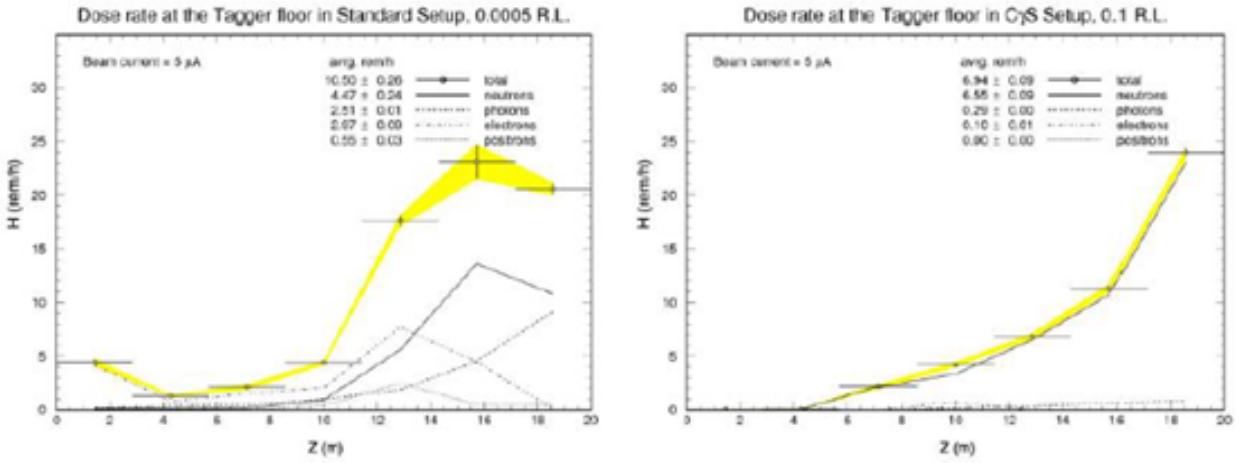

Figure 22: A comparison of dose rate estimates in the Tagger alcove in the two conditions. Left: Nominal Hall D operation with a thin amorphous radiator of 0.05% R.L.. Right: Radiator at 10% R.L., used as part of the CPS setup. This Figure is taken from Ref. [104].

Simulations are being performed in order to optimize the power deposition and shielding distribution. One major difference in the requirements for the different CPS configurations is in the difference in radiation sensitivity in the regions downstream and upstream of the incoming electron beam. The Hall C CPS is situated just over a meter from a polarized target, and therefore has strict constraints on the radiation levels downstream from the CPS. The Hall D CPS has few

beamline elements downstream before the end of the Tagger Hall and continuation of the beamline underground, and so has looser constraints on radiation levels compared to the upstream part of the Hall, where the tagged photon spectrometer, electronics racks, and other equipment is placed.

Additionally, we show in Fig. 22 a comparison of radiation dose rates in the Tagger Hall between a thin amorphous radiator of 0.005% R.L. in the standard GlueX beamline configuration (compare to the nominal amorphous radiator of 0.034% R.L.) and an early configuration of the CPS. Similar levels are seen for both configurations, showing more evidence that the CPS will deliver a level of radiation not higher than what is seen in standard GlueX running.

To summarize: The KLF CPS concept provides the intense photon beam required to produce the K_L beam, and is being developed in collaboration with the CPS Collaboration based on their published conceptual design. The design is being optimized in parallel with calculations for the rest of the beamline, though initial studies show that minor modifications to the baseline design will provide sufficient shielding and heat dissipation for the KLF experiment. The use of lead shielding as opposed to the tungsten powder/lead mix for the baseline CPS design will save on the cost.

5.4 K_L Be Production Target

Calculations for the Kaon production Target (KPT) were performed for different shielding configurations to minimize the neutron and gamma prompt radiation dose rate and cost of the KPT [86].

The prompt background radiation condition is one of the most important parameters of the K_L beam for the JLab KL Facility. Beryllium targets were used for K_L production at SLAC [105] and NINA [106]. We have performed comprehensive simulations of the neutron, gamma, and muon backgrounds and their possible influence on the proposed measurement. The most important and damaging background comes from neutrons. To estimate the neutron and gamma flux in the beam and the neutron prompt radiation dose rate in the experimental hall from scattered neutrons and gammas, we used the MCNP6 N-Particle (MCNP) radiation transport code [103].

For the MCNP calculations (in terms of flux [part/s/cm^2/MeV] or biological dose rate [mrem/h]), many tallies (spots were we calculated a flux or dose rate) were placed along the beam at the experimental hall and alcoves for neutron and gamma fluence estimation. Fluence-to-Effective Dose conversion factors from ICRP 116 [107] were implemented to convert neutron and gamma fluence to effective dose rate. We used the material composition data for the radiation transport modeling from Ref. [108].

The realism of MCNP simulations is based on the advanced nuclear cross section libraries created and maintained by several DOE National Laboratories. The physical models implemented in the MCNP6 code take into account bremsstrahlung photon production, photonuclear reactions, neutron and photons multiple scattering processes. The experimental hall, collimator alcove, and photon beam resulting from the copper radiator within CPS were modeled using the specifications from the layout presented in Figure 19, shown as a 3D graphic model of the experimental setup.

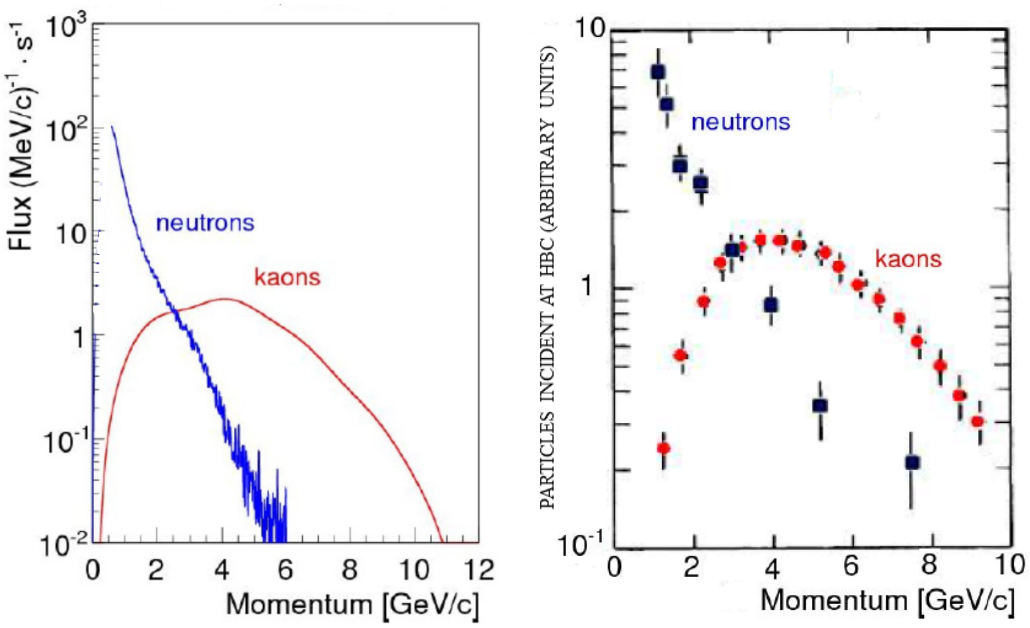

Figure 23: The K_L and neutron momentum spectra on the cryogenic target. Left: Rate of K_L (red) and neutrons (blue) on the LH_2/LD_2 cryogenic target of Hall D as a function of their generated momenta, with a total rate of 1×10^4 K_L/sec and 6.6×10^5 n/sec, respectively. Kaon calculations were performed using Pythia generator [110] while neutron calculations were performed using the MCNP transport code [103]. Right: Experimental data from SLAC measurements using a 16 GeV/c electron beam were taken from Ref. [113] (Figure 3).

5.4.1 Kaon and Neutron Flux:

Neutral kaon production was simulated for a photon bremsstrahlung beam produced by the 12 GeV electron beam in the Hall D CPS. The main mechanism of K_L production in our energy range is via ϕ-meson photoproduction, which yields the same number of K^0 and $\bar{K^0}$. Calculations of the K_L flux [109] are performed using the Pythia MC generator [110], while the neutron flux calculations were performed using the MCNP radiation transport code [103].

The MCNP model simulates a 12 GeV 5 μA electron beam hitting the copper radiator inside of the CPS. Electron transport was traced in the copper radiator, vacuum beam pipe for bremsstrahlung photons, and Be-target. Neutrons and photons were traced in all components of the MCNP model. The areas outside the concrete walls of the collimator alcove and bremsstrahlung photon beam pipe was excluded from consideration to facilitate the calculations. Additionally, we ignore Pair Spectrometer (PS) [112] and KFM magnets but took into account five iron-blocks around beam pipe in front of the GlueX spectrometer.

Figure 23 demonstrates that our simulations for the KLF kaon and neutron flux (Fig. 23 (left)) are in a reasonable agreement with the K_L spectrum measured by SLAC at 16 GeV [113] (Fig. 23 (right)).

5.4.2 Target and Plug Materials:

The K_L beam will be produced with forward emission kinematics due to the interaction of the photon beam with a Be-target. Beryllium is used because lighter elements have a higher photo-

production yield with a lower absorption of kaons, as pointed out in previous SLAC studies [113]. These studies showed that beryllium is the optimal material for neutral kaon photoproduction. Another common target material is carbon, which is easier to handle than beryllium, however the simulations we performed show that a beryllium target performs significantly better than a similar target made of carbon. The Pythia [110] simulations showed that the kaon yield from beryllium is higher than that from carbon at the same radiation length. The ratio of beryllium to carbon gives a factor of 1.51 for kaon yield. At the same time, MCNP simulations demonstrated that the beryllium target reduces the neutron yield more effectively than carbon. The ratio of generated particles from beryllium to the carbon appears to be about ~ 1.45 for neutrons.

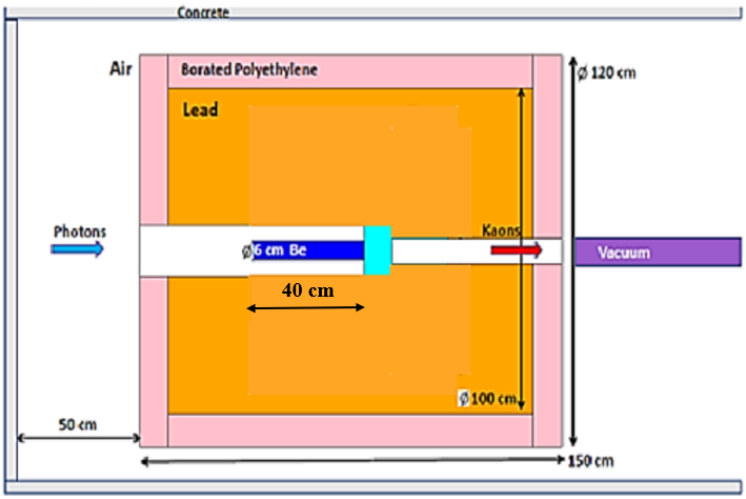

Figure 24: Schematic view of the Be-target (K_L production target) assembly. Concrete, borated polyethylene, lead, tungsten, beryllium, vacuum beam pipe, and air shown by grey, pink, brown, light blue, blue, violet, and white color, respectively. Beam goes from left to right.

A tungsten beam plug of a 10 cm thickness (30 X_0) and 16 cm diameter is attached to the beryllium target (Fig. 24) to clean up the beam and absorb induced radiation. In the same SLAC studies referenced above, it was shown that tungsten is the optimal material for the plug and that tungsten has a lower absorption factor for kaons as compared to copper. Our Pythia simulations showed that the ratio of tungsten to copper (20%) gives 1.16 (1.36) at kaon momentum 1 GeV/c (0.5 GeV/c). Our MCNP simulations additionally demonstrated that the tungsten plug reduces the yield of neutrons and gamma compared to a plug of lead or copper of the same length. The production ratio for lead (copper) to tungsten is 2.25 (9.29) for neutrons and 8.11 (66.8) for gammas.

It was found that increasing the plug diameter will increase the neutron background. For example, increasing the diameter to 24 cm from 16 cm in diameter yields an increase of neutron production by a factor of 2.8. This effect is due to re-scattered neutrons in the plug. There is no effect for gammas. It was also found that increasing the plug length will decrease the neutron background. For example, increasing the length to 15 cm from 10 cm in length gives a factor of 0.60 in neutron production. For gammas, the effect is more significant. However, we will do not plan to not increase the length to prevent similar losses in K_L yield.

5.4.3 Location of the Be-target Assembly:

To reduce the effect of the neutron and gamma background coming from the beryllium target and tungsten plug into the experimental hall, we place the KPT upstream of the GlueX spectrometer in the collimator alcove (Fig. 19). Additional shielding inside the collimator alcove is added to minimize the neutron and γ background in the experimental hall and to satisfy the JLab RadCon requirement establishing the radiation dose rate limit in the experimental hall (1 mrem/h), roughly based on the requirement to limit the yearly dose accumulation at the CEBAF boundary at 10 mrem. The key area for the dose rate evaluation is the area of $(6 \times 6)\ m^2$ on ceiling of the experimental hall centered above the GlueX detector. The dose rate limit at that location roughly correspond to the expected dose rate at the CEBAF fence at the level of 1 μrem/h, both evaluated, and observed at other locations at CEBAF (vicinity of the high power End Stations of Halls A and C). The vacuum beam pipe (between KPT and cryogenic target) prevents neutrons re-scattering in the air in the experimental hall. Directly downstream of the Be target there will be a sweeping magnet with a field integral of $0.8\ T \cdot m$ to clean up the charged particle component from the beam (including muons).

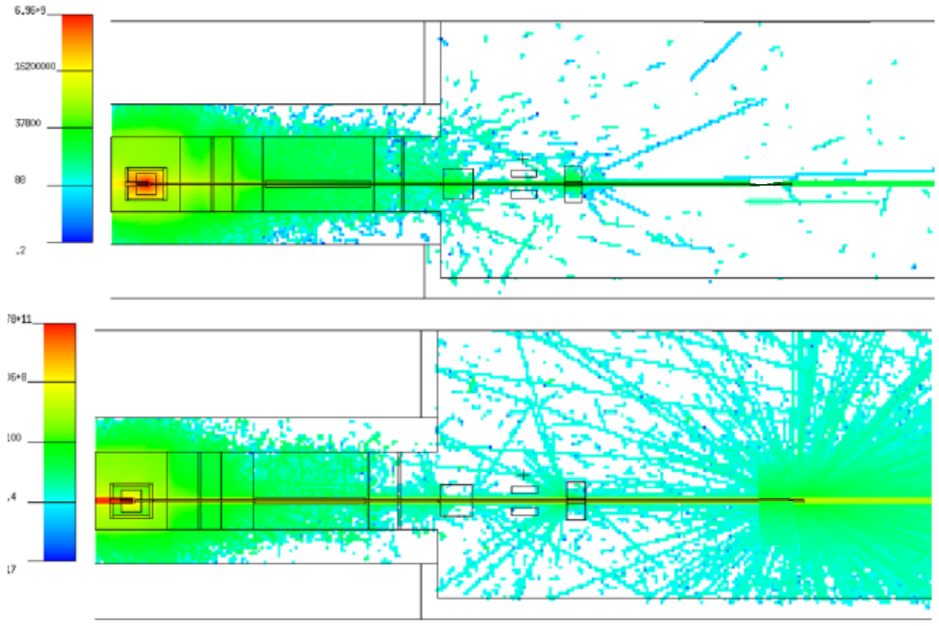

Figure 25: Prompt neutron and gamma yield. Top: (Bottom:) Vertical cross section of the neutron (gamma) flux calculated using the MCNP model. Beam goes from left to right.

5.4.4 Design of the Be Target Assembly:

A schematic view of the Be-target assembly is given in Fig. 24. Changing from the photon to the kaon beam line and vice versa is expected to take about half year or less, and thus should fit well into the breaks of current CEBAF schedule. The collimator alcove has enough space (with 4.52 m width) for Be-target assembly to remain far enough from the beam line (Fig. 19) and to not obstruct GlueX operations in regular photon beam mode. The water cooling is available in experimental hall, and is sufficient to dissipate 6 kW of power delivered by the photon beam to Be-target and W-plug.

The conceptual design of KPT with combination of lead shielding and tungsten plug is shown on Fig 24. The prompt radiation dose rate for neutrons (gammas) in the experimental hall at the key area for RadCon on the ceiling is (0.35±0.17) mrem/h (0.078±0.005 mrem/h). Replacing all tungsten by lead (including plug), one can get (0.61±0.25) mrem/h ((0.527±0.006) mrem/h). Finally, in the case of lead shielding and tungsten plug (Fig. 24), one can get (0.27±0.08) mrem/h ((0.065±0.002) mrem/h). The prompt neutron and gamma yield calculated by MCNP code is demonstrated in Fig. 25.

To summarize: The optimization of the Be-target assembly resulted in the weight of the device 12 t and the estimated cost of $0.134M (note that the final total cost depends on the cost of tungsten).

5.5 K_L Flux Monitor

An accurate determination of the K_L beam flux is necessary to maximize the physics impact of the resulting data [114]. To reach an accuracy of <5 % in the determination of the flux, we plan to build a dedicated flux monitor= which would utilize in-flight decays of the K_L. To account for various possible acceptance effects during K_L beam propagation from the Be-target, we plan to measure the K_L flux upstream of the GlueX detector, utilizing the Hall D Pair Spectrometer [112] as shielding against K_L which have decayed further upstream. The Kaon Flux Monitor (KFM) will measure a small fraction of decayed K_L's, concentrating on the portion decaying within a distance of 2 m downstream of the Pair Spectrometer magnet center (see Fig. 26). The KFM is a combination of solenoid magnetic field spectrometer and a time of flight detectors. The KFM consists of the following major parts: the front cap, forward tracker, backward tracker, endcap, and solenoidal magnet. The KFM can be further equipped with a plastic scintillator barrel, covering inner part of a magnet and a Flux Monitor Start Counter (FMSC), comprising plastic scintillator bars covering the beampipe, from the location of the Pair Spectrometer magnet to the KFM magnet (see Fig. 26). All our MC calculations have been performed for the JLab Hall D beamline geometry.

To be measured by the KFM, both charged particles from the kaon decay need to be incident within the KFM acceptance. Taking into account the different branching ratios, we expect to reconstruct the following number of K_L from various decay channels (see Fig. 27 (left)). One can quantify the expected rate in terms of the achievable statistical error within a one day measurement (see Fig. 27 (right)). For the kaon beam momenta range appropriate for the hyperon program a 1 % statistical error of the K_L flux determination is achievable in less than a day.

An accurate flux monitoring requires determination of the kaon flux as both a function of transversal position within the beampipe and kaon energy. The most inner 3 cm of the transverse beam profile at the position of the KFM would correspond to a 6 cm profile at the cryogenic target. A ∅7 cm beam pipe allows sufficient margins and the clean definition of fiducial regions of the transverse beam profile at the KFM position. All in all we expect to measure 1×10^4 K_L/sec in the KFM.

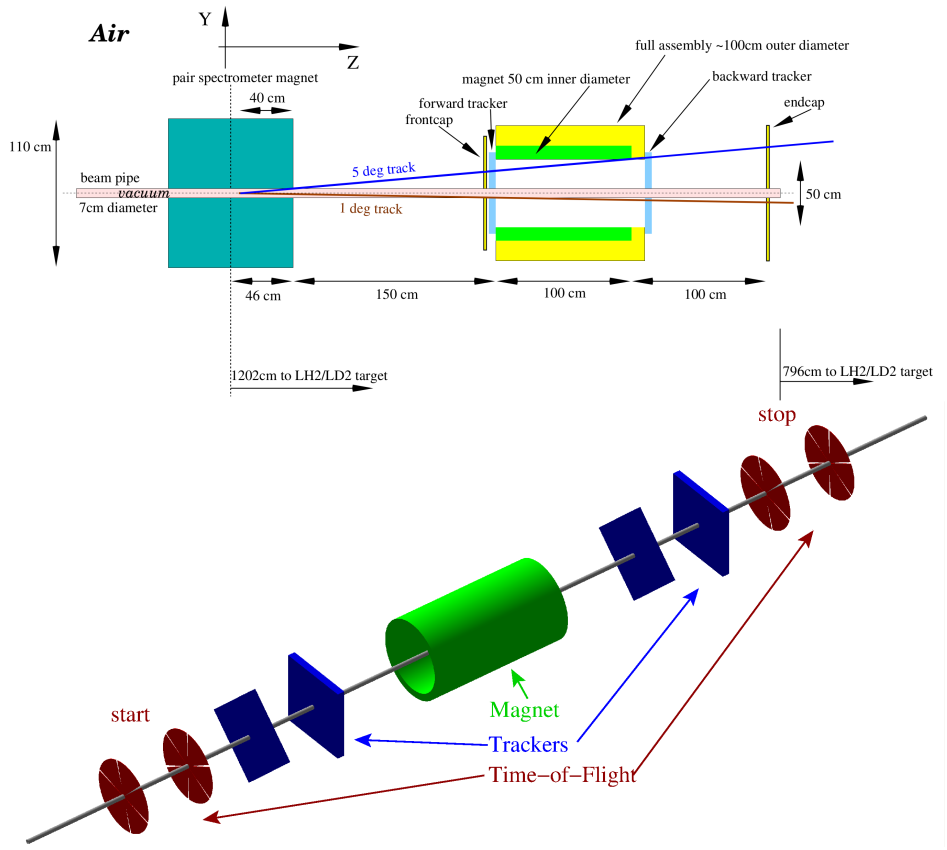

Figure 26: Top: Schematic view of the Kaon Flux Monitor setup. Bottom: Expanded view of the KFM GEANT4 simulation. Beam goes from left to right.

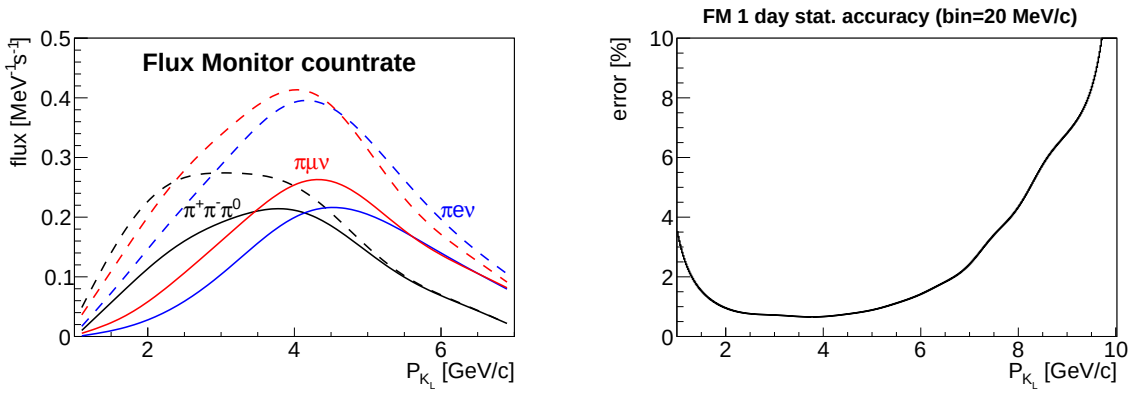

Figure 27: The Kaon Flux Monitor performance. Left: Visible K_L flux for various decay channels within the KFM acceptance. Solid lines correspond to a system with front/end-caps only. Dashed lines show the improvement one can obtain with the additional barrel part extension to the FM. Right: Expected statistical accuracy for 1 day FM measurement ($\pi^+\pi^-\pi^0$ branch only) in 20 MeV/c momentum bin.

5.6 K_L Beam Properties and Neutron, Gamma, and Muon Background

5.6.1 Neutron and Gamma Background:

The neutron flux on the face of the LH_2/LD_2 cryogenic target is found to be 6.6×10^5 n/sec. This energy spectrum of this flux drops exponentially to 10 GeV (Fig. 28 (right)). The SiPM detectors are only sensitive to neutron energies above 1 MeV [115]. The prompt neutron dose rate for the silicon photomultipliers (SiPMs) of the Start Counter (SC) [116–119] and Barrel Electromagnetic Calorimeter (BCAL) [119, 120] is given in Fig. 28 (left). The SiPMs used in the SC and BCAL are expected to tolerate the calculated neutron background shown in Fig. 28. Previous studies state that the dose rate of 30 mreh/h increases a dark current at SiPM by a factor of 5 after 75 days of running period [115], and the expected dose is well below this rate. In the extreme worst case, it is reasonable to expect to replace the affected SiPMs once per year.

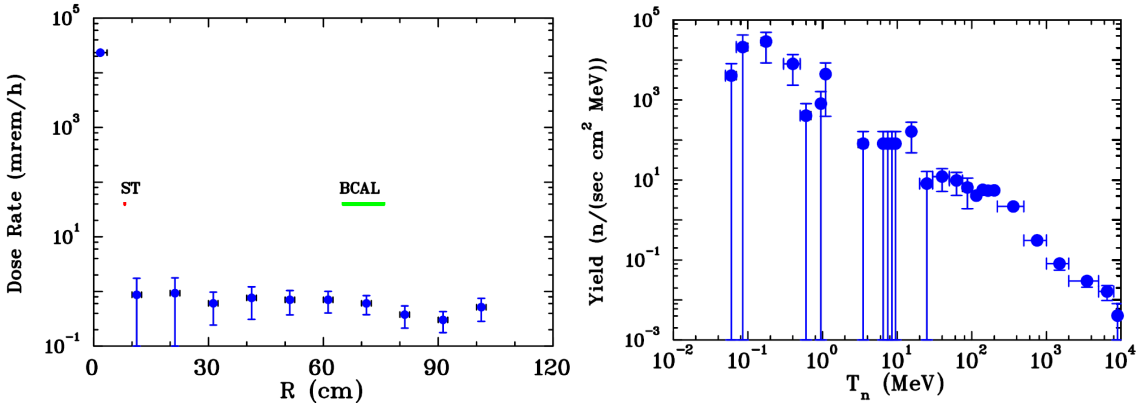

Figure 28: Left: Neutron prompt radiation dose rate background calculated for SiPM of SC and BCAL on the face of the cryogenic target. In this case, we did not take into account additional shieldings in the experimental hall. Right: Neutron energy spectrum at the beam on the face of the cryogenic target.

The flux is additionally not sufficient to provide any significant background in the case of np or nd interactions in the cryogenic target (see Sec. 4.3 for details).

5.6.2 Muon Background:

Following Keller [121], our Geant4 [122] simulations included Bethe-Heitler muon background from KPT and photon dump at CPS, both of which contribute to the background at the GlueX detector and the muon dose rate outside Hall D [109]. The number of produced muons in the Be-target and W-plug are about the same, but muons originating in tungsten have much softer momenta. The estimated number of produced muons is less than 10^7 μ/sec. Their momentum spectrum is shown in Fig. 29. Half of the muons will have momenta higher than 2 GeV/c, 10% of them will have momenta higher than 6 GeV/c, and 1% will have momenta above 10 GeV/c. Overall, the muon flux for the KLF experiment is tolerable to the RadCon requirement, and such muons are deflected well by the sweeping magnet downstream of the target.

To summarize: Calculations for KPT were performed for different shielding configurations to minimize the neutron and gamma prompt radiation dose rate and the cost of KPT. Our studies have shown that the KPT will produce a high K_L flux of the order of 1×10^4 K_L/sec and the neutron

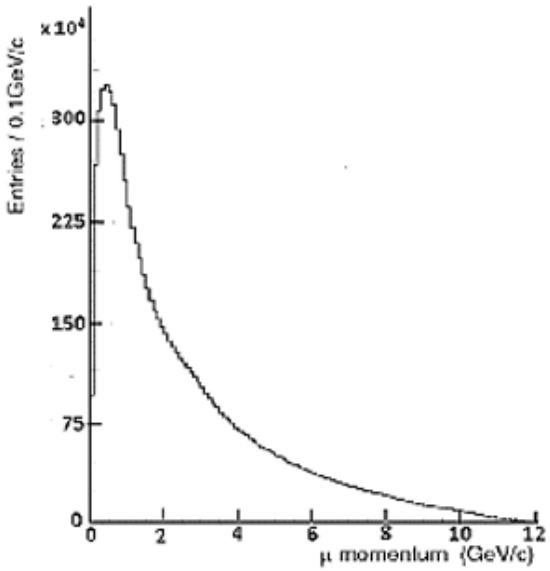

Figure 29: Muon momentum spectrum for the Bethe-Heitler (see details in text).

and gamma fluxes and prompt dose rates for the KLF experiment are below the JLab RadCon requirement establishing the radiation dose rate limits in the experimental hall.

5.7 K_L Momentum Determination and Beam Resolution

The mean lifetime of the K_L is 51.16 nsec ($c\tau = 15.3$ m) whereas the mean lifetime of the K^- is 12.38 nsec ($c\tau = 3.7$ m) [1]. For this reason, it is much easier to perform measurements of $K_L p$ scattering at low beam energies compared with $K^- p$ scattering.

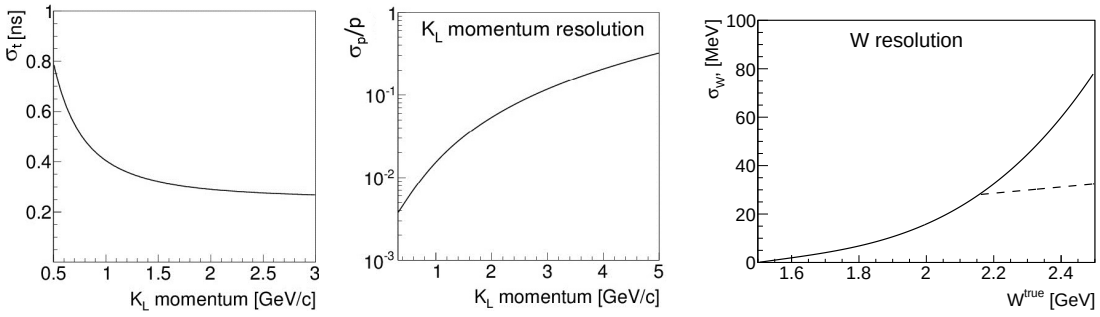

Figure 30: Left: Time resolution (σ_t) for K_L beam as a function of K_L-momentum. Middle: Momentum resolution (σ_p/p) as a function of momentum (note, log scale). Right: Energy resolution (σ_W) as a function of energy. The dashed line shows approximate W resolution from reconstruction of the final-state particles.

The momentum of a K_L beam will be measured using time-of-flight (TOF) - the time between the accelerator bunch (RF signal from CEBAF) and the reaction in the LH_2/LD_2 target as detected by

the GlueX spectrometer. Thus the TOF resolution is a quadratic sum of accelerator time and GlueX spectrometer time resolutions. Since the accelerator signal has a very good time resolution on the order of few picoseconds, the TOF resolution will be defined mainly by the GlueX detector. In our calculations, we used currently achieved Start Counter (SC) time resolution of 250 psec to show the time and beam momentum resolution vs. kaon momentum (Fig. 30). All hyperon production reactions have very similar TOF and final state reconstructed W-resolution.

To get precise TOF information, the electron beam needs to have a narrow bunch time structure. As discussed in Sec. 5.1, the electron beam can be delivered with predetermined repetition rate. For the K_L experiment, the 64 nsec bunch spacing structure is an optimal choice. It allows no cross-bunch overlap for the full range of kaon beam momentum from p > 320 MeV/c.

The uncertainty in a neutral kaon production position at lower momenta (p < 0.5 GeV/c) affects timing resolution caused by the TOF difference between the photon and kaon time traversing the Be target, however, as $\Delta p/p = \gamma^2 \Delta t/t$ momentum resolution is below 1 % at lower momenta. The TOF resolution is flat for momenta higher than 1 GeV/c. The momentum resolution decreases with momentum: for 1 GeV/c it is $\sim$1.5 % and for 2 GeV/c it is $\sim$5 %. For fully reconstructed final states W can be reconstructed directly, providing a better resolution in the region where the TOF method deteriorates, W > 2.2 GeV (see dashed curve in Fig. 30 (right)).

The K_L beam momentum and time resolution are governed by the time resolution provided by the GlueX detector from the reconstruction of charged particles produced in the LH_2/LD_2 target. There are three detector systems that can provide precision timing information for reconstructed charged particles in GlueX: the SC [117], Barrel Calorimeter (BCAL) [120], and the TOF detectors. In the current studies, we rely on the SC for beam momentum determination.

The GlueX SC is a cylindrical plastic scintillator detector surrounding the LH_2/LD_2 target, with 3 mm thick scintillator bars and a tapered nose region that bends toward the beamline at the downstream end. The scintillation light from each of the 30 scintillator bars is detected by an array of four 3×3 mm^2 Hamamatsu S10931-050P surface mount silicon photomultipliers (SiPMs) [118]. The time resolution of the SC was determined to be 250 psec during the 2016 and 2017 GlueX run periods and thus provided adequate separation of the 250 MHz photon beam bunch structure delivered to Hall D during that time. This performance was achieved using the recommended operating gain and bias voltages supplied by Hamamatsu to provide both the FADC 250 analog signals and precision F1TDC discriminator signals used in the GlueX reconstruction.

To summarize: The simulation studies in this proposal have assumed a time resolution of 250 psec, which is adequate for the proposed physics program. With the current detector, the overall K_L-momentum resolution will be determined by utilizing the timing information from the SC, BCAL, and TOF detectors and will probably overshoot a very conservative 250 psec specification. Finally, we are exploring potential upgrades to improve the SC time resolution significantly; however, such improvements would not influence much on the resonance parameters extracted by the PWA, hence they have low priority for the proposed hyperon spectroscopy program.

5.8 LH_2/LD_2 Cryogenic Target for KL Beam at Hall D

The proposed experiment will utilize the existing GlueX liquid hydrogen cryogenic target (Fig. 31) modified to accept a larger diameter target cell [123]. The GlueX target is comprised of a kapton cell containing liquid hydrogen at a temperature and pressure of about 20 K and 19 psia, respectively. The 100 ml cell is filled through a pair of 1.5 m long stainless steel tubes (fill and return) connected to a small container where hydrogen gas is condensed from two room-temperature storage tanks. This condenser is cooled by a pulse tube refrigerator with a base temperature of 3 K and cooling power of about 20 W at 20 K. A 100 W temperature controller regulates the condenser at 18 K.

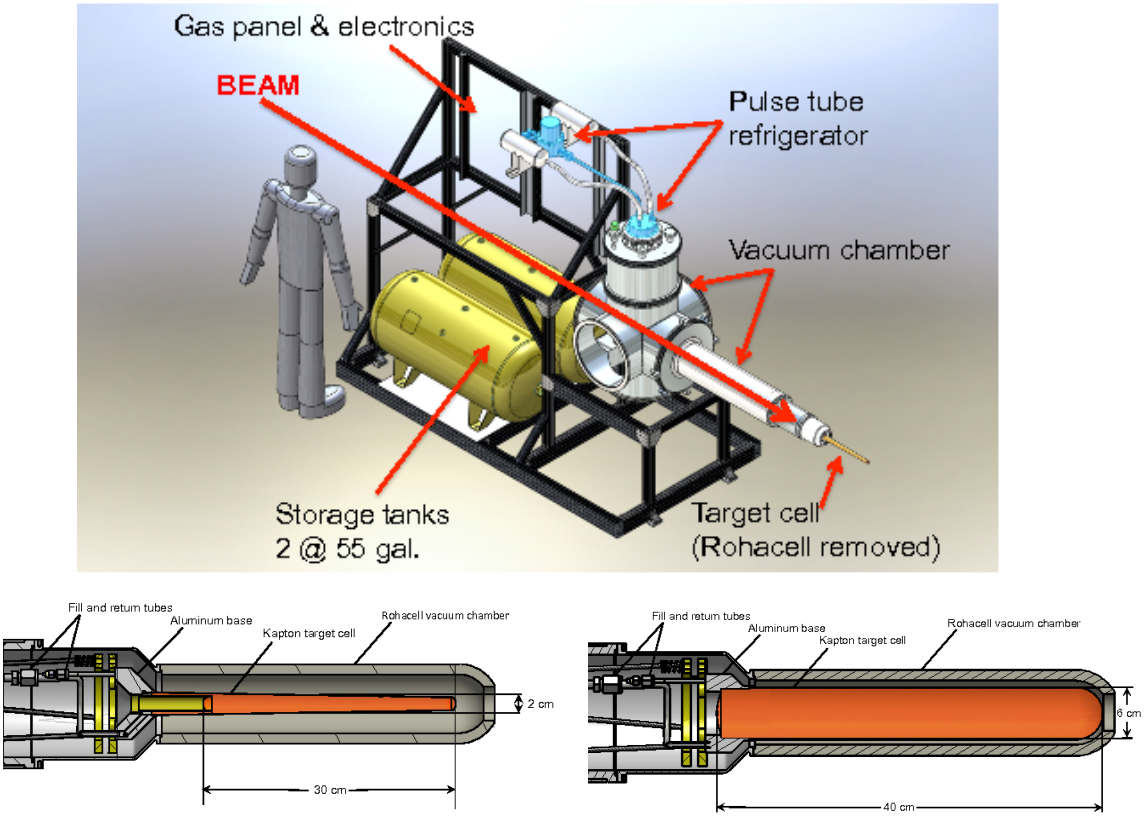

Figure 31: Top: The GlueX liquid hydrogen target. Bottom left: Kapton target cell for the GlueX LH_2/LD_2 cryogenic target. Bottom right: Conceptual design for a larger target cell for the proposed K_L beam at Hall D experiment.

The entire target assembly is contained within an "L"-shaped stainless steel and aluminum vacuum chamber with a Rohacell extension surrounding the target cell. The SC for the GlueX experiment fits snugly over this extension. The vacuum chamber, along with the hydrogen storage tanks, gas handling system, and control electronics, is mounted on a custom-built beamline cart for easy insertion into the Hall D solenoid. A compact I/O system monitors and controls the performance of the target, while hardware interlocks on the target temperature and pressure and on the chamber vacuum ensure the system's safety and integrity. The target can be cooled from room temperature

and filled with liquid hydrogen in about 5 hours. For empty target runs, the liquid can be boiled from the cell in about 20 minutes (the cell remains filled with cold hydrogen gas), and then refilled with liquid in about 40 minutes.

The GlueX cell (Fig. 31 (bottom left)) is closely modeled on those utilized at Hall B for more than a decade and is a horizontal, tapered cylinder about 0.38 m long with a mean diameter of 0.02 m. The cell walls are 130 μm kapton glued to an aluminum base. A $\varnothing$0.02 m reentrant beam window defines the length of LH_2/LD_2 in the beam to be about 0.30 m. Both entrance and exit windows on the cell are 75 μm kapton. In normal operation, the cell, the condenser, and the pipes between them are all filled with liquid hydrogen. In this manner, the liquid can be subcooled a few degrees below the vapor pressure curve, greatly suppressing bubble formation in the cell. In total, about 0.4 liter of LH_2 is condensed from the storage tanks, and the system is engineered to recover this quantity of hydrogen safely back into the tanks during a sudden loss of insulating vacuum, with a maximum allowed cell pressure of 49 psia [124].

A conceptual design for the neutral kaon beam target is also shown in Fig. 31 (bottom right). The proposed target cell has a $\varnothing$0.06 m and a 0.40 m length from entrance to exit windows, corresponding to a volume of about 1.1 liter, which will require filling the existing tanks on the target cart to about 50 psia. The Collaboration will work with the JLab Target Group to investigate alternative materials and construction techniques to increase the strength of the cell. As an example, the LH_2 target cell recently developed for Hall A is $\varnothing$0.063 m, 0.18 m long and has a wall thickness of approximately 0.2 mm. The cell is machined from a high-strength aluminum alloy, AL7075-T6, and has a maximum allowed pressure of about 100 psia. It is expected that minor modifications to the cryogenic target's piping systems will also be required to satisfy the increased volume of condensed hydrogen.

The proposed system is expected to work equally well with liquid deuterium, which condenses at a slightly higher temperature than hydrogen (23.3 K versus 20.3 K at atmospheric pressure). The expansion ratio of LD_2 is 13 % higher, which implies a storage pressure of about 60 psia. Therefore, the new target cell must be engineered and constructed to work with both LH_2 and LD_2.

6 Project Planning

The KLF Collaboration represents a substantial community interested in the physics of strange quark hadrons, whose membership includes people currently involved in the physics of Hall D and those from outside the currently established Collaborations. A growing core group is actively involved in the hardware and analysis activities required for this project.

We show the key KLF beamline and detector system projects in Tables 6, along with the personnel currently involved in each project. The main additional hardware required for the KLF are the new beamline components for the neutral kaon beam. These components have been previously described in detail in Sec. 5, and they are listed in Table 6 along with the Collaboration members currently involved in their design. The CPS for Hall D is being designed in collaboration with the CPS Collaboration, in order to leverage their experience with designing a CPS for Halls A/C.

Group	Members
CPS	**Sean Dobbs**, Donal Day, Pavel Degtyarenko, Gabriel Niculescu, Tim Whitlatch, Todd Satogata, **Igor Strakovsky**, Bogdan Wojtsekhowski, Eugene Chudakov
KPT	**Igor Strakovsky**, Pavel Degtyarenko, Tim Whitlatch, Eugene Chudakov
KFM	**Mikhail Bashkanov**, Nick Zachariou, Dan Watts, Tim Whitlatch, **Moskov Amaryan**, Shankar Adhikari
Electron Beamline	**Todd Satogata**
Secondary particle yields	**Igor Strakovsky**, **Ilya Larin**, **Moskov Amaryan**
Cryogenic Target	**Chris Keith**
Trigger / DAQ	**Sergey Furletov**, **Alexander Somov**

Table 6: Topical groups for the various detector systems and beamline components being developed or upgraded for the KLF experiment. Working group coordinator(s) are listed in bold text.

The KPT and KFM are smaller projects, and their designs are advanced and well-matched for the expertise of their working group members.

An initial high-level list of tasks required for these hardware projects and the estimated time to complete each of them is given in Fig. 32. With reasonable assumptions of the available resources, we expect that the new beamline elements could be built and fully installed by the beginning of 2024.

In addition, a growing range of members have been working on performing the detailed simulation and PWA studies shown in this proposal, and have been continuing to build the physics and analysis frameworks needed for the determination of resonance pole parameters and other physics goals described in this proposal. The physics topics covered by these efforts include the primary hyperon and meson spectroscopy program, as well as studies of neutron-induced reactions and other physics possibilities with the KLF facility, as described in the body of the proposal and the appendices. The range of active experimental and theoretical activities is illustrated by the range of talks presented at the regularly schedule KLF Collaboration Meetings [216].

7 Summary and Beam Time Request

We propose to perform strange hadron spectroscopy with a secondary K_L beam in the GlueX setup at JLab. Precise new experimental data (both differential cross sections and recoil polarization of hyperons) for K_Lp scattering with good kinematic coverage will be obtained. This will allow predictions from the CQM and LQCD to be checked for all families of excited Λ^*, Σ^*, Ξ^*, and Ω^* hyperon resonances for the first time. In addition, it will permit a search for the possible existence of hybrids in the hyperon sector as predicted by the lattice calculations [125].

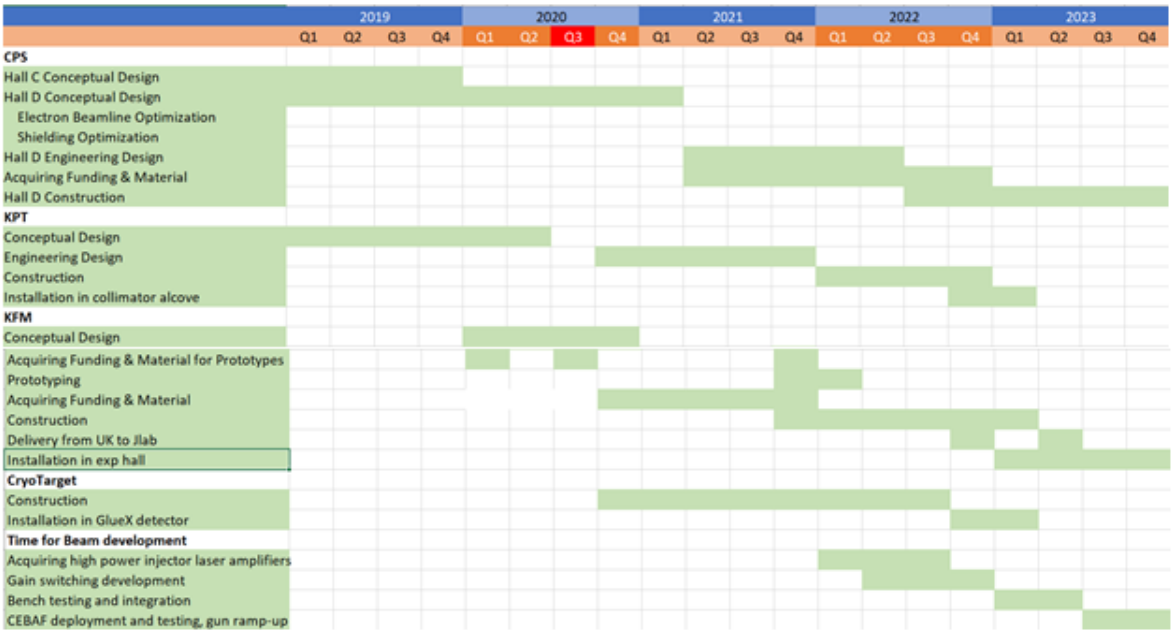

Figure 32: Diagram illustrating a potential timeline for the different stages of the design, construction, and installation of the K_L beamline.

A complete understanding of three-quark bound states requires accurate measurements of the full spectra of hyperons with their spin-parity assignments, pole positions, and branching ratios. An important impact of these strange hyperon spectroscopy measurements is their significance for the thermodynamic properties of the early universe at freeze-out, which is one of the main physics topics at heavy-ion colliders.

Besides hyperon spectroscopy, the experimental data obtained in the strange meson sector in the reactions $K_L p \to K^{\pm}\pi^{\mp}p$ and $K_L p \to K_S\pi^{\pm}n(p)$ will provide precise and statistically significant data for experimental studies of the $K\pi$ system. This will allow a determination of quantum numbers of strange meson resonances in S- (including $\kappa(800)$), P-, D-, and higher-wave states. It will also allow a determination of phase shifts to account for final-state $K\pi$ interactions. Measurements of $K\pi$ form factors will be important input for Dalitz-plot analyses of D-meson and charmless B mesons with $K\pi$ in final state.

The K_L facility at JLab will be *unique in the world*. The high-intensity secondary beam of K_L (1×10^4 K_L/s) would be produced in EM interactions using the high-intensity and high-duty-factor CEBAF electron beam with very low neutron contamination as was done at SLAC in the 1970s [34]; but now, with three orders of magnitude higher intensity. The possibility to perform similar studies with charged kaon beams is under discussion at J-PARC with intensities similar to those proposed for the K_L beam at JLab. If these proposals are approved, the experimental data from J-PARC will be complementary to those of the proposed K_L measurements.

In Table 7, we present the expected statistics for 100 days of running with a LH_2 target in the GlueX setup at JLab. The expected statistics for the 5 major reactions are very large. There are however, two words of cautions at this stage. These numbers correspond to an inclusive reaction

Reaction	Statistics (events)
$K_L p \to K_S p$	2.7M
$K_L p \to \pi^+ \Lambda$	7M
$K_L p \to K^+ \Xi^0$	2M
$K_L p \to K^+ n$	60M
$K_L p \to K^- \pi^+ p$	7M

Table 7: Expected statistics for differential cross sections of different reactions with LH_2 and below W = 3.0 GeV for 100 days of beam time.

reconstruction, which is enough to identify the resonance, but might not be enough to uncover its nature. The need for exclusive reconstruction is essential to extract polarization observables was highlighted in Sections 4.1 and Ref. [25]. It further decrease the expected statistics, e.g., from 2M to 200k events in the $K\Xi$ case. These statistics, however, would allow a precise measurement of the double-differential polarization observables with statistical uncertainties on the order of 10 %. Secondly, kaon flux has a maximum around W = 3 GeV, which decreases rapidly towards high/low W's. Thus, the 100 days of beam time on the LH_2 are essential to maximize the discovery potential of the K_L Facility and uncover the densely populated hyperon states at low-W.

There are no data on "neutron" targets and, for this reason, it is hard to make a realistic estimate of the statistics for $K_L n$ reactions. If we assume similar statistics as on a proton target, the full program will be completed after running 100 days with LH_2 and 100 days with LD_2 targets.

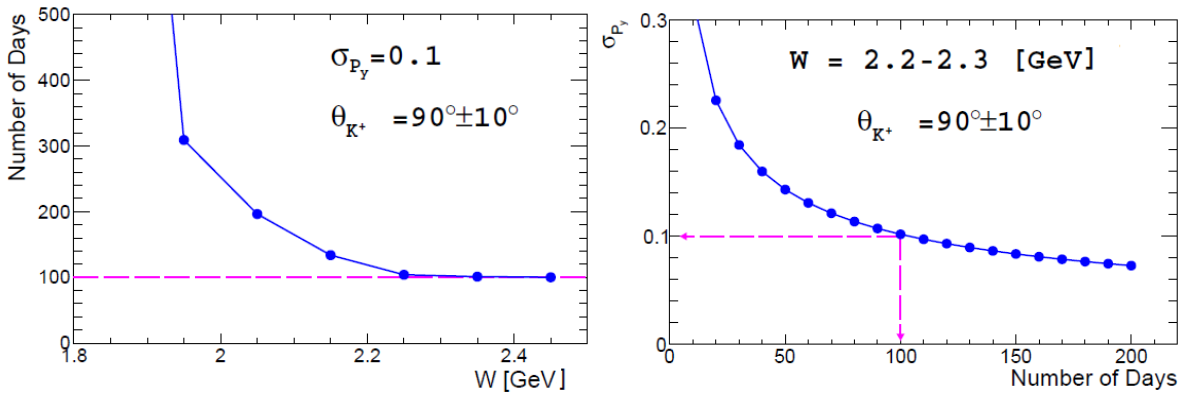

Figure 33: Required a beam time of the experiment for the $K_L p \to K^+ \Xi$ reaction. Left: To reach 10 % polarization uncertainty as a function of W. Right: Reachable polarization uncertainty at W = 2.2 GeV and $\theta_{K+} = 90°$.

7.1 Expected Statistical Accuracy:

A coupled-channel PWA is the most direct and least model-dependent way to extract resonance properties. However, as shown in Appendix. A.3, it requires knowledge of both the differential and polarization observables at the same CM energy. In order to ensure that the duration of the experiment would be adequate to extract all observables with sufficient accuracy, dedicated studies were performed. One can determine the recoil polarization utilizing large self-analysing powers of hyperon decays. In this case, the errors on the polarization measurement are essentially of statistical nature, hence one can infer desired accuracy in the polarization measurement to a required beam time of experiment in a straightforward way. From theoretical perspective, the polarization error on the order of 0.1 looks essential in getting an unambiguous PWA solution (see Sec. A.3.12). Polarization errors larger than 0.5 would have no influence on convergence of the PWA fit, hence will be discarded. This tight theoretical constrains impose strict requirement for the duration of experiment to collect sufficient statistics in each channel. Fig. 33 shows the expected error in measurement of polarization observable as a function of CM energies (left) and experiment duration (right) for the key reaction $K_L p \to K^+\Xi^0$. The expected error is a complex three-fold function of kaon flux (Fig. 33 (left)) with maximum at W = 3 GeV), cross section (Ref. [35]) and detector acceptance. In case of $K_L p \to K^+\Xi^0$ reaction, it lead to a maximum statistics reachable in the range of 2.2 < W < 2.7 GeV.

A similar study can be performed for the another reaction channel, $K_L p \to \pi^+\Lambda$, see Fig. 34.

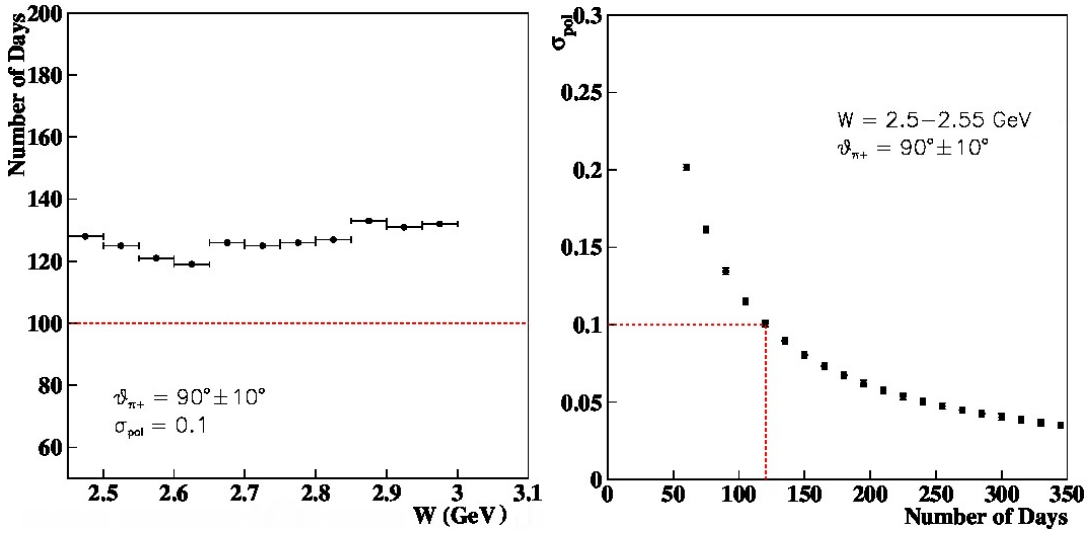

Figure 34: Required a beam time of the experiment for the $K_L p \to \pi^+\Lambda$ reaction. Left: To reach 10 % polarization uncertainty as a function of W. Right: Reachable polarization uncertainty at W = 2.525 GeV and $\theta_{\pi^+} = 90°$.

This reaction requires finer binning to disentangle various $\Lambda - \Sigma$ mixing effects leading to a similar experiment duration as in $K\Xi$ case, despite larger production cross sections.

To summarize: All channels we have considered so far require about 100 days beamtime for a nominal flux of $1\times10^4\ K_L/sec$ to exhibit the beauty of strangeness physics in details and maximize the discovery potential of the KL Facility. Expected statistics for differential cross sections of different reactions with LH_2 and below W = 3.0 GeV for 100 days of beam time, for instance, is given in Table 7.

As it was already mentioned in the Section 4.2, running KLF for 100 days on hydrogen target will increase the world statistics by about two orders of magnitude, while also providing a data in completely unmeasured region of $M(K\pi) < 0.8$ GeV, which will result in significant improvement in determination of the pole position and the width of the κ scalar meson.

7.2 Expected Systematic Uncertainties:

Systematic uncertainties with K_L beam will be reaction and kinematics dependent. The total systematic errors include three major sources: detector related, induced by the reconstruction algorithms, and overall flux estimation. The first two sources can be linked to the current GlueX program. Indeed after several years of running our understanding of the GlueX detector performance is in quite advanced state. The K_L program will utilize this knowledge. Hence, we expect the detector related systematical errors to be of the similar size to that of the photon program and below ≈3 % [6]. The only source of uncertainty which cannot be estimated from ongoing GlueX program is K_L flux related ambiguity. A dedicated K_L Flux Monitor will be able to provide a flux determination with an accuracy better than 5 %.

Additional source of systematical uncertainties in the determination of resonance parameters is related to theoretical extraction of "true" observables from experimental data. Theoretical uncertainty is two-folded: the first part related to the absence of experimental data, e.g., the absence of polarization observables, or non-existence of measurements on neutron target; the second one is associated with particular theoretical methods employed to extract resonance parameters. We, in KLF, will attack this problem from both directions: precise experimental measurements will cover gaps in existing database, while comprehensive theoretical analysis of competing theoretical groups (SAID, BnGa, GW-Jülich, MAID, or Kent State) with uncorrelated method-dependent systematics will eliminate the second source of uncertainties.

In the case of strange meson spectroscopy, non-$K\pi$ scattering backgrounds are likely to play a role leading to systematic errors. One source of the background could be the higher mass baryon resonances in the case of $K^{\pm}\pi^{\mp}p$ final states. In the case when the final system is $K^-\pi^0\Delta^{++}$, one source of uncertainties is due to the background under the π^0 peak, which according to the current GlueX measurement [6] is estimated to be on the order of less than 1%. Another source of systematic uncertainties is stemming from the K_L beam flux normalization systematics, which will be on the order of 5%. In the case of $\pi^-\Delta^{++}(K_L)$ an additional uncertainty may come from the $\Lambda\pi^+(\pi^0)$ background, which should be vetoed by selecting events, where invariant mass of $p\pi^-$ lies above ground state $\Lambda(1116)$. Overall for the reactions with Δ^{++}, we expect systematic uncertainties to be on the order $\sim\ 5\%$, while in the neutral pion exchange reactions systematic errors may be higher.

Systematic uncertainties for the κ pole position determination from $K\pi$ scattering have already been taken into account in the estimation of the precision for its mass and width with KLF data in the summary Appendix A.4 of the $K\pi$ scattering.

A Appendices

Contents

A.1 Interest of the RHIC/LHC Community in Excited Hyperon Measurements

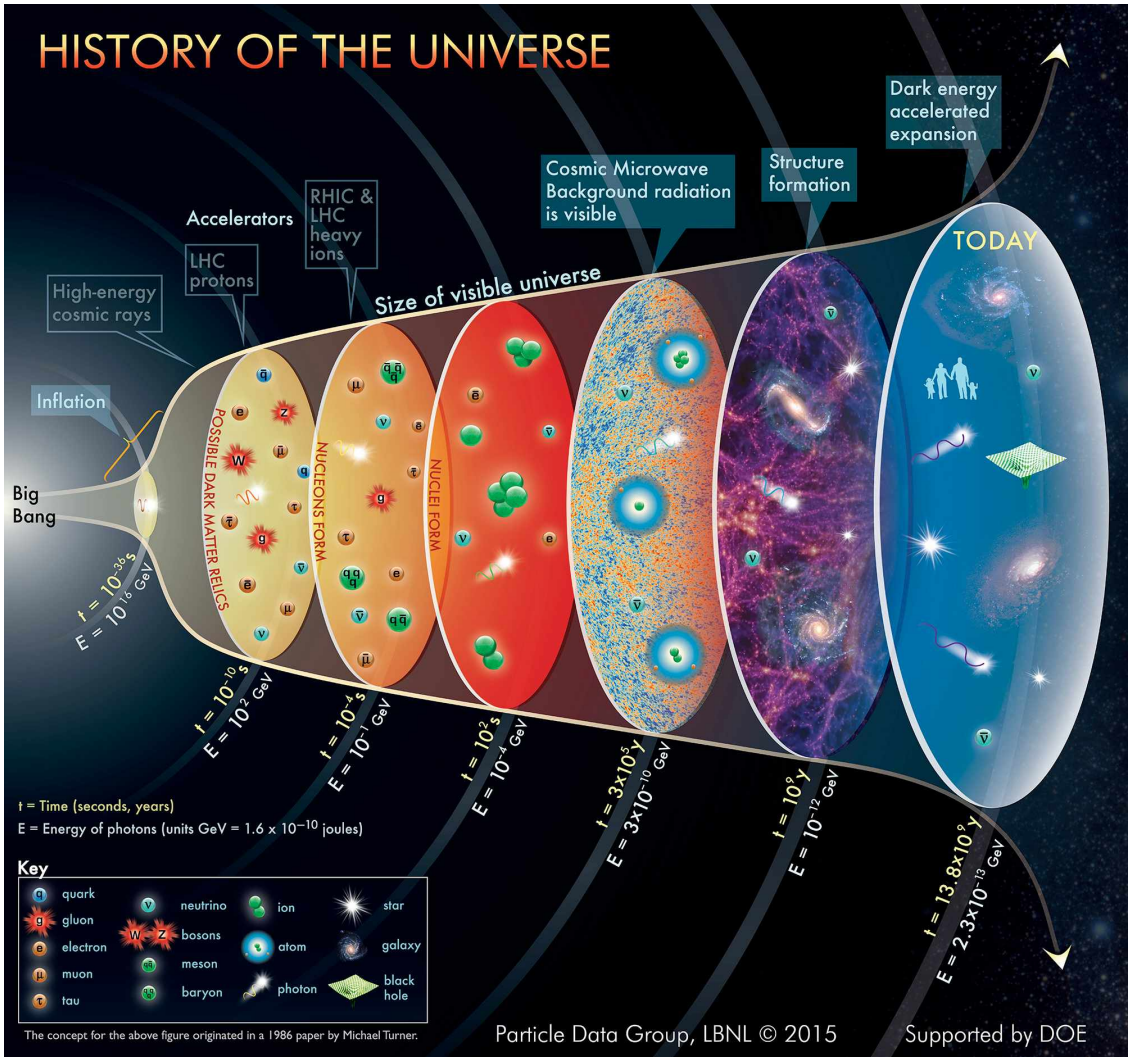

Figure 35: KLF Project will provide a valuable missing input needed to shed a light on thermodynamic properties of the Early Universe around 1 μs after the Big Bang.

At temperatures on the order of the pion mass strongly interacting matter undergoes a transition (rapid crossover) from the confined phase with hadronic degrees of freedom to a deconfined phase with partonic degrees of freedom, Quark-Gluon Plasma (QGP). A reverse process, hadronization has taken place shortly after the Big Bang when the matter in the Universe started cooling down and underwent a chain of transitions, as illustrated in Fig. 35. The properties of the strongly interacting matter under extreme temperatures and densities and the transition to QGP are under intense study at the Relativistic Heavy-Ion Collider (RHIC) at BNL and the Large Hadron Collider (LHC) at CERN. To relate experimentally measured particle yields to theoretically predicted thermodynamic observables, a detailed understanding of the hadronization process of light and strange degrees of freedom is required.

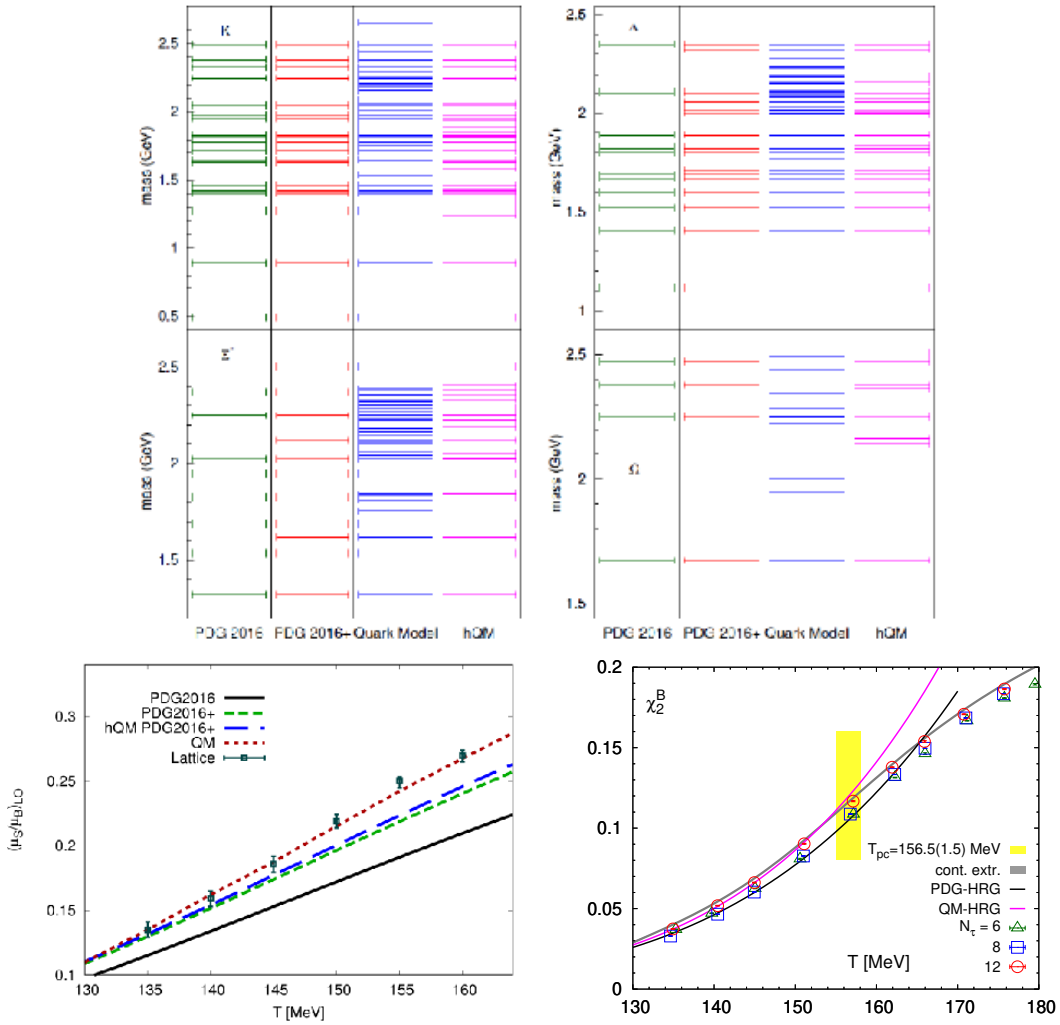

Figure 36: Top: Comparison of predicted and measured excited strange hadronic states in PDG2018, PDG2018+ (including one star states), QM, and hQM. Bottom left: Lattice QCD calculations of the temperature dependence of the leading order susceptibility ratio (μ_s/μ_B) compared to results from HRG model calculations with varying number of hadronic states. Bottom right: Lattice QCD calculations of the temperature dependence of the baryon number susceptibility χ_B^2 compared to results from HRG model calculations with varying number of hadronic states.

The relativistic heavy-ion community at the RHIC and LHC has recently embarked on specific analyses to address the issue of strangeness hadronization. LQCD calculations in the QCD crossover transition region between a deconfined phase of quark and gluons and a hadronic resonance gas have revealed a potentially interesting sub-structure related to the hadronization process. Studies of flavor-dependent susceptibilities, which can be equated to experimental measurements of conserved quantum-number fluctuations, seem to indicate a slight flavor hierarchy in the three-quark sector (u,d,s) in thermalized systems. Specifically, the ratios of higher-order susceptibilities in the strange sector show a higher transition temperature than in the light sector [126]. Recently, original estimates of the pseudo-critical temperature [127, 128] have been significantly improved placing

the transition at $T_c = (156.5 \pm 1.5)$ MeV [129], $T_c = (158.0 \pm 0.6)$ MeV [130]. Ref. [130] has also estimated the width of the transition to be around $\Delta T = 15$ MeV. The difference of the specific susceptibilities calculated in Ref. [126] is around 18 MeV and well outside their individual uncertainties. At the same time the pseudo-critical temperature associated with strangeness observables is certainly not consistent with the most recent estimates of the pseudo-critical temperatures based on the chiral condensate and related observables. This warrants a more detailed analysis of the strangeness sector, both in terms of the partonic and hadronic degrees of freedom.

This difference seems to be confirmed by statistical thermal-model calculations that try to describe the yields of emitted hadrons from a QGP based on a common chemical freeze-out temperature. Although the yields measured by ALICE at the LHC in 2.76 TeV PbPb collisions can be described by a common temperature of 156$\pm$2 MeV, with a reasonable χ^2, the fit improves markedly if one allows the light quark baryons to have a lower temperature than the strange quark baryons [131]. A similar result has been found when the thermal fluctuations of particle yields as measured by the STAR Collaboration [132, 133], which can be related to the light quark dominated susceptibilities of the electric charge and the baryon number on the lattice, have been compared to statistical model calculations [134].

If one assumes that strange and light quarks indeed prefer different freeze-out temperatures, then the question arises how this could impact the hadronization mechanism and abundance of specific hadronic species. In other words, is the production of strange particles, in particular excited resonant states, enhanced in a particular temperature range in the crossover region? Strange ground-state particle production shows evidence of enhancement, but the most likely scenario is that the increased strange quark abundance will populate excited states; therefore, the emphasis of any future experimental program trying to understand hadron production is shifting towards strange baryonic resonance production. Furthermore, recent LHC measurements in small systems, down to elementary proton-proton collisions, have revealed that even in these small systems there is evidence for deconfinement, if the achieved energy density, documented by the measured charged particle multiplicity is large enough [135]. Therefore, future measurements of elementary collisions in the K-Long Facility experiment at JLab might well provide the necessary link to future analysis of strange resonance enhancements in heavy-ion collisions at RHIC and the LHC and a deeper understanding of the hadronization process.

This statement is also supported by comparisons between the aforementioned LQCD calculations and model predictions based on a non-interacting hadronic resonance gas. The Hadron Resonance Gas (HRG) model [136–139] yields a good description of most thermodynamic quantities in the hadronic phase up to the pseudo-critical temperature. The idea that strongly interacting matter in the ground state can be described in terms of a non-interacting gas of hadrons and resonances, which effectively mimics the interactions of hadrons by simply increasing the number of possible resonant states exponentially as a function of temperature, was proposed early on by Hagedorn [140]. The only input to the model is the hadronic spectrum: usually it includes all well-known hadrons in the *Review of Particle Physics*, namely the ones rated with at least two stars. Recently, it has been noticed that some more differential observables present a discrepancy between lattice and HRG model results. The inclusion of not-yet-detected states, such as the ones predicted by the original Quark Model (QM) [141, 142] has been proposed to improve the agreement [143, 144]. A systematic study based on a breakdown of contributions to the thermodynamic

pressure given by particles grouped according to their quantum numbers (in particular baryon number and strangeness) enables us to infer in which hadron sector more states are needed compared to the well-known ones from the PDG [145]. In case of a flavor hierarchy in the transition region, one would expect the number of strange resonances to increase, due to a higher freeze-out temperature, compared to the number of light-quark resonances. Figure 36 shows the effect of different strange hadron input spectra to the HRG model in comparison to LQCD. Figure 36 (top) shows the number of states in PDG2018 [1], PDG2018+ (including one star states), the standard QM, and a Quark Model with enhanced quark interactions in the hadron (hyper-central model hQM [146]). Fig. 36 (bottom left) shows a comparison of the HRG results to a leading-order LQCD calculation of μ_s/μ_B; i.e., the ratio to strange to baryon number susceptibility [145]. Recent extensions of the HRG model, for instance, accommodating repulsive mean-field [147] also indicate that inclusion of the predicted by the Quark Model states improves the agreement between HRG and LQCD results.

An interesting conclusion that arises from these studies is that the improvement in the listing of strange resonances between PDG2008 [148] and PDG2018 [1] definitely brought the HRG calculations closer to the LQCD data. By looking at details in the remaining discrepancy, which is in part remedied by including one-star rated resonances in PDG2018, it seems that the effect is more carried by singly strange resonances rather than multi-strange resonances, also in light of comparisons to quark models that include di-quark structures [149] or enhanced quark interactions in the baryon (hypercentral models [146]). This is good news for the experiments since the Λ and Σ resonances below 2 GeV are well within reach of the KLF experiment and, to a lesser significance, the RHIC/LHC experiments. In this context it is also important to point out that the use of both hydrogen and deuterium targets in KLF is crucial since it will enable the measurement of charged and neutral hyperons. A complete spectrum of singly strange hyperon states is necessary to make a solid comparison to first-principle calculations.

The possible effect of missing states on the QCD thermodynamics is also quite pronounced in the baryon sector. Fig. 36 (bottom right) shows the fluctuations of the baryon number computed in LQCD [150] and compared to the HRG model. While the HRG model with the PDG spectrum undershoots the continuum-extrapolated lattice data, adding the Quark Model predicted states brings the HRG result into closer agreement with LQCD.

To summarize: Any comparisons between experimentally verified strange quark-model states from YSTAR and LQCD will shed light on a multitude of interesting questions relating to hadronization in the non-perturbative regime, exotic particle production, the interaction between quarks in baryons and a possible flavor hierarchy in the creation of confined matter.

A.2 Strangeness Physics within Neutron Stars

One of the main goal of nuclear physics is to obtain a comprehensive picture of the strong interaction, which can be accessed by introducing the strangeness degree of freedom in the, now well-understood, nucleon-nucleon (NN) interaction. The NN interaction has a long history of detailed studies, and currently phenomenological approaches can describe observed phenomena with high accuracy [151]. On the other hand, the interaction between Hyperons and Nucleons (YN) is very

poorly constrained, mainly due to difficulties associated with performing high-precision scattering experiments involving short-lived hyperon beams (currently only $\sim$1300 events from bubble chamber experiments exist on the interaction between hyperons and protons). This interaction, however, provides the key in understanding properties and phenomena associated with Neutron stars [152, 153].

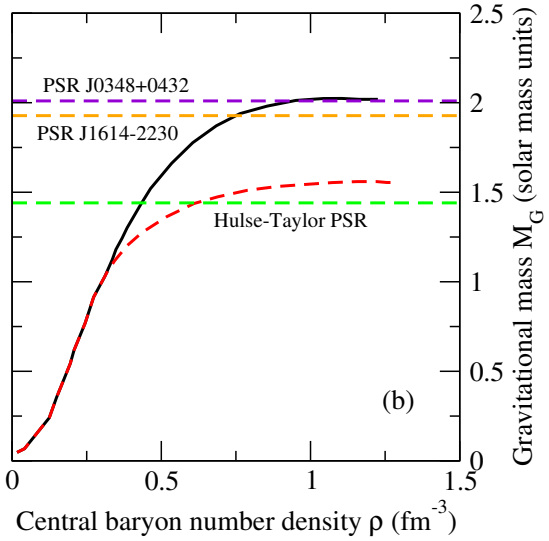

Figure 37: Effect of hyperons on EoS of neutron stars using a generic model with (black solid line) and without (red dashed line) hyperons. The horizontal lines shows the observational mass of the Hulse-Taylor [154] pulsar and the observed PSR J1614-2230 [155] and PSR J0348+0432 [156]. Figure from Ref. [157].

Hyperons are expected to appear within the core of Neutron stars at densities about 2-3 times the nuclear saturation density. In fact, contrary to terrestrial conditions, where hyperons are unstable and decay into nucleons via the weak interaction in a matter of nanoseconds, the conditions in neutron stars can make the inverse process more energetically favourable; with their subsequent decay blocked by the Pauli principle. Because of this, the existence of hyperons in Neutron stars has been a very hot topic in the past years as it is predicted to have a very strong effect on the Equation of State of the neutron star (see Fig. 37) [152].

Obtaining a detailed understanding of the YN interaction will allow us to address the so called “hyperon puzzle," which reflects how theoretical approaches cannot reconcile the predicted role of hyperons within neutron stars using our current poor understanding of the interaction between hyperons and nucleons [153].

With the recent advancement of detector and accelerator technologies we can obtain a more direct access on the YN interaction by studying final state interaction in exclusive hyperon photoproduction. This approach is complementary to the alternative hypernuclear studies [158], which are important in obtaining the many-body effects but fail in accessing the bare YN interaction. For KLF, these studies will focus on obtaining a data set in which a hyperon beam, produced on a nucleon and tagged by the detection of the pion ($K_L p \to \pi^+ \Lambda/\Sigma$) or kaon ($K_L p \to K^+ \Xi$), rescatters with

a secondary nucleon within the target cell. Large acceptance detectors, like the GlueX detector, allows a full reconstruction of the event by the detection of the hyperons decay products. The KLF, which facilitates a copious production of hyperons, will provide us with unprecedented statistics to study the YN interaction. Utilising the self-analyticity of hyperons allows us to obtain further stringent constraints on the underlying dynamics and address the “hyperon puzzle". Experiments with deuterium target can also be used to study the isospin dependence of the YN interaction for the first time. Such approaches have been successfully applied to data from CLAS [159, 160] with results being prepared for publication. The KLF facility, will allow a much more precise measurement as it will provide ~ 40 times higher statistics and a significant increase in kinematical coverage. Figure 38 shows the projected KLF cross section measurement uncertainties (magenta points) and how these compare to existing world data.

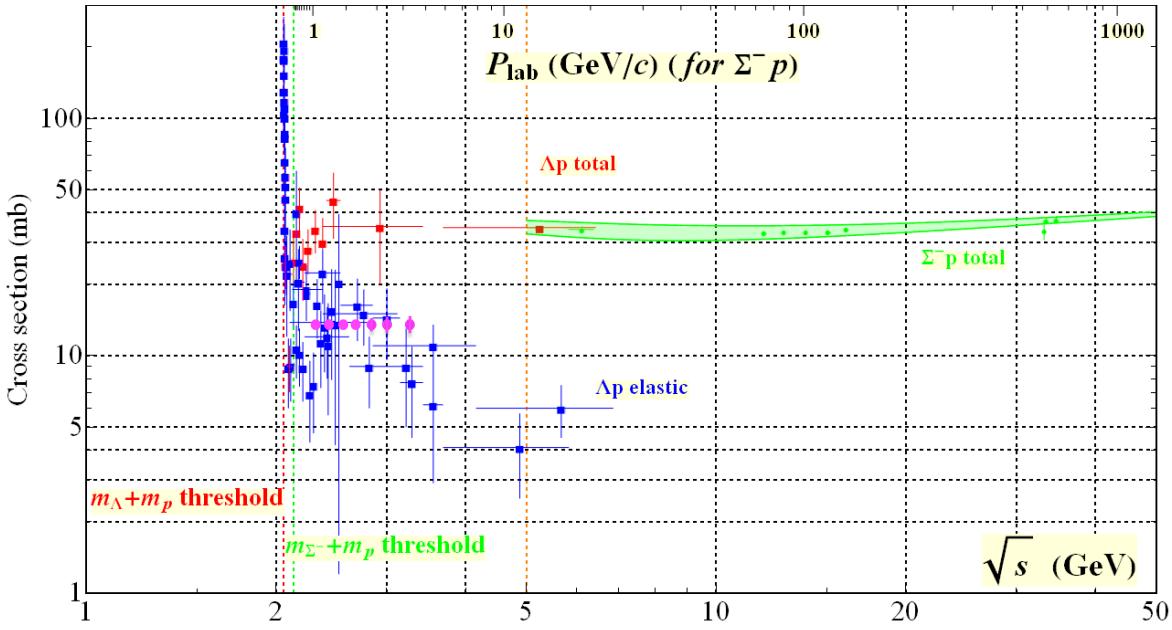

Figure 38: Total cross section for hyperon-nucleon scattering. Magenta points indicate the projected measurement and statistical uncertainties from KLF and how these compare to existing world data.

To summarize: Providing direct experimental constraints on the Equation of State of neutron stars is important for the following reason: while non-perturbative ab initio lattice QCD calculations are very successful in the region of the phase diagram with high temperatures and low densities, the region of high densities and almost zero temperature, relevant for neutron stars, is completely out of reach for non-perturbative LQCD calculations. As a result, a theoretically sound Equation of State with fully controlled systematics for strongly interacting matter at high density is not presently available.

A.3 Hyperon Spectroscopy

The present experimental knowledge of the spectra of strange hyperons remains remarkably incomplete. For example, only the lowest negative-parity doublet and the positive parity singlet of the Λ hyperon are well established. In the case of the Σ and Ξ hyperons, only the lowest decuplet resonance states $\Sigma(1385)$ and $\Xi(1530)$ are well established. In this section, we discuss this context for the proposed hyperon spectroscopy program and a few highlights of proposed measurements which will address the outstanding questions in the field.

A.3.1 Previous Measurements for Hyperons:

While a formally complete experiment requires the measurement, at each energy, W, and angle, θ, of at least three independent observables, the current database for $K_Lp \to \pi Y$ and KY is populated mainly by unpolarized cross sections. Figure 39 illustrates this quite clearly.

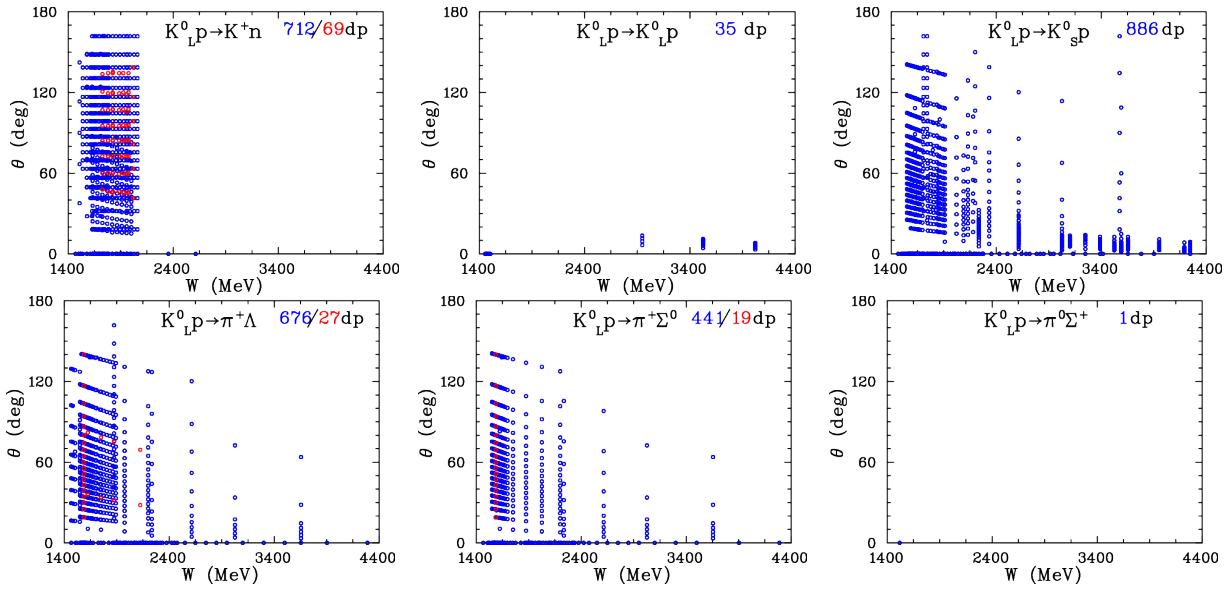

Figure 39: Experimental data available for $K_Lp \to K^+n$, $K_Lp \to K_Lp$, $K_Lp \to K_Sp$, $K_Lp \to \pi^+\Lambda$, $K_Lp \to \pi^+\Sigma^0$, and $K_Lp \to \pi^0\Sigma^+$ as a function of CM energy W [161]. The number of data points (dp) is given in the upper righthand side of each subplot [blue (red) shows the amount of unpolarized (polarized) observables]. Total cross sections are plotted at zero degrees.

The initial studies of the KLF program at GlueX will likely focus on two-body and quasi-two-body processes: elastic $K_Lp \to K_Sp$ and charge-exchange $K_Lp \to K^+n$ reactions, then two-body reactions producing $S = -1$ ($S = -2$) hyperons as $K_Lp \to \pi^+\Lambda$, $K_Lp \to \pi^+\Sigma^0$, and $K_Lp \to \pi^0\Sigma^+$ ($K_Lp \to K^+\Xi^0$). Most of the previous measurements induced by a K_L beam, were collected for W = 1454 MeV and with some data up to W = 5054 MeV. Experiments were performed between 1961 and 1982 with mostly hydrogen bubble chambers at ANL, BNL, CERN, DESY, KEK, LRL, NIMROD, NINA, PPA, and SLAC. Note that some of data were taken at EM facilities at NINA [106] (a short overview about NINA experiments is given by Albrow recently [162]) and SLAC [105]. The goal of the Manchester University group that worked at the Daresbury 5-GeV electron synchrotron NINA was CP-violation, which was a hot topic back to the mid 1960s. The main physics topics

that the SLAC group addressed were studies of the systematics for particle/anti-particle processes through the intrinsic properties of the K-longs.

The first paper that discussed the possibility of creating a practical neutral kaon beam at an electron synchrotron through photoproduction was an optimistic prediction for SLAC by Drell and Jacob in 1965 [163]. With significant developments in technology, high-quality EM facilities, such as JLab [17], are now able to realize a complete hyperon spectroscopy program.

The overall systematics of previous K_Lp experiments varies between 15 % and 35 %, and the energy binning is much broader than hyperon widths. The previous number of K_L-induced measurements (2426 $d\sigma/d\Omega$, 348 σ^{tot}, and 115 P observables) [161] was very limited. Additionally, we are not aware of any measurements on a "neutron" target.

Our knowledge about the non-strange sector is more advanced vs. the strange one [1]. For the non-strange case, for instance, phenomenology has access to 51k data of $\pi N \to \pi N$ and 39k data of $\gamma N \to \pi N$ below W = 2.5 GeV [93].

A.3.2 Partial-Wave Analysis for Hyperons:

Here, we summarize some of the physics issues involved with K_L scattering processes. Following Ref. [164], the differential cross section and polarization for $K_L p$ scattering are given by

$$\frac{d\sigma}{d\Omega} = \lambda\!\!\!^{-2}(|f|^2 + |g|^2) \qquad \text{and} \qquad P\frac{d\sigma}{d\Omega} = 2\lambda\!\!\!^{-2}\mathrm{Im}(fg^*), \tag{8}$$

where $\lambda\!\!\!^{-} = \hbar/k$, with k the magnitude of CM momentum for the incoming meson. Here $f = f(W,\theta)$ and $g = g(W,\theta)$ are the usual spin-non-flip and spin-flip amplitudes at CM energy W and meson CM production angle θ. In terms of partial waves, f and g can be expanded as

$$f(W,\theta) = \sum_{l=0}^{\infty}[(l+1)T_{l+} + lT_{l-}]P_l(\cos\theta), \tag{9}$$

$$g(W,\theta) = \sum_{l=1}^{\infty}[T_{l+} - T_{l-}]P_l^1(\cos\theta), \tag{10}$$

where l is the initial orbital angular momentum, $P_l(\cos\theta)$ is a Legendre polynomial, and $P_l^1(\cos\theta)$ is an associated Legendre function. The total angular momentum for the amplitude T_{l+} is $J = l+\frac{1}{2}$, while that for the amplitude T_{l-} is $J = l - \frac{1}{2}$. For hadronic scattering reactions, we may ignore small CP-violating terms and write

$$K_L = \frac{1}{\sqrt{2}}(K^0 - \overline{K^0}) \qquad \text{and} \qquad K_S = \frac{1}{\sqrt{2}}(K^0 + \overline{K^0}). \tag{11}$$

We may generally have both $I = 0$ and $I = 1$ amplitudes for KN and $\bar{K}N$ scattering, so that the amplitudes $T_{l\pm}$ can be expanded in terms of isospin amplitudes as

$$T_{l\pm} = C_0 T^0_{l\pm} + C_1 T^1_{l\pm}, \tag{12}$$

where $T^I_{l\pm}$ are partial-wave amplitudes with isospin I and total angular momentum $J = l \pm \frac{1}{2}$, with C_I the appropriate isospin Clebsch-Gordan coefficients.

We plan to do a coupled-channel PWA with new KLF data in combination with available new J-PARC K^- measurements when they will come. Then the best fit will allow to determine model-independent (data-driven) partial-wave amplitudes and associated resonance parameters (pole positions, residues, BW parameters, etc.) as the GWU/SAID group does, for instance, for the analysis of πN-elastic, charge-exchange, and $\pi^- p \to \eta n$ data [165].

In the following sections, we outline some of the outstanding questions in the hyperon spectrum, overview the available data on KN scattering and introduce theoretical predictions for the unexplored domain of measurements with "neutron" targets.

A.3.3 The $\Lambda(1405)1/2^- - \Lambda(1520)3/2^-$ Doublet:

In the quark model, the $\Lambda(1405)1/2^- - \Lambda(1520)3/2^-$ doublet is a flavor singlet of three quarks (*uds*). Dynamical versions of this model, with two-body interactions between the quarks can describe the low mean energy of this multiplet, but not the 115 MeV splitting between them. This has led to suggestions that there may even be two different 1/2$^-$ states – one dynamical low $\overline{K}N$ resonance at 1405 MeV, and an unresolved higher state close to 1520 MeV [166]. A two pole structure of $\Lambda(1405)$ was indeed found in Ref. [167]. The narrow pole lies slightly below $\bar{K}N$ threshold, and is fixed by the scattering data rather well, see Ref. [168] for the comparison of different coupled-channel approaches. However, the position of the second pole is determined less precisely, and may lie much further below $\bar{K}N$ threshold and deeper in the complex plane. Recent photoproduction data on $\pi\Sigma$ by CLAS [40] may be used to reduce the theoretical ambiguity on this (second) pole of $\Lambda(1405)$ [38] and a single pole structure is not ruled out [169]. Modern lattice QCD (LQCD) calculations also support the view that its structure is a $\bar{K}N$ state [170, 171]. In Skyrme's topological soliton model for the baryons, the low-lying $\Lambda(1405)$ state also appears naturally as a mainly 5-quark state [172, 173]. Lattice calculations based on the sequential Bayesian do, however, indicate that the multiplet may have a mainly 3-quark structure [174].

In the case of those lowest energy flavor-singlet $1/2^-$ - $3/2^-$ parity doublets in the strange, charm and bottom hyperon spectra: $\Lambda(1405) - \Lambda(1520)$, $\Lambda_c(2595) - \Lambda_c(2625)$, $\Xi_c(2790) - \Xi_c(2815)$, and $\Lambda_b(5912) - \Lambda_b(5920)$ [1] the ratio between the splittings in these three doublets are 14.4:3.7:3.1:1.0. These ratios agree qualitatively and within 30% with the corresponding inverse ratios of the K, D, and B meson masses: 10.7:2.8:1.0. As these resonances all contain one light quark pair the latter is what one should expect from the gradual approach to heavy-quark symmetry with increasing meson (or constituent quark) mass if the quark structure of these three multiplets is similar. As described in Sec. A.3.12, data on neutron targets described in this proposal have the potential to provide key insights into settling the nature of the $\Lambda(1405)$.

A.3.4 Low-Lying Positive-Parity Resonances:

In the spectra of the nucleon and the Λ and Σ hyperons, the lowest positive-parity resonances all lie below the lowest negative-parity multiplets except for the flavor singlet doublet $\Lambda(1405)1/2^- - \Lambda(1520)3/2^-$. This reversal of normal ordering cannot be achieved in the constituent quark model with purely color-spin dependent quark interactions. These low-lying positive-parity resonances are the $N(1440)$, $\Lambda(1600)$, and $\Sigma(1660)1/2^+$ states. Their low masses do however appear naturally, if the interactions between the quarks are flavor dependent [175]. Present day LQCD calculations have not yet converged on whether these low-lying states can be described as having a mainly three-quark structure [174, 176, 177].

In the spectrum of the Ξ, the $\Xi(1690)$, or possibly the recently discovered $\Xi(1620)$ [178] may be such a 1/2$^+$ state as well, although the quantum numbers of those states are yet to be determined.

In the corresponding decuplet spectra, a similar low-lying positive-parity state has so far only been definitely identified in the $\Delta(1232)$ spectrum: namely, the $\Delta(1600)3/2^+$. The $\Sigma(1840)3/2^+$ resonance very likely represents the corresponding positive-parity Σ^* state. It should be important to identify the corresponding $3/2^+$ state in the spectrum of the Ξ^*.

A.3.5 Negative-Parity Hyperon Resonances:

In the spectrum of the nucleon, two well-separated groups of negative-parity resonances appear above the 1/2$^+$ state $N(1440)$. This lowest energy group consists of the $N(1535)1/2^-$ and the $N(1520)3/2^-$ resonances. There is a direct correspondence in the $\Lambda(1670)1/2^-$ and the $\Lambda(1690)3/2^-$ resonances. There is also a repeat of this group in the spectrum of the Σ hyperon in the two resonances $\Sigma(1620)1/2^-$ (tentative) and $\Sigma(1670)3/2^-$.

The $N(1535)$ resonance has a large (32–52 %) decay branch to ηN, even though its energy lies very close to the ηN threshold. This pattern repeats in the case of the $\Lambda(1670)$, which also has a substantial (10–25 %) decay branch to the corresponding $\eta\Lambda$ state. As the still uncertain $\Sigma(1620)1/2^-$ resonance is located almost exactly at the threshold for $\eta\Sigma$, there is naturally no signal for an $\eta\Sigma$ decay from it.

In the spectrum of the Ξ hyperon, none of the hitherto determined negative-parity multiplets is complete. The state $\Xi(1820)3/2^-$ may be the analog in the Ξ spectrum of the states $N(1520)$, $\Lambda(1670)$, and $\Sigma(1670)$. It should be important to identify the lowest $1/2^-$ resonance in the Ξ spectrum. If that resonance lacks an η decay branch, it would demonstrate that the η decay of the $1/2^-$ resonances in the spectra of the nucleon, Λ and Σ involves two quarks.

It should also be important to determine whether the uncertain "bumps" referred to in the Particle Data Tables labelled $\Sigma(1480)$, $\Sigma(1560)$, and $\Xi(1620)$ represent true resonances [1].

About 120 MeV above the $1/2^- - 3/2^-$ pair of nucleon resonances $N(1535)$ and $N(1520)$, the nucleon spectrum has three negative-parity resonances close in energy to one another. This multiplet is formed of the $N(1650)1/2^-$, $N(1700)3/2^-$, and $N(1675)5/2^-$ resonances.

The analogs in the spectrum of the Λ of the first and last of these nucleon resonances are the $\Lambda(1800)1/2^-$ and the $\Lambda(1830)5/2^-$ resonances. The missing 3/2$^-$ state in this Λ resonance multiplet has not yet been identified. A common feature of all the 1/2$^-$ resonances in these multiplets is their substantial η decay branch.

A.3.6 Excited $S = -2$ and $S = -3$ Baryons:

$SU(3)$ flavor symmetry allows as many $S = -2$ baryon resonances as there are N and Δ resonances combined ($\sim$27); however, until now only three states, $\Xi(1322)1/2^+$, $\Xi(1530)3/2^+$, and $\Xi(1820)3/2^-$, have their quantum numbers assigned and only a few more states have been observed [1]. For the discovery of excited cascade baryons, we envision a PWA similar to the $S = -1$ sector but more complicated as one is dealing with a three-body final state.

The experimental situation with Ω^{-*}s is even worse than for the Ξ^* case – there are very few data for excited states [179]. The main reason for such a scarce dataset is the very low cross section for their indirect production with pion or photon beams.

A major effort in LQCD calculations involves the determination of inelastic and multi-hadron scattering amplitudes, and the first calculation to study an inelastic channel was recently performed [57,180]. For lattice calculations involving baryons that contain one or more strange quarks an advantage is that the number of open decay channels is generally smaller than for baryons comprised only of the light u and d quarks.

A.3.7 Heavy Quark Symmetry and the Hyperons:

Heavy quark symmetry [181] provides a powerful tool for comparing the structure of hyperons with heavy (charm and bottom) flavor quarks to those with strange quarks. This symmetry follows from the fact that the strength of quark spin-orbit couplings scale with the inverse of the constituent mass. In the case of hyperons with light and heavy quarks this implies that the heavy quark spin decouples from those of the light quarks. Heavy quark symmetry suggests, that the ratio of the sizes of such spin-orbit splittings in the corresponding multiplets in the spectra of the strange, charm and beauty hyperons should approximately correspond to the ratio of the inverses of the corresponding constituent quark (or approximately) meson (K, D, B) masses. Where the spin-orbit splittings conform to this scaling law the implication is that the structure of the corresponding hyperon resonances in the different flavor sectors are similar.

The approach to this symmetry can used as a phenomenological tool to compare the spin-orbit splittings between the Ξ hyperons in the different flavor sectors. Hitherto such comparable splittings are only known for the lowest negative parity doublets in the strange, charm and beauty hyperon spectra, with two light-flavor and only one single heavy quark. The recent observation of a rich spectrum of narrow Ξ_{cc} [182, 183], Ξ_b [184], and Ω_c [185] states has yielded significant theoretical developments in heavy quark spectroscopy. The determination of the mass spectrum and quantum numbers of the $S = -2$ Cascade resonances beyond the $\Xi(1530)$ at KLF will be essential to test these developments to the strange quark sector and compare with recent and forthcoming LQCD calculations [24]. This is *a fortiori* the case for the spectrum of the Ω hyperons.

A.3.8 KN and $\bar{K}N$ Final States:

A fair amount of data are available for the reaction, $K^+n \to K^0p$, measured on a deuterium target. Figure 40 shows a sample of available differential cross sections for $K_Lp \to K_Sp$ compared with predictions determined from a recent PWA of $\bar{K}N \to \bar{K}N$ data [186,187], combined with $KN \to KN$ amplitudes from the SAID database [93]. The predictions at lower and higher energies tend to agree less well with the data.

A.3.9 $\pi\Lambda$ Final States:

The $K^-p \to \pi^0\Lambda$ and $K_Lp \to \pi^+\Lambda$ amplitudes imply that observables for these reactions measured at the same energy should be the same except for small differences due to the isospin-violating mass differences in the hadrons. No differential cross section data for $K^-p \to \pi^0\Lambda$ are available at CM energies W < 1540 MeV, although data for $K_Lp \to \pi^+\Lambda$ are available at such energies. At 1540 MeV and higher energies, differential cross section and polarization data for the two reactions are in fair agreement, as shown in Figs. 40 and 41. It should be stressed that polarized measurements are tolerable for any PWA solutions (Fig. 41).

A.3.10 $\pi\Sigma$ Final States:

Figure 40 shows a comparison of differential cross section data for K^-p and K_Lp reactions leading to $\pi\Sigma$ final states at W = 1660 MeV (or P_{lab} = 716 MeV/c). The curves are based on energy-dependent isospin amplitudes from a recent PWA [186, 187]. No differential cross section data are

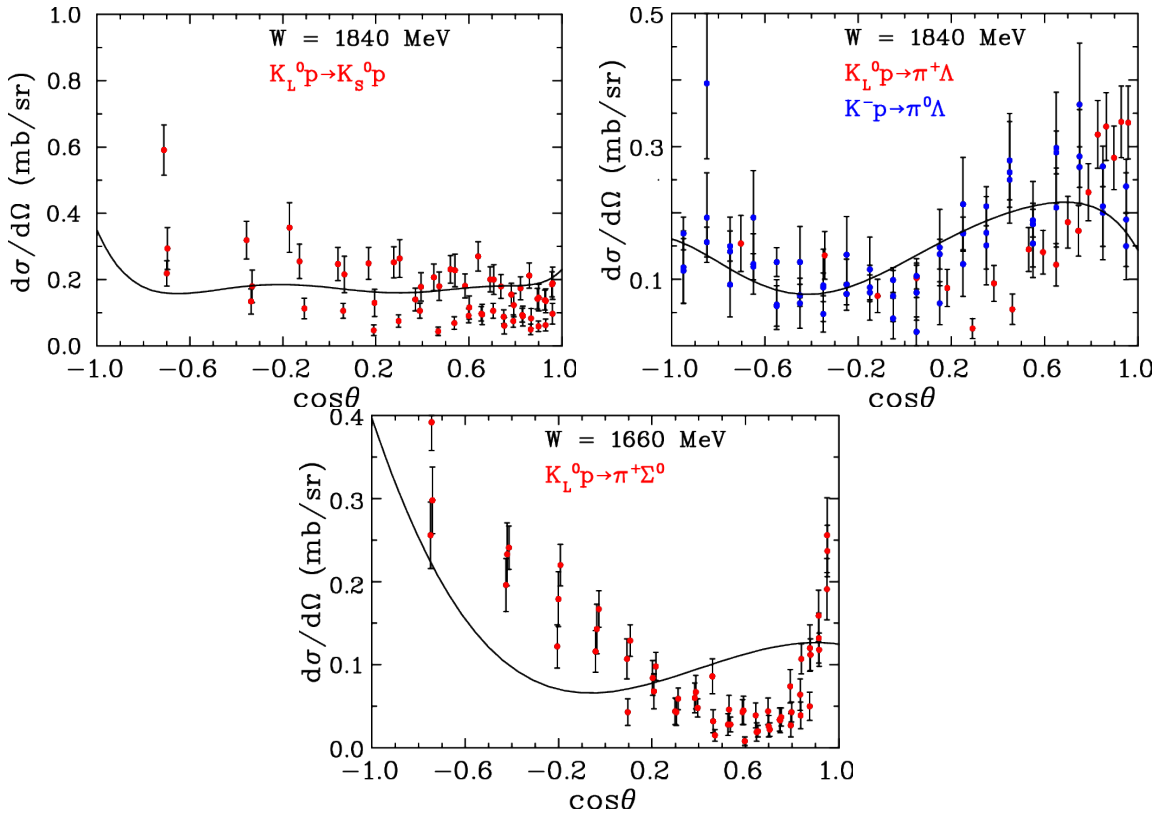

Figure 40: Selected differential cross section data for $K_Lp \to K_Sp$ (left), $K_Lp \to \pi^+\Lambda$ (middle) at W = 1840 MeV and $K_Lp \to \pi^0\Sigma^+$ at W = 1660 MeV (right) from Ref. [188]. The plotted data from previously published experimental data are those data points within 20 MeV of the kaon CM energy indicated on each panel [93]. Plotted uncertainties are statistical only. The curves are predictions using amplitudes from a recent PWA [186, 187], combined with $KN \to KN$ amplitudes from the SAID database [93].

available for $K_Lp \to \pi^0\Sigma^+$. As this example shows, the quality of the K_Lp data is comparable to that for the K^-p data. It would, therefore, be advantageous to combine the K_Lp data in a new coupled-channel PWA with available K^-p data. Note that the reactions $K_Lp \to \pi^+\Sigma^0$ and $K_Lp \to \pi^0\Sigma^+$ are isospin selective (only $I = 1$ amplitudes are involved) whereas the reactions $K^-p \to \pi^-\Sigma^+$ and $K^-p \to \pi^+\Sigma^-$ are not. New measurements with a K_L beam would lead to a better understanding of Σ^* states and would help constrain the amplitudes for K^-p scattering to $\pi\Sigma$ final states.

A.3.11 $K\Xi$ Final States:

The threshold for K^-p and K_Lp reactions leading to $K\Xi$ final states is fairly high ($W_{\rm thresh}$ = 1816 MeV). There are no differential cross section data available for $K_Lp \to K^+\Xi^0$ and very few (none recent) for $K^-p \to K^0\Xi^0$ or $K^-p \to K^+\Xi^-$. Measurements for these reactions would be very helpful, especially for comparing with predictions from dynamical coupled-channel (DCC) models [189, 190] and other effective Lagrangian approaches [191]. The *Review of Particle Physics* [1] lists only two states with branching ratios (BR) to $K\Xi$, namely, $\Lambda(2100)7/2^-$ (BR $<$ 3 %) and $\Sigma(2030)7/2^+$ (BR $<$ 2 %). A recent theoretical prediction of the total cross section for the $K^+\Xi^0$ process was provided in Ref. [193].

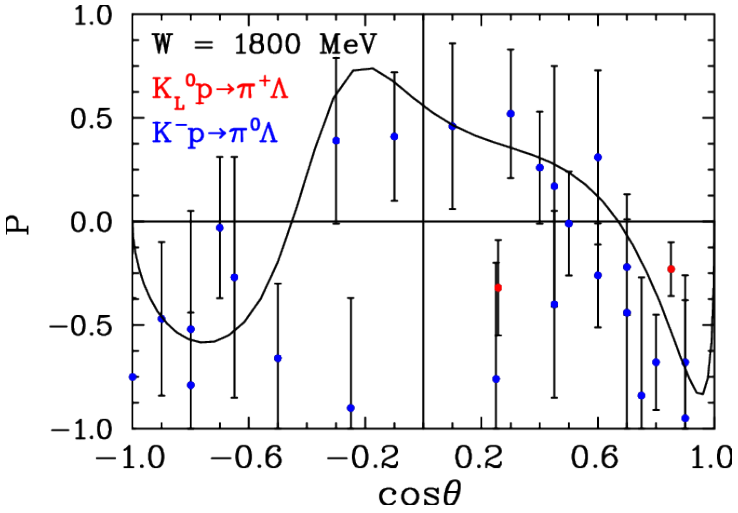

Figure 41: Comparison of selected polarization data for $K^- p \to \pi^0 \Lambda$ and $K_L p \to \pi^+ \Lambda$ at W = 1880 MeV, from Ref. [188]. The plotted data from previously published experimental data are those data points within 20 MeV of the kaon CM energy indicated on each panel [93]. The curves are from a recent PWA of $K^- p \to \pi^0 \Lambda$ data [186, 187].

A.3.12 Theory for "Neutron" Target Measurements:

The so-called coupled-channel Chiral Unitary approaches (UChPT) implement unitarity exactly via a re-summation of a chiral potential to a certain chiral order. They successfully describe all available anti-kaon-nucleon scattering data and predict the mass and width of the sub-threshold resonance in the Isospin $I = 0$ channel, the $\Lambda(1405)1/2^-$. Furthermore, such models lead to the prediction of the second pole in the complex energy plane with the same quantum numbers as $\Lambda(1405)1/2^-$. This is usually referred to as the two-pole structure of the $\Lambda(1405)1/2^-$, see the current review by the Particle Data Group [1] for more details.

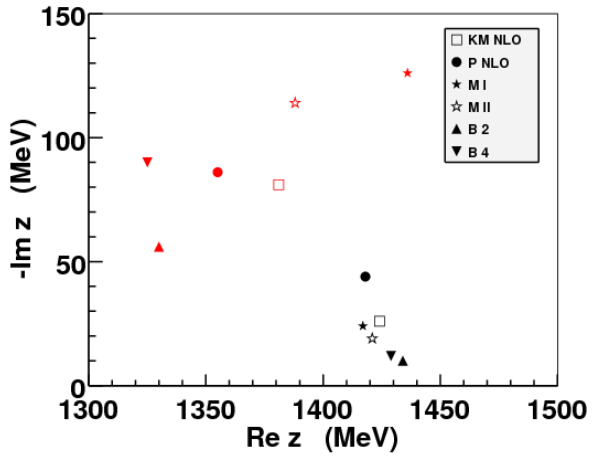

Figure 42: Pole positions of $\Lambda(1405)$ in chiral unitary approaches - KM from Ref. [39], B from Ref. [38], M from Ref. [192], and P from Ref. [194] as compared in Ref. [168]. Each symbol represents the position of the first (black) and second (red) pole in each model.

In the most recent formulation, such UChPT approaches rely on a chiral amplitude for meson-baryon scattering up to next-to-leading chiral order. The unitarity constraint is imposed via the Bethe-Salpeter equation either in the full off-shell formulation [36, 37] or in the so-called on-shell approximation [38, 39], while the off-shell effects are rather small [36]. Among the on-shell approaches [38, 39, 192, 194] a quantitative comparison was performed in Ref. [168], which shown that using the available experimental data, the models predict very different behavior of the scattering amplitude on and off the real energy-axis. This systematic uncertainty becomes evident, when comparing the pole positions of the $\Lambda(1405)1/2^-$ in these models, see Fig. 42. The position

of the narrow (first) pole seems to be constrained rather well, while the predictions for the position broad (second) pole cover a very wide region of the complex energy-plane. This uncertainty is present even within models of the same type. This ambiguity can be traced back to the fact that the experimental data used to fix the parameters of the models is rather old and imprecise.

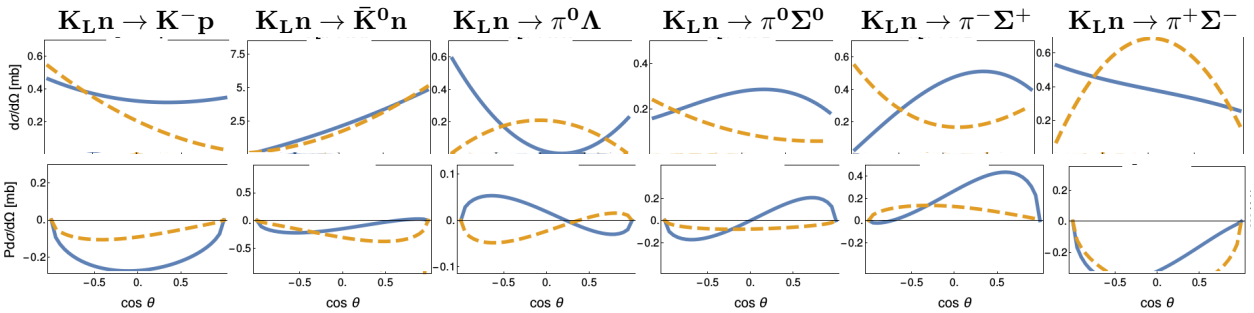

Figure 43: Theoretical predictions for $d\sigma/d\Omega$ (top) and $Pd\sigma/d\Omega$ (bottom) as a function of CM cos of a meson production angle for kaon lab-momentum of 300 MeV/c of initial neutral kaon beam. Orange dashed and blue solid lines show predictions within Model-B2 and Model-B4, respectively.

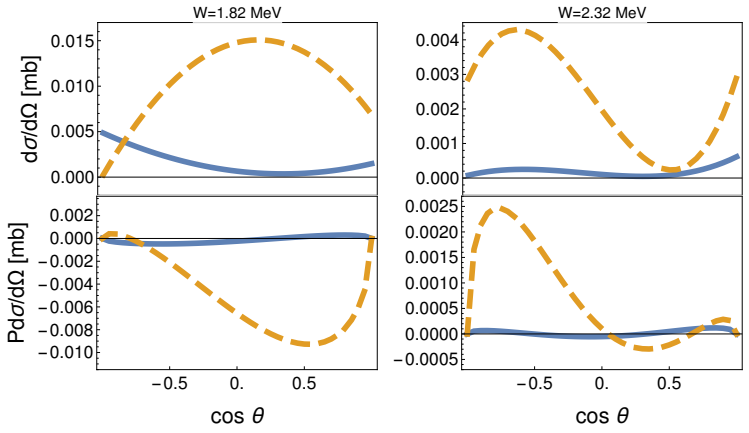

Figure 44: Predictions for $d\sigma/d\Omega$ and $Pd\sigma/d\Omega$ as a function of CM cos of a meson production angle, θ, for the reaction $K_L n \to K^+\Xi^-$. Each column is associated with kaon laboratory momentum of 300 and 700 MeV/c of initial neutral kaon beam. Orange (dashed) and blue lines show predictions within Model-B2 and Model-B4, respectively.

The K_L beam scattered off a neutron target, while measuring the strangeness $S = -1$ of the final meson-baryon states, will become a strongly desired new source of experimental data to pinpoint the properties of the anti-kaon-nucleon scattering amplitude. To make this statement more quantitative, we compare predictions of both solutions of the model from Ref. [38]. These solutions agree with all scattering, threshold as well as the photoproduction data for the $\Sigma\pi$ line shapes by the CLAS Collaboration [40]. The predicted differential cross sections ($d\sigma/d\Omega$) as well as polarized ones ($P \cdot d\sigma/d\Omega$) for the $K_L n$ scattering with the final states $K^- p$, $\bar{K}^0 n$, $\pi^0\Lambda$, $\pi^{0/+/-}\Sigma^{0/-/+}$ are presented in Fig. 43. There is no evident agreement between both prediction of these observables in the energy range aimed to study in the proposed K_L experiment. This is very encouraging since the actual data can sort out one (or both) solutions as unphysical, which was not possible using the present experimental data. As for the $K\Xi$ final states being measured at KLF, both solutions of the here presented model can be used for a theoretical estimate. The reason of being able to do so is that $K^+\Xi^-$ and $K^0\Xi^0$ channels are part of the channel space of ground state octet mesons-baryon channels dynamically implemented into the present model. The result of such a prediction is depicted and addressed further in Fig. 44.

To Summarize: The pole positions have been determined for several Λ^*s and Σ^*s but the information about the pole positions have not been determined for Ξ or Ω hyperons [1]. Our plan is to do a coupled-channel PWA with new KLF data in combination with available and new J-PARC K^-p measurements when they will be available. Then the best fit will allow the determination of data-driven (model independent) partial-wave amplitudes and associated resonance parameters (pole positions, residues, BW parameters, and so on). See Appendix A.3 for a more detailed discussion. Additionally, PWAs with new KLF data will allow a search for "missing" hyperons via looking for new poles in complex plane positions. It will provide a new benchmark for comparisons with QCD-inspired models and LQCD calculations.

A.3.13 Partial-Wave Analysis for Hyperons:

In spite of their model dependence, partial-wave BW parameters have for quite some time been the preferred connection between experiment and QCD in hadronic spectroscopy. More recently, however, pole parameters (e.g., pole positions and residues) have justifiably become the preferred connection, and this fact has also been recognized by the Particle Data Group in recent editions of the *Review of Particle Physics* [1]. Therefore, the extraction of pole parameters from experimental data becomes a procedure of utmost importance.

Extraction of pole parameters is usually performed in two ways:
(a) in an energy-dependent way (ED) or
(b) in an energy-independent procedure through SES PWAs.
In an ED procedure, one measures as many observables as possible to be close to the complete set and then fits the observables with parameters of a well-founded theoretical model that describes the reaction in question. Continuity in energy is enforced by the features of the theoretical model. In a SE procedure, one again measures as many observables as possible but attempts to extract partial waves by fitting energy-binned data independently, therefore, reducing the theoretical input. A discrete set of partial waves is obtained, and the issues of achieving continuity in energy have recently been extensively discussed either by introducing the constraints in analyticity [195] or through angle- and energy-dependent phase ambiguity [196, 197].

In energy-dependent models, pole parameters have been extracted in various ways. The most natural way is the analytic continuation of theoretical model solutions into the complex-energy plane. Simpler single-channel pole extraction methods have been developed such as the speed plot [198], time delay [199], the N/D method [200], regularization procedures [201], and Padé approximants [202], but their success has been limited. In single-energy analyses, the situation is even worse: until recently no adequate method has been available for the extraction of pole parameters. All single-channel methods involve first- or higher-order derivatives, so partial-wave data had to be either interpolated or fitted with an unknown function, and that introduced additional and, very often, uncontrolled model dependencies.

That situation has been recently overcome when a new Laurent+Pietarinen (L+P) method applicable to both, ED and SES models, has been introduced [203–207]. The driving concept behind the single-channel (and later multichannel) L+P approach was to replace solving an elaborate theoretical model and analytically continuing its solution into the full complex-energy plane, with an approximation actualized by local power-series representation of partial-wave amplitudes having well-defined analytic properties on the real energy axis, and fitting it to the given input. In such a way, the global complexity of a model is replaced by a much simpler, and almost model-

independent expansion, limited to the regions near the real energy axis. And this is sufficient to obtain poles and their residues. This procedure gives the simplest function with known analytic structure that fits the data. Formally, the introduced L+P method is based on the Mittag-Leffler expansion [3] of partial-wave amplitudes near the real-energy axis, where we represented the regular background term by a conformal-mapping-generated, fastly converging power series called a Pietarinen expansion [4]. In practice, the regular background part is usually fitted with three Pietarinen expansion series. Each of them approximates the most general function which describes the background, and has a branch point at x_{bp}, while all free parameters are then fitted to the chosen channel input. The first Pietarinen expansion with branch-point x_P which is restricted to an unphysical energy range represents all left-hand cut contributions. The next two Pietarinen expansions describe background in the physical range, and the used branch points x_Q and x_R are defined by the analytic properties of the analyzed partial wave. A second branch point is usually fixed to the elastic channel branch point describing threshold effects, and the third one is either fixed to the dominant channel threshold value, or let free.

Thus, solely on the basis of general physical assumptions about analytic properties of the fitted process like number of poles and number and location of conformal mapping branch points, the pole parameters in the complex energy plane are obtained. In such a way, the simplest analytic function with a set of poles and branch points which is fitting the input is actually constructed. This method is equally applicable to both theoretical and experimental input [5].

The transition amplitude of the multichannel L+P model is parametrized as

$$T^a(W) \;=\; \sum_{j=1}^{N_{pole}} \frac{g_j^a}{W_j - W} + \sum_{i=1}^{3} \sum_{k_i=0}^{K_i^a} c_{k_i}^a \left(\frac{\alpha_i^a - \sqrt{x_i^a - W}}{\alpha_i^a + \sqrt{x_i^a - W}} \right)^{k_i} , \tag{13}$$

where a is a channel index, W_j are pole positions in the complex W (energy) plane, g_i^a coupling constants. The x_i^a define the branch points, $c_{k_i}^a$, and α_i^a are real coefficients. K_i^a, $i = 1, 2, 3$ are Pietarinen coefficients in channel a. The first part represents the poles and the second term three branch points. The first branch point is chosen at a negative energy (determined by the fit), the second is fixed at the dominant production threshold, and the third branch point is adjusted to the analytic properties of fitted partial wave.

[3] Mittag-Leffler expansion [208] is the generalization of a Laurent expansion to a more-than-one pole situation. For simplicity, we call it Laurent expansion.

[4] This type of conformal mapping expansion was introduced by Ciulli and Fisher [209, 210]. It was described in details and also used in pion-nucleon scattering by Pietarinen [211, 212]. The procedure was named Pietarinen expansion by Höhler in Ref. [164].

[5] Observe that fitting partial wave data originating from experiment as energy independent analysis is even more favorable.

To enable the fitting, a reduced discrepancy function D_{dp} is defined as

$$
\begin{aligned}
D_{dp} &= \sum_{a}^{all} D_{dp}^{a}; \\
D_{dp}^{a} &= \frac{1}{2\,N_W^a - N_{par}^a} \times \sum_{i=1}^{N_W^a} \left\{ \left[\frac{\mathrm{Re}\,T^a(W^{(i)}) - \mathrm{Re}\,T^{a,exp}(W^{(i)})}{Err_{i,a}^{\mathrm{Re}}} \right]^2 \right. \\
&+ \left. \left[\frac{\mathrm{Im}\,T^a(W^{(i)}) - \mathrm{Im}\,T^{a,exp}(W^{(i)})}{Err_{i,a}^{\mathrm{Im}}} \right]^2 \right\} + \mathcal{P}^a,
\end{aligned}
$$

where

$$
\mathcal{P}^a = \lambda_{k_1}^a \sum_{k_1=1}^{K^a} (c_{k_1}^a)^2\, {k_1}^3 + \lambda_{k_2}^a \sum_{k_2=1}^{L^a} (c_{k_2}^a)^2\, {k_2}^3 + + \lambda_{k_3}^a \sum_{m=1}^{M^a} (c_{k_3}^a)^2\, {k_3}^3
$$

is the Pietarinen penalty function, which ensures fast and optimal convergence. N_W^a is the number of energies in channel a, N_{par}^a the number of fit parameters in channel a, $\lambda_c^a, \lambda_d^a, \lambda_e^a$ are Pietarinen weighting factors, $Err_{i,a}^{\mathrm{Re,\,Im}}$ ... errors of the real and imaginary part, and $c_{k_1}^a, c_{k_2}^a, c_{k_3}^a$ real coupling constants.

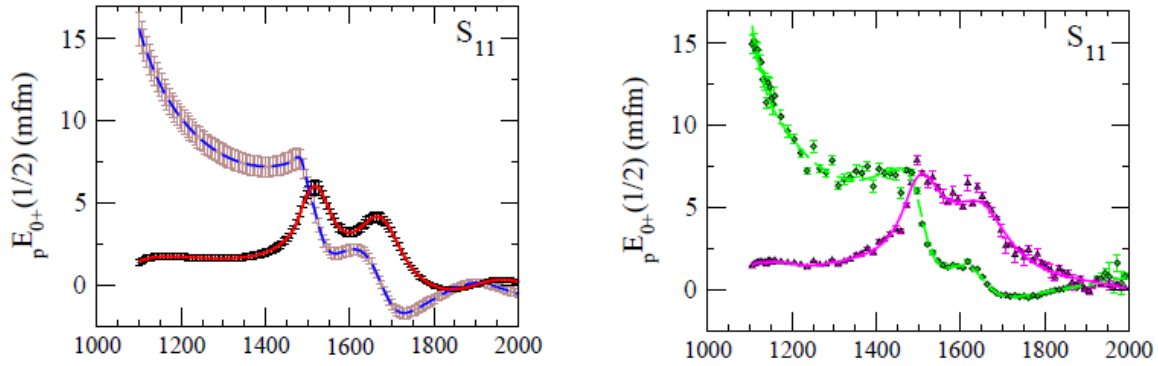

Figure 45: L+P fit to CM12 GW/SAID pion photoproduction ${}_pE_{0+}$ ED and SESs [213].

In order to obtain reliable answers in the L+P model we have to build knowledge about the analytic structure of the fitted partial wave into the fitting procedure. Because we are looking for poles, we only have to define which branch points to include. Their analytic form will be determined by the number of Pietarinen coefficients. As we have only three branch points at our disposal we expect that the first branch-point will describe all subthreshold and left-hand cut processes, the second

one is usually fixed to the dominant channel opening, and the third one is to represent background contributions of all channel openings in the physical range. So, in addition to choosing the number of relevant poles, our anticipation of the analytic structure of the observed partial wave is of great importance for the stability of the fit.

The L+P model has been successfully applied to both theoretical models and discreet partial-wave data. As an example, in Fig. 45, we give the achieved quality of the fit for the CM12 GW/SAID pion photoproduction amplitudes [213].

A.3.14 Strange Hadrons from the Lattice:

Our knowledge of the excited-state spectrum of QCD through the solution of the theory on a Euclidean-space lattice has undergone tremendous advances over the past several year. What we characterize as excited states are resonances that are unstable under the strong interaction, and their properties are encapsulated in momentum-dependent scattering amplitudes.

The methodology for obtaining momentum-dependent phase shifts for elastic scattering from the shifts in energy levels on a Euclidean lattice at finite volume was provided many years ago [214] and extended to systems in motion [215], but its implementation for QCD remained computationally elusive until recently. A combination of theoretical, algorithmic, and computational advances has changed this situation dramatically, notably in the case of mesons. There have been several lattice calculations of the momentum-dependent phase shift of the ρ mesons [217–223]. This has now been extended to $K\pi$ scattering [224] in both P- and S-wave.

The formulation to extract amplitude information has been extended to the coupled-channel case [225–233], and applied to the case of the coupled $K\bar{K} - \pi\pi$ [234] system describing the ρ resonance to the $\eta K - \eta\pi$ system [57,180], and to the emblematic isoscalar sector [235,236]. Most recently, a calculation of coupled isoscalar $\pi\pi$, $K\bar{K}$, and $\eta\eta$ scattering for both S and D wave has been performed [235], revealing a qualitative interpretation of σ, f_0, and f_2 mesons similar to that seen in experiment. Collectively, these papers provide a comprehensive picture of SU(3) nonets both in the tensor and scalar sectors, albeit at unphysically large pion mass.

The application to baryons is far more limited, but nonetheless, important insights have been gained. In an approach in which the excited-state hadrons are treated as stable particles, a spectrum of baryons at least as rich as that of the quark model is revealed [237, 238], and evidence has been presented for “hybrid" baryon states, beyond those of the quark model, in which gluon degrees of freedom are essential [125]. Notably, this picture extends to the spectrum of Λ, Σ, Ξ, and Ω states where the counting of states reflects $SU(6) \times O(3)$ symmetry, and the presence of hybrids is common across the spectrum. In Fig. 46, baryon spectra from [24] are presented in units of Ω mass from LQCD calculations with ensemble $m_\pi = 391$ MeV (not yet at physical m_π).

The calculations for the baryon sector are incomplete, in that the momentum-dependent scattering amplitudes characterizing multi-hadron states have not been extracted. In comparison with the calculations for mesons cited above, the challenges are more computational than theoretical or conceptual. Nonetheless, the first direct calculation of the $I = 3/2$ $N\pi$ system in P-wave has now been performed [239], revealing a BW description of the amplitude commensurate with a phenomenological description of the Δ resonance. Thus we can be confident that the progress made in the meson sector will be reflected for the case of baryons in the coming years. Indeed,

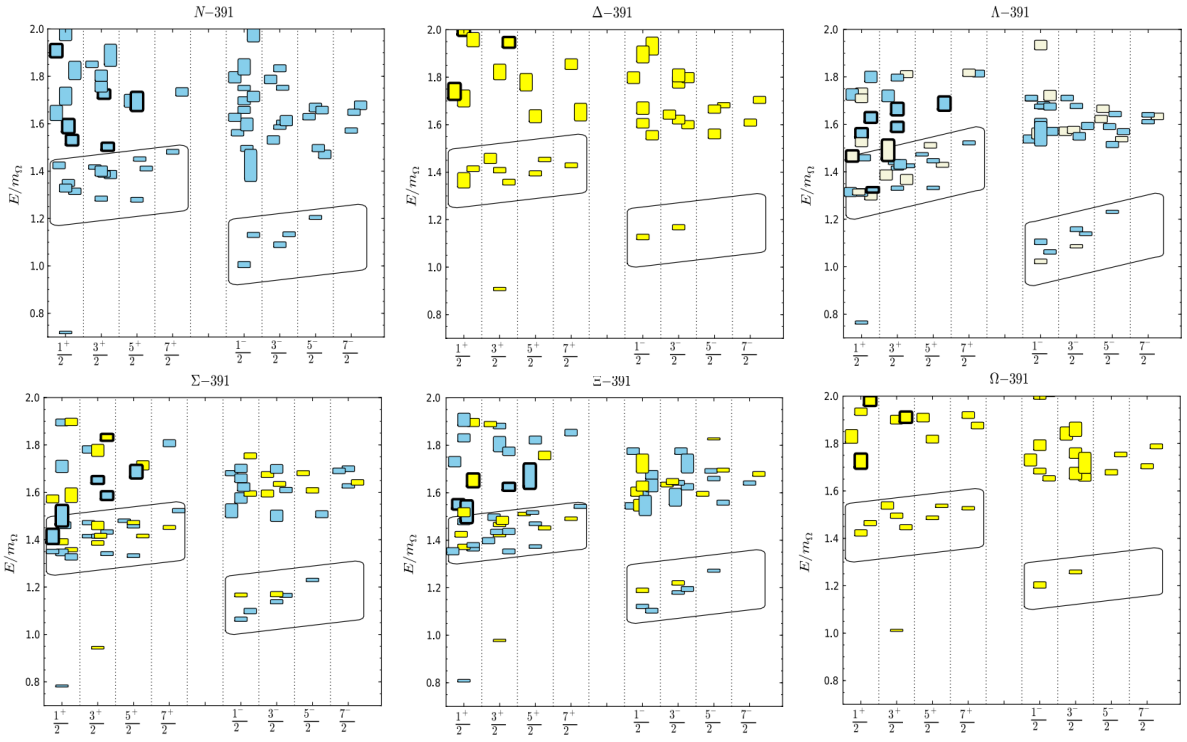

Figure 46: Results for baryon excited states using an ensemble with $m_\pi = 391$ MeV are shown versus J^P [24]. Colors are used to display the flavor symmetry of dominant operators as follows: blue for 8_F in N, Λ, Σ, and Ξ; beige for 1_F for Λ; yellow for 10_F in Δ, Σ, Ξ, and Ω. The lowest bands of positive- and negative-parity states are highlighted within slanted boxes. Hybrid states, in which the gluons play a substantive role, are shown for positive parity by symbols with thick borders.

many of the algorithmic and computational challenges, notably the need to perform calculations at physical quark masses, and the increasing complexity of the Wick contractions as the number of hadrons, and therefore quarks, is increased, are being addressed with the recently launched Exascale Computing Project of the DOE and NNSA, whose application to lattice QCD is described in Ref. [240].

A.4 πK Scattering Amplitudes and Strange Meson Resonances

It is instructive to compare the spectrum of the kaons to the corresponding spectra of the D and D_s mesons (see Ref. [241]). With exception of the still uncertain spin 0 state κ or $K_0^*(700)$ the known parts of the kaon, the D and D_s mesons are qualitatively very similar, but with somewhat different orderings [1].

The established part of the strange meson spectrum [1, 241] begins with the 0^- ground state, followed by the 1^- $K^*(892)$ vector meson meson state, which is followed by the two 1^+ states $K_1(1270)$, $K_1(1400)$, and then the recurrence $K^*(1410)$ of the 1^- vector meson state and the scalar meson state $K_0^*(1430)$. The spectrum of the D meson differs only in that the corresponding

scalar meson state $D_0^*(2400)$ slightly below, rather than slightly above the two 1^+ states $D_1(2420)$ and $D_1(2430)$.

This comparison of the spectra of the K, D and D_s mesons reveals the importance of settling the existence of the κ or $K_0^*(700)$, as its existence would settle the existence of a light scalar nonet below 1 GeV. This can be compared to the corresponding low-lying scalar meson states in the spectra of the charm and charm-strange mesons. In all these spectra, the first recurrence of that low scalar meson is well established by the states $K_0^*(1430)$, $D_0^*(2400)$, and $D_{s0}^*(2317)$. Given the very large width of the non-strange scalar meson $f_0(500)$ (or σ), it may be expected that the κ and the lowest charm strange, charm and charm-strange mesons will have similar large widths and threshold effects. Moreover, establishing firmly the existence of the $\kappa/K_0^*(700)$, with similar characteristics to the $\sigma/f_0(500)$, would also kill the glueball interpretations of the latter [242] or the dilatonic interpretation [243].

A.4.1 Previous Measurements for Strange Mesons:

Most of experimental data on $K\pi$ elastic scattering are obtained from KN scattering data under the assumption that they occur in reactions with one pion exchange. First measurements of $K\pi$ scattering in the reaction $K^-d \to p_s p K^-\pi^-$ produced in deuterium bubble chamber at 5.5 GeV/c were performed at Argonne [28], then in the reaction $K^-d \to p_s p K^-\pi^-$ in the deuterium bubble chamber at 3 GeV/c were performed at Saclay [29], in the reaction $K^\pm N$ in hydrogen bubble chamber in the momentum range 2.0 to 12.0 GeV/c were produced at CERN [30], in the reaction $K^-p \to K^-\pi^-\Delta^{++}$ at 4.25 GeV/c in hydrogen bubble chamber were produced at CERN as well [31]. Finally, high statistics measurements for reactions $K^\pm p \to K^\pm\pi^+ n$ and $K^\pm p \to K^\pm\pi^-\Delta^{++}$ at 13 GeV/c using spectrometers were performed at SLAC [26] and in the reaction $K^-p \to K^-\pi^+ n$ at 11 GeV/c were performed with the LASS Spectrometer [27].

A.4.2 Strange Exotics:

Two important motivations for new measurements of πK scattering amplitudes, are the attention received by Chiral Perturbation Theory [48–50, 244], resonance and unitarized models [61–65], and the need to confirm the existence of the exotic κ meson (or $K_0^*(700)$) in the $I = 1/2$ S-wave. This state would be the strange counterpart of the σ (or $f_0(500)$) meson which is now rather well established from $\pi\pi$ scattering (see the review [245]).

For spectroscopy, the relevance of this state, which according to the Review of Particle Physics [1] still "needs confirmation", is twofold:
First, establishing firmly its existence will settle the longstanding debate on whether there is a low-lying scalar nonet, with the $\sigma/f_0(500)$, $f_0(980)$, and $a_0(980)$ as partners.
But, second, because there is mounting evidence that such a nonet is actually exotic, i.e., not an ordinary quark-antiquark state [84, 246–254].

For Chiral Perturbation Theory the interest is on the low energy parameters, particularly the scalar scattering lengths. Below, we discuss the existing tension between dispersive analyses of experimental data [79, 255], theoretical predictions from Chiral Perturbation Theory [49, 50], and lattice calculations [52, 54, 56, 256]. One of the main difficulties for extracting reliable values form experiment is that the existing πK data starts at 750 MeV, and one needs an extrapolation down to the threshold at $\sim$635 MeV. Thus, the new KLF input at low energies, together with the general

improvement in statistics, will settle this issue.

At this point, it is worth noting the decisive role that the precise low-energy data from the NA48/2 experiment [257] played for the revision of the $\sigma/f_0(500)$ in the PDG2018. In this regard, improved measurements of the S-wave πK phase-shifts at low energy ($E \lesssim 1$ GeV) would be highly desirable in order to play a similar role for the $\kappa/K_0^*(700)$. Precision measurements of the S-wave phase-shifts would allow application of the Padé approximant method for determining the positions of the resonances (see, e.g., [202]. This method has been recently applied to πK scattering, and a κ pole has been found in Ref. [85] using as an input the fit to data constrained with Forward Dispersion Relations obtained in Ref. [79].

Alternatively, the most rigorous way to determine this resonance pole is using Roy-Steiner (RS) type equations [258, 259]. These equations rely on the first principles like analyticity, crossing as well as data. They provide a suitable framework for performing extrapolations in the low energy region, E < 1 GeV, of the S and P partial waves given sufficiently precise inputs at higher energies, essentially in the range 1 – 2 GeV. Extrapolations to complex values of the energies can be performed with the same accuracy as on the real axis. Unlike the Padé approximant approach, the extrapolation of the $I = 1/2$ S-wave from the RS equations requires inputs from other partial waves as well since the equations form a coupled system. Based on the existing data set, an estimate of the κ pole position from the RS equations was performed in Ref. [11]. Note that no input on πK scattering in the scalar partial waves below 1 GeV was used for this estimate. Using this RS equations with the data produced in KLF would produce an actual experimental and rigorous determination of the κ pole.

In the P-wave, finally, the studies by the LASS Collaboration [27, 260] have identified besides the well known $K^*(892)$ a new meson, the $K^*(1410)$. This meson has an unexpectedly low mass as it appears to be essentially degenerate with the non-strange $\rho(1450)$ or $\omega(1420)$ vector mesons. Its properties are not very precisely known at present.

A.4.3 Status of πK Scattering Measurements:

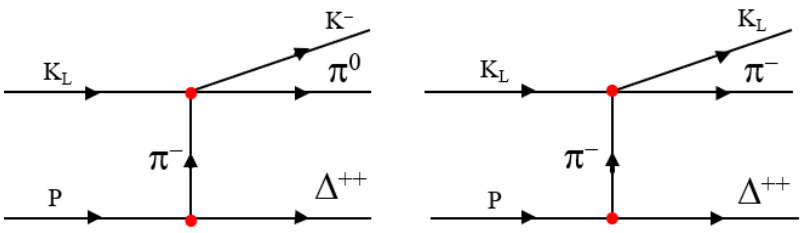

Figure 47: Illustration of the contribution from one-pion exchange, which is dominant at small momentum transfer, to the production amplitude. Left: $K_L p \to K^- \pi^0 \Delta^{++}$ or Right: $K_L p \to K_L \pi^- \Delta^{++}$.

The traditional method for measuring $\pi K \to \pi K$ amplitudes is from production experiments like

$$Kp \to K\pi p, \quad Kp \to K\pi n, \quad Kp \to K\pi\Delta \tag{14}$$

focusing on the region of small momentum transfers $|t| < 0.1 - 0.2\,\text{GeV}^2$, which is accessible with kaon beams of a few GeV. In this region, the amplitude is dominated by the one pion exchange (OPE) contribution, see Fig. 47. Depending on the particular production process Eq. (14), these

will carry different Clebsch-Gordan coefficients for combinations of the $I = 1/2$ and $I = 3/2$ $K\pi$ scattering amplitudes. For example, the reaction $K_L p \to K^- \pi^0 \Delta^{++}$ (Fig. 47 (left)) is proportional to $(1/3) \cdot (-T^{1/2} + T^{3/2})$ while reaction $K_L p \to K_L \pi^- \Delta^{++}$ (Fig. 47 (right)) is proportional to $(1/3) \cdot (T^{1/2} + 2T^{3/2})$, where $T^{1/2}$ and $T^{3/2}$ correspond to the $K\pi$ scattering isospin $I = 1/2$ and $I = 3/2$ amplitudes, respectively. These two independent measurements in principle allow a separation of isospin $1/2$ and $3/2$ amplitudes. A similar method (OPE approximation) was used for the extraction of $\pi\pi \to \pi\pi$ elastic scattering amplitudes, further details can be found in the book [261] or in the recent review by Peláez [245]. The two experiments performed at SLAC [26, 27] have the largest statistics and provide the best determinations of the πK scattering amplitudes at present. They cover the energy ranges $0.73 \leq E \leq 1.85$ GeV (Ref. [26]) and $0.83 \leq E \leq 2.52$ GeV (Ref. [27]), respectively. References to earlier works can be found in the review [262]. -

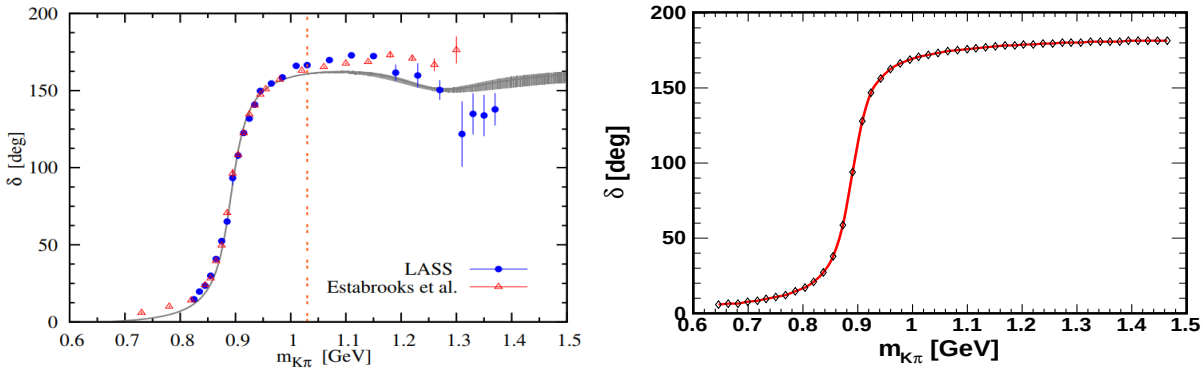

Figure 48: Phase of the πK vector form factor. Left: Experimental data from Estabrooks *et al.* [26] and LASS Collaboration [27]. The opening first inelastic $K^*\pi$ channel is indicated by the dashed vertical line. The gray band represents the extrema from the fits of Table 3 in the paper by Boito *et al.* [76] constrained by the data on $\tau \to K\pi\nu_\tau$ decay from Belle experiment [77] with additional constrains from a compilation of K_{l3} decay analyses [264]. Right: 100 days of running with KLF, simulated with the $K^{*-}(892)$ (see text for details).

A completely different approach to measuring the πK phase-shifts makes use of the Watson's theorem for weak decay form factors. In this manner, the phase-shift difference $\delta_S - \delta_P$ was determined by analyzing the $D^+ \to K^- \pi^+ e^+ \nu$ by the *BABAR* Collaboration [263]. The results are in agreement with the LASS determination but more statistics are needed before one reaches a comparable precision. Similarly, from the measurement of the energy distribution in the decay $\tau^- \to K_S \pi^- \nu$ by the Belle Collaboration [77] the P-wave phase has been determined [76], relying on the analyticity properties of the form factor. Their result is shown in Fig. 48 (left). While Fig. 48 (right) shows the expected results for 100 days of running with KLF, simulated with $K^{*-}(892)$ only. As one can see the proposed measurement will dramatically increase statistical precision of the world data and extend the measurement to the very low mass elastic scattering, as well as high mass inelastic scattering regions.

Since Watson's theorem is valid in the energy region of elastic scattering, these alternative phase determinations provide important information on the effective onset of inelastic scattering in the

various partial waves. This figure also shows that the determination of the phase shift in the region of the $K^*(1410)$ resonance is not very precise and could be improved.

The same form factors which appear in the $\tau \to K\pi\nu$ decays are also involved in the K_{l3} decay amplitudes: $K \to \pi e\nu$, $K \to \pi\mu\nu$. A series of new K_{l3} experiments were undertaken recently in order to improve the determination of V_{us} (see Ref. [264]). As shown in Ref. [264], an optimal analysis of the K_{l3} data is achieved by using a description of the two form factors involved based on phase dispersive representations rather than phenomenological polynomial or pole forms as done previously.The πK scattering also plays an important role in a number of three-body decays, like $D \to K\pi\pi$. Recently, a method was developed [265] which allows to compute the effect of the three-body re-scattering in terms of the known two-body $\pi\pi$ and πK T-matrices. This could be useful for identifying small CP violating effects in the charm sector.

A.4.4 Theory:

Up to now the only experimental data on s-wave for both isospin states $I = 1/2$ and $I = 3/2$ from the same experiment were obtained at SLAC by Estaabrooks *et al.* [26]. This limits precision to extract the mass and the width of the κ. On the left panel of Fig. 49, the SLAC data are presented with the theoretical extrapolation of the Roy-Steiner dispersive equations from Ref. [255]). On the right panel of Fig. 49, the S-wave phase shifts are presented with statistics based on 100 days of running with KLF. As one can see there is dramatic improvement not only in statistical uncertainties, but also in the number of points reaching to the much lower invariant masses of $K\pi$ system. The simulated data are obtained from the reactions $K_L p \to K^- \pi^0 \Delta^{++}$ and $K_L p \to (K_L)\pi^- \Delta^{++}$, where the K_L in the latter case is reconstructed via missing mass technique.

More details about MC simulations of $K\pi$ scattering can be found in Ref. [78].

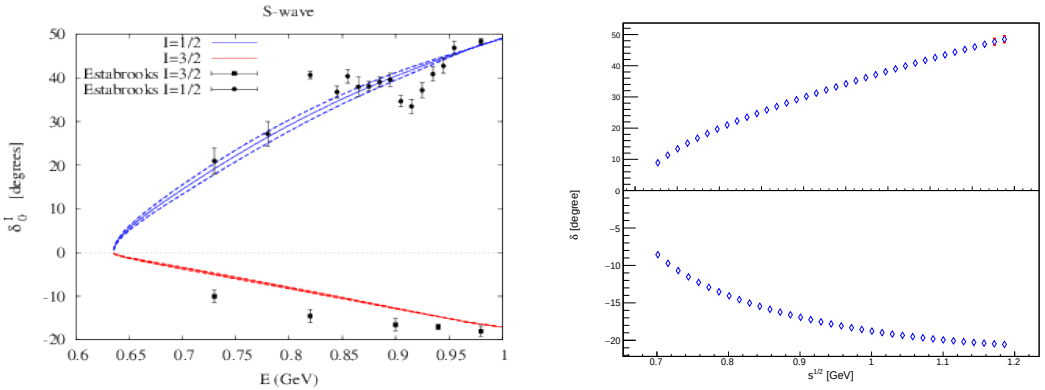

Figure 49: Left: Results for the S-wave phase shifts extrapolated below 1 GeV based on the Roy-Steiner dispersive equations (from Ref. [255]) compared with the experimental data from Ref. [26]. Right: Expected phase shift statistics for S-wave isospin $I = 1/2$ (upper half) and $I = 3/2$ (lower half) states simulated for 100 days of running with KLF. In both panels, phase shifts are plotted as a function of invariant mass of $K\pi$ system.

Pions and kaons are QCD pseudo-Goldstone bosons, therefore the πK amplitudes at low energy can be expressed as a chiral expansion. The NLO calculation was performed in Ref. [49] who

predict the following results for the scattering lengths,

$$a_0^{1/2} = 0.19 \pm 0.02, \quad a_0^{3/2} = -0.05 \pm 0.02 \tag{15}$$

(in units of m_π^{-1}). Verifying these predictions would provide an important check of the three-flavor chiral expansion. Based on experimental phase-shift measurements this is possible, in principle, using dispersion relations for extrapolating down to the threshold. The Roy-Steiner equations provide a suitable framework for that. This is illustrated in Fig. 49 which shows the extrapolated results for the S-waves in the region $E \leq 1$ GeV, based on experimental inputs from Refs. [26, 27] in the region $E > 1$ GeV. It is clear that the availability of more precise data in the range $E \leq 1$ GeV would greatly strengthen the efficiency of this method. We note that a direct experimental estimate of the scattering length difference was performed recently [266] based on the lifetime of the π^+K^- atom at the DIRAC experiment at CERN. Unfortunately, the experimental errors are still too large and do not provide really precise information about the pion-kaon scattering lengths.

Alternatively, scattering phase shifts can be computed in lattice QCD using Lüscher's method [214]. Results for πK phase shifts were first obtained in Refs. [55, 267] and in Ref. [57]. In this last work, the influence of one inelastic scattering two-body channel is accounted for and m_π = 391 MeV. Very recently, results for m_π = 230 MeV have been presented [224]. Once physical values for m_π are reached, these lattice QCD results can be compared directly to experimental measurements of the πK phase shifts which provides a direct probe of the quality of the numerical QCD solution.

To Summarize: As it is discussed above, there are many aspects of πK scattering that require improvement on the existing measurements. First of all, it is the quest to establish existence or non-existence of scalar κ meson either to complete scalar meson nonet or to find an alternative way to explain well established non-strange σ, a_0, and f_0 meson family. Besides there are some fundamental questions that need to be clarified. In particular, currently there is a sizable tension between the values of scattering lengths obtained from dispersive analyses of data [79, 255], on one side, and the predictions from Chiral Perturbation Theory [49, 50] and lattice calculations [52, 54, 56, 256], on the other side. The values of the threshold parameters are related to two important questions. On the one hand, for phenomenology, establishing the convergence and reliability of SU(3) Chiral Perturbation Theory. On the other hand, for the foundations of QCD, the size of the strange versus the non-strange chiral condensate, i.e., the detailed pattern of the QCD spontaneous chiral symmetry breaking is very important.

As previously noticed and as shown in Fig. 49, the existing πK data starts at 750 MeV, and one needs an extrapolation down to the threshold at $\sim$635 MeV. Hence, the new KLF data at low energies, together with the general improvement in statistics, will be determinant to resolve this tension.

A.5 Current Hadronic Projects

Past measurements involving kaon scattering measurements were made at a variety of laboratories, mainly in the 1960s and 1980s when experimental techniques were far inferior to the standards of today (short summary is given in Appendices A.3.1 and A.4.1. It is important to recognize that

current projects are largely complementary to the proposed JLab KL hadron beam facility. We summarize the status of the J-PARC, Belle, *BABAR* PANDA, COMPASS, and LHCb efforts here.

A.5.1 J-PARC, Japan:

While J-PARC has a whole program of charged strange particle and hypernuclear reactions [268], the photon beam at KLF allows unique access to other channels. J-PARC provides separated secondary beam lines up to 2 GeV/c (Table 8). The operation of the Hadron Experimental Facility resumed in April of 2015 following a two-year suspension to renovate the facility after the accident that occurred in May 2013 [270]. The primary beam intensity is currently 50 kW, and can be upgraded to 85 kW. This will correspond to $\sim 10^9$ ppp (particles per pulse) for pion beam intensity and to $\sim 10^6$ ppp for negative kaon beam flux. The K/π ratio is expected to be close to 10, which is realized with double-stage electrostatic separators. One of the main problems in the K/π separation is a high duty-factor of the J-PARC Complex.

Beamline	Particle	Momentum (GeV/c)	Number of particles per spill	Characteristics
K1.8	$K^{\pm}$, $\pi^{\pm}$	<2.0	10^6 K^-	separated
K1.8BR	$K^{\pm}$, $\pi^{\pm}$	<1.1	10^5 K^-	separated
KL	K_L	2.1 in ave.	10^7 K_L	to 16°
High-p	p		10^{10} p	primary protons
	$\pi^{\pm}$	<31	10^7 π	
K1.1	$K^{\pm}$, $\pi^{\pm}$	<1.2	10^6 K^-	separated
		0.7∼0.8		lower momentum [K1.1BR]
HIHR	$\pi^{\pm}$	<2.0	2.8×10^8 π^-	separated $\times 10$ better $\Delta p/p$
K10	$K^{\pm}$, $\pi^{\pm}$, $\bar{p}$	<10	10^7 K^-	separated
new KL	K_L	5.2 in ave.	10^8 K_L	to 5° n/K_L optimized

Table 8: J-PARC beamlines in the Hadron Experimental Facility from Ref. [269]. Top part of Table gives information about beamlines in the present hall, while bottom part information is about new beamlines in the extended area.

With K^- beams, currently there is no proposal specific for $S = -1$ hyperons, but the cascades will be studied in the early stage of E50 [271], hopefully in a few years. The beam momentum bite, $\Delta p/p$, is strongly depending on the configuration of the beam line spectrometer, but one can determine beam momentum with the resolution of $\Delta p/p \sim 10^{-3}$ or 10^{-4}. One can think that the systematic study for $S = -1$ hyperons even with charged kaons is desirable and J-PARC folks think that such a study is definitely needed but currently there is no room to accept a new proposal to require a long beamline. J-PARC is focusing on hypernuclei physics [272].

There is no K_L beamline for hyperon physics at J-PARC. It is 100 % dedicated to the study of CP-violation. The momentum is spread out from 1 to 4 GeV/c, there is no concept of $\Delta p/p$ since the beam cannot be focused with EM devices.

A.5.2 Belle, Japan:

At B Factories large samples of charmed baryons are produced in the decays of B mesons as well as from the $e^+e^- \to c\bar{c}$ continuum [273]. The masses, widths and branching fractions of many ground state singly-charmed baryons and their excitations have been measured at Belle [274], like $\Xi_c(2645)^{0,+}$, $\Xi_c(2790)^{0,+}$, $\Xi_c(2815)^{0,+}$, $\Xi_c(2980)^{0,+}$, Ξ_c' [275–277]; $\Sigma_c(2455)^{0,++}$, and $\Sigma_c(2520)^{0,++}$ [278].

Many charmed baryons and their decay modes have been discovered at Belle [279] or confirmed after LHCb recently, for example: $\Xi_c(3055)^+$ [280]; $\Lambda_c^+ \to pK^+\pi^-$ [281]; $\Xi_c(3055)^0$, $\Xi_c(3055)^+/\Xi_c(3080)^+ \to \Lambda D^+$ [282]; $\Omega_c(3000)$, $\Omega_c(3050)$, $\Omega_c(3066)$, $\Omega_c(3090)$ [283]; $\Xi_c^0 \to \Xi^-\pi^+$, $\Xi_c^0 \to \Lambda K^-\pi^+$, $\Xi_c^0 \to pK^-K^-\pi^+$ [284]; $\Xi_c^+ \to \Xi^-\pi^+\pi^+$, $\Xi_c^+ \to pK^-\pi^+$ [285]. Fifty times larger data sample expected from Belle II will open new era in the precision studies of charmed baryons in the coming decade [286].

Recently, the Belle Collaboration posted an article in arXiv where it studies $D^0 \to K - \pi^+\eta$ decay [287]. In this analysis, it is clearly shown that along with the contribution from higher mass K^*'s the S-wave below $K^*(892)$ is needed to get a reasonable fit to the experimental squared invariant mass distribution of $K^-\pi^+$ from the threshold up to 1.8 GeV^2 (see Fig. 50). Actually,

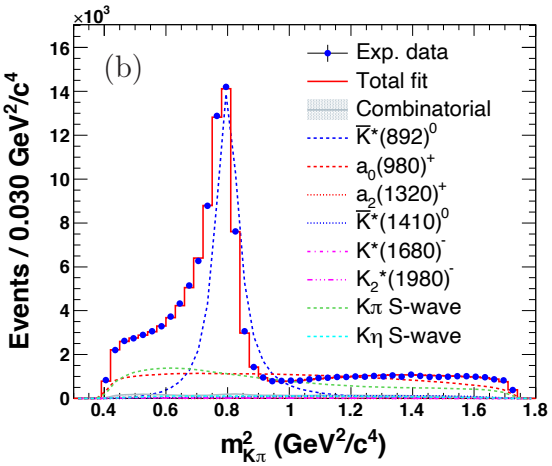

Figure 50: Squared $K^-\pi^+$ invariant mass distribution from Dalitz plot analysis of $D^0 \to K^-\pi^+\eta$ decay at Belle.

predictions for a sizeable S-wave $\bar{K}\pi$ contribution in addition to $\bar{K}^*$ excitation have already been done in the related reaction $\bar{B}^0 \to J/\psi\pi^+K^-$ reaction (see Fig. 6 of Ref. [288]).

A.5.3 *BABAR* USA:

Charmonium decays can be used to obtain new information on light meson spectroscopy. In e^+e^- interactions, samples of charmonium decays can be obtained using different processes, in particular η_c decays can be produced in two-photon interactions. In this process, events are selected in which the e^+ and e^- beam particles are scattered at small angles and remain undetected. Two-photon events are isolated from background requiring the conservation of the transverse momentum with respect to the beam axis. The study of the η_c three-body hadronic decays is found to proceed almost entirely through the intermediate production of scalar meson resonances.

BABAR experiment has performed Dalitz plot analyses of $\eta_c \to K^+K^-\eta$ ($\eta \to \gamma\gamma$ and $\eta \to \pi^+\pi^-\pi^0$), $\eta_c \to K^+K^-\pi^0$, and $\eta_c \to K^0_S K^\pm\pi^\mp$. These three η_c decays have provided new information on the properties of the strange scalar mesons.

The isobar model Dalitz plot analysis of the $\eta_c \to K^+K^-\eta$ has provided the unexpected observation of $K^*_0(1430) \to K\eta$ [289]. The Dalitz plot projection on the $m^2(K^\pm\eta)$ is shown in Fig. 51 (left), togheter with the fit projection. A clear signal of $K^*_0(1430)$ can be observed.

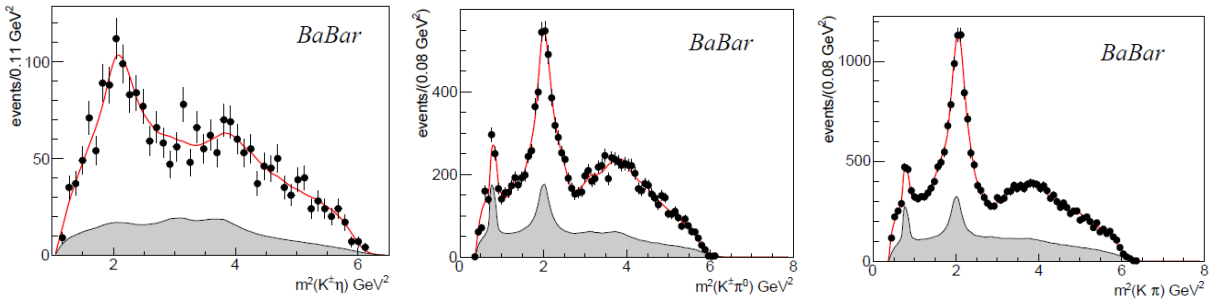

Figure 51: Left: The $m^2(K^\pm\eta)$ from $\eta_c \to K^+K^-\eta$ Dalitz plot projection from *BABAR*. The superimposed curve results from the Dalitz plot analysis. The shaded region show the background estimate obtained by interpolating the results of the Dalitz plot analyses of the sideband regions. Middle: The $m^2(K^\pm\pi^0)$ from $\eta_c \to K^+K^-\pi^0$ Dalitz plot projection from *BABAR*. The superimposed curve results from the Dalitz plot analysis. The shaded region show the background estimate obtained by interpolating the results of the Dalitz plot analyses of the sideband regions. Right: The $m^2(K\pi)$ from $\eta_c \to K^0_S K^\pm\pi^\mp$ Dalitz plot projection from *BABAR*. The superimposed curve results from the Dalitz plot analysis. The shaded region show the background estimate obtained by interpolating the results of the Dalitz plot analyses of the sideband regions.

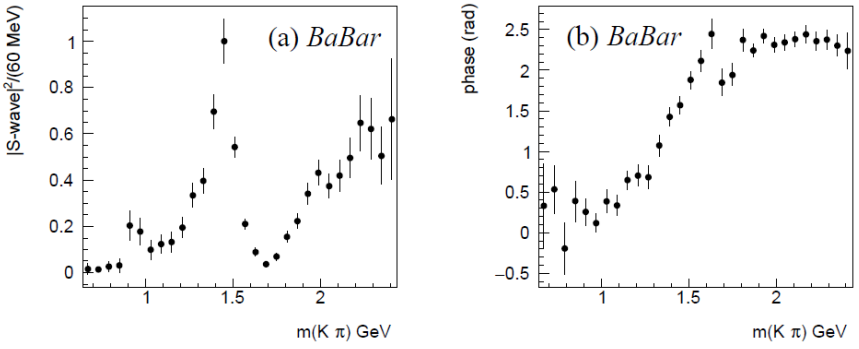

Figure 52: (a) Squared $K\pi$ $\mathcal{S}$-wave and (b) phase from the QMI analysis of $\eta_c \to K^+K^-\pi^0$, and $\eta_c \to K^0_S K^\pm\pi^\mp$ decays.

The corresponding $m^2(K^\pm\pi^0)$ projection from the $\eta_c \to K^+K^-\pi^0$ Dalitz plot analysis is shown in Fig. 51 (middle). The decay is dominated by the $K^*_0(1430)K$ final state.

In the Dalitz plot analysis of $\eta_c \to K^+K^-\pi^0$, a likelihood scan allows to obtain the best-fit param-

eters for the $K_0^*(1430)$:

$$\begin{aligned} m(K_0^*(1430)) &= (1438 \pm 8 \pm 4)\ \text{MeV} \\ \Gamma(K_0^*(1430)) &= (210 \pm 20 \pm 12)\ \text{MeV}. \end{aligned} \tag{16}$$

The observation of the $K_0^*(1430)$ in both the $K\eta$ and $K\pi^0$ decay modes permits a measurement of the corresponding branching ratio:

$$\frac{BR(K_0^*(1430) \to \eta K)}{BR(K_0^*(1430) \to \pi K)} = 0.092 \pm 0.025^{+0.010}_{-0.025}. \tag{17}$$

BABAR has also performed a Quasi Model Independent Partial Wave Analysis (QMI) [290] of $\eta_c \to K^+K^-\pi^0$, and $\eta_c \to K^0_S K^\pm\pi^\mp$ decays [291]. In the QMI, the $K\pi$ mass spectrum is divided into 30 equally spaced mass intervals 60 MeV wide and for each bin two new free parameters are added to the fit, the amplitude and the phase of the $K\pi$ $\mathcal{S}$-wave. The corresponding Dalitz plot projection on $m^2(K\pi)$ from $\eta_c \to K^0_S K^\pm\pi^\mp$ is shown in Fig. 51 (right) and is dominated by the $K_0^*(1430)$ resonance.

The resulting $K\pi$ $\mathcal{S}$-wave squared amplitude and phase, averaged over the two η_c decay modes, is shown in Fig. 52. The $K\pi$ $\mathcal{S}$-wave is dominated by the $K_0^*(1430)$ resonance, with little evidence of $\kappa(700)$. The phase motion shows the expected behaviour for the $K_0^*(1430)$ resonance.

A.5.4 PANDA, Germany:

The PANDA experiment [292] will measure annihilation reactions of antiprotons with nucleons and nuclei in order to provide complementary and in part uniquely decisive information on a wide range of QCD aspects. The scientific scope of PANDA is ordered into several pillars: hadron spectroscopy, properties of hadrons in matter, nucleon structure and hypernuclei. Antiprotons are produced with a primary proton beam, collected and phase-space cooled in the Collector Ring (CR), and then transferred to the High Energy Storage Ring (HESR) where they are stacked, further phase-space cooled, and then directed onto an internal target located at the center of the $\overline{P}$ANDA detector. The facility will start with a luminosity of 10^{31} cm^2/s and a momentum resolution of $\Delta p/p = 10^{-4}$, and later improve to 2×10^{32} and 4×10^{-5}, respectively. The large cross section into baryon-antibaryon final states (e.g., $\sim$1 μb for $\Xi\overline{\Xi}$ or 0.1 μb for $\Omega\overline{\Omega}$) make spectroscopic studies of excited multi-strange hyperons a very compelling part of the initial program of PANDA, which is expected to commence by 2025 [293].

A.5.5 COMPASS, CERN:

In 2008 and 2009, the COMPASS experiment at CERN used a negatively charged hadron beam with a momentum of 190 GeV/c to study the light meson spectrum. This secondary beam from the CERN SPS accelerator was composed of 97% pions, which produced a world-leading data set of diffractively produced three-pion final states [294]. An admixture of about 2.6% of kaons in the beam was tagged by Cherenkov detectors in the beam line, which allows the COMPASS collaboration to investigate the spectrum of strange mesons in various final states. The number of signal events in the sample of Kaon diffraction into $K^-\pi^-\pi^+$, for instance, surpasses any previous measurement by a factor of 4 [295]. An elaborate partial-wave decomposition revealed signals in the mass region of well-known states, such as $K_1(1270)$ and $K_1(1400)$. In addition, potential signals from excited states, such as $K_1(1650)$, were observed.

As a continuation of these effort, the newly formed COMPASS++/AMBER collaboration has included a kaon spectroscopy program in its Letter of Intent [296]. By installing a radio-frequency (RF) separation stage in the beam line, the kaon contribution in the beam can be considerably enhanced, aiming at a 20-times larger data set compared to what has been measured so far. The energy of the kaon beam would be somewhere between 50 GeV and 75 GeV, where diffractive production via Pomeron exchange is the dominant process and kaon beam diffraction can be well separated from target excitation. The charged kaon beam can also be used to extend the ongoing χPT investigations [297] into the strangeness sector, e.g., to measure the polarizability of the kaon.

Since the program with RF-separated kaon beams will require a considerable commitment by CERN to upgrade the existing beam line infrastructure, it was not included in the SPSC proposal for COMPASS++/AMBER Phase-1 [298]. The full project described in the Letter of Intent is expected to stretch across the next 10 to 15 years.

A.5.6 LHCb, CERN:

The LHCb experiment is designed to study the properties and decays of heavy flavored hadrons produced in proton-proton collisions at the LHC. The collisions production recorded between 2010 and 2016 provided the world's largest data sample of beauty and charm hadrons. Various spectroscopy studies have been conducted in LHCb collaborations for such states. Recently, important results in exotics hadron search have been obtained, such as the discovery of the first pentaquark states [299] and the existence confirmation of the exotic meson $Z_c(4430)$ [300], these results have increased the interest in spectroscopy of heavy hadrons. Moreover, LHCb collaboration published several spectroscopy studies of unexplored charmed baryons, for example the observation of new Ω_c states [185] and the observation of the Ξ_{cc} [301]. Regarding the spectroscopy studies of bottom baryons, LHCb collaboration published many interesting achievements in this topic, among them the recently observed Ω_b states via strong decays to $\Xi_b^0 K^-$ [302], observed in Tevateron a decade ago. In the mesonic sector, divers spectroscopy studies has been performed, for example, in the charmonium sector [303] and the search for the excited D_s and B_s mesons [304–307].

A.6 Additional Physics Potential with a K_L Beam

There are two particles in the reaction $K_L p \to \pi Y$ and KY that can carry polarization: the target and recoil baryons. Hence, there are two possible double-polarization experiments: target/recoil. The total number of observables is three. The formalism and definitions of observables commonly used to describe the reaction $K_L p \to KY$ is given in Appendix A.3. Although one cannot easily measure recoil polarization with GlueX, the self-analyzing decay of hyperons makes this possible. Double-polarization experiments, using, e.g., a polarized target like FROST [123], will however be left for future proposal(s).

As stated in the summary of Mini-Proceedings of the Workshop on Excited Hyperons in QCD Thermodynamics at Freeze-Out (YSTAR2016) [308] (see Appendix A.1): a very interesting further opportunity for the KL Facility is to investigate KL reactions on complex nuclei. By requiring an appropriate beam momentum along with a fast forward-going pion, events can be identified in which a hyperon is produced with low relative momentum with respect to the target nucleus, or even hypernuclear bound states. Baryons with strangeness embedded in the nuclear environment,

hypernuclei or hyperatoms, are the only available tool to approach the many-body aspect of the three-flavor strong interaction. Furthermore, appropriate events with a forward-going K^+ could deposit a doubly-strange hyperon into the nucleus, enabling searches for and studies of double-Λ hypernuclei.

Similarly, the scattering of kaons from nuclear targets could be a favorable method to measure the matter form factor (and, therefore, neutron skin) of heavy nuclei, with different and potentially smaller systematics than other probes. The character of the neutron skin, therefore, has a wide impact and the potential to give important new information on neutron star structure and cooling mechanisms [309–313], searches for physics beyond the standard model [314, 315], the nature of 3-body forces in nuclei [316, 317], collective nuclear excitations [318–321] and flows in heavy-ion collisions [322, 323]. Theoretical developments and investigations will be required to underpin such a program, but science impact of such measurements would be high.

The high flux K_L beam allows a first measurement of a K_L beta-decay, $K_L^0 \rightarrow K^+ e^- \bar{\nu}_e$ [324], having about 700 in-flight beta-decay events produced during 200 days of the beam with ability to measure about 20-30 of these rare decay events. A fairly simple dedicated detector system might be necessary for achieving decent detection efficiency for this extremely rare decay branch, $BR \sim 4 \times 10^{-9}$ [324].

Further potential exists to search for—or exclude—possible exotic baryonic states that cannot easily be described by the usual three-valence-quark structure. Recent results from LHCb provide tantalizing hints for the existence of so-called pentaquarks that include a charm valence quark [299]; however, the interpretation of those results is under discussion. In contrast, elastic scattering of K_L with a hydrogen target gives unambiguous information on the potential existence of such states in the strange sector. With the given flux of K_L at the proposed facility, a clear proof of existence or proof of absence will be obtained within the integrated luminosity required for the excited hyperon spectroscopy program that forms the basis of this proposal.

The physics potential connected with studies of CP-violating decays of the K_L is very appealing; however, that topic is not currently the focus of this proposal, since a detailed comparison with the competition from existing and upcoming experiments is needed in order to identify the most attractive measurements that could be done at the proposed KL Facility at JLab.

References

[1] M. Tanabashi *et al.* [Particle Data Group], "Review of Particle Physics," Phys. Rev. D **98**, no. 3, 030001 (2018).

[2] B. M. K. Nefkens, "The Crystal Ball baryon resonance program," πN Newslett. **14**, 150 (1998).

[3] R. Koniuk and N. Isgur, "Where have all the resonances gone? An analysis of baryon couplings in a Quark Model With Chromodynamics," Phys. Rev. Lett. **44**, 845 (1980).

[4] A. Aprahamian *et al.*, *Reaching for the Horizon: The 2015 Long Range Plan for Nuclear Science*: http://science.energy.gov/np/nsac/.

[5] A. AlekSejevs *et al.* [GlueX Collaboration], "An initial study of mesons and baryons containing strange quarks with GlueX," arXiv:1305.1523 [nucl-ex].

[6] H. Al Ghoul *et al.* [GlueX Collaboration], "Measurement of the beam asymmetry Σ for π^0 and η photoproduction on the proton at $E_\gamma = 9$ GeV," Phys. Rev. C **95**, no. 4, 042201 (2017).

[7] Y. Qiang, Y. I. Azimov, I. I. Strakovsky, W. J. Briscoe, H. Gao, D. W. Higinbotham, and V. V. Nelyubin, "Properties of the $\Lambda(1520)$ resonance from high-precision electroproduction data," Phys. Lett. B **694**, 123 (2011).

[8] W. J. Briscoe, M. Döring, H. Haberzettl, D. M. Manley, M. Naruki, I. I. Strakovsky, and E. S. Swanson, "Physics opportunities with meson beams," Eur. Phys. J. A **51**, no. 10, 129 (2015).

[9] C. Amsler, S. Eidelman, T. Gutsche, C. Hanhart, S. Spanier, and N. A. Törnqvist, "Note on scalar mesons below 2 GeV," in: Ref. [10].

[10] C. Patrignani *et al.* [Particle Data Group], "Review of particle physics," Chin. Phys. C **40**, no. 10, 100001 (2016).

[11] S. Descotes-Genon and B. Moussallam, "The K*0 (800) scalar resonance from Roy-Steiner representations of pi K scattering," Eur. Phys. J. C **48**, 553 (2006).

[12] Web page of the Workshop on *Physics with Neutral Kaon Beam at JLab* (KL2016), JLab, Newport News, VA, USA, Feb. 2016: https://www.jlab.org/conferences/kl2016/ contains presentations.

[13] Web page of the Workshop on *Excited Hyperons in QCD Thermodynamics at Freeze-Out* (YSTAR2016), JLab, Newport News, VA, USA, Nov. 2016: https://www.jlab.org/conferences/YSTAR2016/ contains presentations.

[14] Web page of the Workshop on *New Opportunities with High-Intensity Photon Sources* (HISP2017), CUA, Washington, DC, USA, Feb. 2017: https://www.jlab.org/conferences/HIPS2017/ contains presentations.

[15] Web page of the Workshop on *Pion-Kaon Interactions* (PKI2018), JLab, Newport News, VA, USA, Feb. 2018: https://www.jlab.org/conferences/pki2018/ contains presentations.

[16] M. Amaryan, U.-G. Meißner, C. Meyer, J. Ritman, and I. Strakovsky, eds., Mini-Proceedings, *Workshop on Physics with Neutral Kaon Beam at JLab* (KL2016); arXiv:1604.02141 [hep–ph].

[17] *Physics opportunities with secondary K_L beam at JLab*, Spokesperson: M. Amaryan [GlueX Collaborations], JLab LoI12–15–001, Newport News, VA, USA, 2015.

[18] *Strange hadron spectroscopy with a secondary KL beam at GlueX*, Spokespersons: M. J. Amaryan, M. Bashkanov, J. Ritman, J. R. Stevens, and I. I. Strakovsky [GlueX Collaboration], JLab Proposal PR12–17–001, Newport News, VA, USA, 2017; arXiv:1707.05284 [hep–ex].

[19] *Photoproduction of the very strangest baryons on the proton target in CLAS12*, Spokespersons: L. Guo, M. Dugger, J. Goetz, E. Pasyuk, I.I. Strakovsky, D.P. Watts, N. Zachariou, and V. Ziegler [Very Strange Collaboration for CLAS Collaboration], JLab Proposal E12–11–005A, Newport News, VA, USA, 2013.

[20] *Nucleon resonance structure studies via exclusive KY electroproduction at 6.6 GeV and 8.8 GeV*, Spokespersons: D.S. Carman, R. Gothe, and V. Mokeev [CLAS Collaboration], JLab E12–16–010A, Newport News, VA, USA, 2016.

[21] M. Amaryan, E. Chudakov, K. Rajagopal, C. Ratti, J. Ritman, and I. Strakovsky, eds., Mini-Proceedings, *Workshop on Excited Hyperons in QCD Thermodynamics at Freeze-Out* (YSTAR2016); arXiv:1701.07346 [hep–ph].

[22] T. Horn, C. Keppel, C. Munoz-Camacho, and I. Strakovsky, eds., Mini-Proceedings, *Workshop on High-Intensity Photon Sources* (HIPS2017); arXiv:1704.00816 [nucl–ex].

[23] M. Amaryan, C. Meyer, U.-G. Meißner, J. Ritman, and I. Strakovsky, eds., Mini-Proceedings, *Workshop on Pion-Kaon Interactions* (PKI2018); arXiv:1804.06528 [hep–ph].

[24] R. G. Edwards *et al.* [Hadron Spectrum Collaboration], "Flavor structure of the excited baryon spectra from lattice QCD," Phys. Rev. D **87**, no. 5, 054506 (2013).

[25] M. Bashkanov, N. Zachariou, K. Park, S, Taylor, and I. Strakovsky, "KLF Analysis Report: Hyperon Spectroscopy Simulation Studies," KLF Note, 2020; https://wiki.jlab.org/klproject/images/4/46/KLF-Analysis-Report.pdf .

[26] P. Estabrooks, R. K. Carnegie, A. D. Martin, W. M. Dunwoodie, T. A. Lasinski, and D. W. G. S. Leith, "Study of K pi scattering using the reactions K+- p —> K+- pi+ n and K+- p —> K+- pi- Delta++ at 13-GeV/c," Nucl. Phys. B **133**, 490 (1978).

[27] D. Aston *et al.*, "A study of K- pi+ scattering in the reaction K- p —> K- pi+ n at 11-GeV/c," Nucl. Phys. B **296**, 493 (1988).

[28] Y. Cho *et al.*, "Study of k- pi- scattering using the reaction k- d —> k- pi- p p(s)," Phys. Lett. **32B**, 409 (1970).

[29] A. M. Bakker *et al.*, "A determination of the i=3/2 k pi elastic-scattering cross section from the reaction k- n —> p k- pi- at 3 GeV/c," Nucl. Phys. B **24**, 211 (1970).

[30] D. Linglin *et al.*, "K- pi- elastic scattering cross-section measured in 14.3 GeV/c k- p interactions," Nucl. Phys. B **57**, 64 (1973).

[31] B. Jongejans, R. A. van Meurs, A. G. Tenner, H. Voorthuis, P. M. Heinen, W. J. Metzger, H. G. J. M. Tiecke, and R. T. Van de Walle, "Study Of The I = 3/2 K- Pi- Elastic Scattering From The Reaction K- P —> K- Pi- P Pi+ At 4.25-GeV/c Incident K- Momentum," Nucl. Phys. B **67**, 381 (1973).

[32] H. Al Ghoul *et al.* [GlueX Collaboration], "First results from the GlueX Experiment," AIP Conf. Proc. **1735**, 020001 (2016).

[33] P. Capiluppi, G. Giacomelli, G. Mandrioli, A. M. Rossi, P. Serra-Lugaresi, and L. Zitelli, "A Compilation of K0(L) p Cross-sections," IFUB-81-25.

[34] R. Yamartino *et al.*, "A Study of the Reactions anti-K0 p —> Lambda pi+ and anti-K0 p —> Sigma0 pi+ from 1-GeV/c to 12-GeV/c," Phys. Rev. D**10**, 9 (1974); Ph. D Thesis, SLAC Stanford University, 1974; SLAC-R-0177, SLAC-R-177, SLAC-0177, SLAC-177.

[35] D. A. Sharov, V. L. Korotkikh, and D. E. Lanskoy, "Phenomenological model for the Kbar N –> K Xi reaction," Eur. Phys. J. A **47**, 109 (2011).

[36] M. Mai and U.-G. Meißner, "New insights into antikaon-nucleon scattering and the structure of the Lambda(1405)," Nucl. Phys. A **900**, 51 (2013).

[37] P. C. Bruns, M. Mai, and U.-G. Meißner, "Chiral dynamics of the S11(1535) and S11(1650) resonances revisited," Phys. Lett. B **697**, 254 (2011).

[38] M. Mai and U.-G. Meißner, "Constraints on the chiral unitary $\bar{K}N$ amplitude from $\pi\Sigma K^+$ photoproduction data," Eur. Phys. J. A **51**, no. 3, 30 (2015).

[39] Y. Ikeda, T. Hyodo, and W. Weise, "Chiral SU(3) theory of antikaon-nucleon interactions with improved threshold constraints," Nucl. Phys. A **881**, 98 (2012).

[40] K. Moriya *et al.* [CLAS Collaboration], "Measurement of the $\Sigma\pi$ photoproduction line shapes near the $Lambda(1405)$," Phys. Rev. C **87**, no. 3, 035206 (2013).

[41] C. M. Jenkins *et al.*, "Existence Of Ξ Resonances Above 2-GeV," Phys. Rev. Lett. **51**, 951 (1983).

[42] D. Cline, J. Penn, and D. D. Reeder, "The k+ n charge-exchange reaction at 5.5 GeV/c," Nucl. Phys. B **22**, 247 (1970).

[43] P. Baillon, Y. Declais, M. Ferro-Luzzi, P. Jenni, J.-M. Perreau, J. Seguinot, and T. Ypsilantis, "Measurement of the Real Part of the Forward Amplitude in K- n and K+ n Elastic Scattering at 10-GeV/c and a New K+- n Dispersion Relation," Nucl. Phys. B **134**, 31 (1978).

[44] A. V. Sarantsev, "The recent results in the analysis of the meson production reactions," EPJ Web Conf. **199**, 01009 (2019).

[45] M. A. Matveev and A. Sarantsev, "The Bonn-Gatchina analysis of the data from the Kp collision reactions," PoS Hadron **2017**, 069 (2018).

[46] I. G. Alekseev *et al.* [EPECUR Collaboration], "High-precision measurements of πp elastic differential cross sections in the second resonance region," Phys. Rev. C **91**, no. 2, 025205 (2015).

[47] A. Sarantsev, talk at the KLF Collaboration meeting on Feb. 12, 2020, `https://wiki.jlab.org/klproject/index.php/February_12th,_2020`.

[48] V. Bernard, N. Kaiser, and U. G. Meißner, "pi K scattering in chiral perturbation theory to one loop," Nucl. Phys. B **357**, 129 (1991).

[49] V. Bernard, N. Kaiser, and U. G. Meißner, "Threshold parameters of pi K scattering in QCD," Phys. Rev. D **43**, 2757 (1991).

[50] J. Bijnens, P. Dhonte, and P. Talavera, "pi K scattering in three flavor ChPT," JHEP **0405**, 036 (2004).

[51] C. Miao, X. i. Du, G. w. Meng, and C. Liu, "Lattice study on kaon pion scattering length in the I = 3/2 channel," Phys. Lett. B **595** 400-407 (2004).

[52] S. R. Beane *et al.*, "pi K scattering in full QCD with domain-wall valence quarks," Phys. Rev. D **74**, 114503 (2006).

[53] J. Nagata, S. Muroya, and A. Nakamura, "Lattice study of K pi scattering in I = 3/2 and 1/2," Phys. Rev. C **80**, 045203 (2009).

[54] Z. Fu, "Lattice study on πK scattering with moving wall source," Phys. Rev. D **85**, 074501 (2012).

[55] C. B. Lang, L. Leskovec, D. Mohler, and S. Prelovsek, "K pi scattering for isospin 1/2 and 3/2 in lattice QCD," Phys. Rev. D **86**, 054508 (2012).

[56] K. Sasaki *et al.* [PACS-CS Collaboration], "Scattering lengths for two pseudoscalar meson systems," Phys. Rev. D **89**, no. 5, 054502 (2014).

[57] D. J. Wilson, J. J. Dudek, R. G. Edwards, and C. E. Thomas, "Resonances in coupled $\pi K, \eta K$ scattering from lattice QCD," Phys. Rev. D **91**, no.5, 054008 (2015).

[58] C. Helmes *et al.* [ETM Collaboration], "Hadron-Hadron Interactions from $N_f = 2 + 1 + 1$ Lattice QCD: $I = 3/2$ πK Scattering Length," Phys. Rev. D **98**, no.11, 114511 (2018).

[59] D. J. Wilson, R. A. Briceno, J. J. Dudek, R. G. Edwards and C. E. Thomas, "The quark-mass dependence of elastic πK scattering from QCD," Phys. Rev. Lett. **123**, no.4, 042002 (2019).

[60] C. K. Guruswamy, U. G. Meißner and C. Y. Seng, "Contraction Diagram Analysis in Pion-Kaon Scattering," [arXiv:2002.01763 [hep-lat]].

[61] Z. H. Guo and J. A. Oller, "Resonances from meson-meson scattering in U(3) CHPT," Phys. Rev. D **84**, 034005 (2011).

[62] A. Dobado and J. R. Peláez, "A global fit of pi pi and pi K elastic scattering in ChPT with dispersion relations," Phys. Rev. D **47**, 4883 (1993).

[63] A. Gomez Nicola and J. R. Peláez, "Meson meson scattering within one loop chiral perturbation theory and its unitarization," Phys. Rev. D **65**, 054009 (2002).

[64] M. Jamin, J. A. Oller, and A. Pich, "S wave K pi scattering in chiral perturbation theory with resonances," Nucl. Phys. B **587**, 331 (2000).

[65] J. Nebreda and J. R. Peláez, "Strange and non-strange quark mass dependence of elastic light resonances from SU(3) Unitarized Chiral Perturbation Theory to one loop," Phys. Rev. D **81**, 054035 (2010).

[66] A. V. Anisovich and A. V. Sarantsev, "K matrix analysis of the K pi S wave in the mass region 900-MeV - 2100-MeV and nonet classification of scalar q anti-q states," Phys. Lett. B **413**, 137 (1997).

[67] J. A. Oller and E. Oset, "Chiral symmetry amplitudes in the S wave isoscalar and isovector channels and the σ, $f_0(980)$, $a_0(980)$ scalar mesons," Nucl. Phys. A **620**, 438 (1997); Erratum: [Nucl. Phys. A **652**, 407 (1999)].

[68] C. Cawlfield *et al.* [CLEO Collaboration], "Measurement of interfering K*+ K- and K*- K+ amplitudes in the decay D0 —> K+ K- pi0," Phys. Rev. D **74**, 031108 (2006).

[69] R. Delbourgo and M. D. Scadron, "Dynamical generation of linear sigma model SU(3) Lagrangian and meson nonet mixing," Int. J. Mod. Phys. A **13**, 657 (1998).

[70] M. D. Scadron, F. Kleefeld, G. Rupp, and E. van Beveren, "Meson form-factors and the quark level linear sigma model," Nucl. Phys. A **724**, 391 (2003).

[71] Z. Y. Zhou and H. Q. Zheng, "An improved study of the kappa resonance and the non-exotic s wave πK scatterings up to $\sqrt{s} = 2.1$ GeV of LASS data," Nucl. Phys. A **775**, 212 (2006).

[72] E. M. Aitala *et al.* [E791 Collaboration], "Dalitz plot analysis of the decay $D^+ \to K^-\pi^+\pi^+$ and indication of a low-mass scalar $K\pi$ resonance," Phys. Rev. Lett. **89**, 121801 (2002).

[73] J. Z. Bai *et al.* [BES Collaboration], "Evidence of kappa particle in $J/\psi \to K*(892)^0 K^+\pi^-$," hep-ex/0304001.

[74] J. H. Friedman and R. R. Ross, "Production and decay properties of the K0 (892) produced in the reaction $K^- p \to p\bar{k}^0\pi^-$ At 2.1-GeV/c, 2.45-GeV/c, and 2.64-GeV/c," Phys. Rev. Lett. **16**, 485 (1966).

[75] V. Bernard, "First determination of $f_+(0)|V_{us}|$ from a combined analysis of $\tau \to K\pi\nu_\tau$ decay and πK scattering with constraints from $K_{\ell 3}$ decays," JHEP **1406**, 082 (2014).

[76] D. R. Boito, R. Escribano, and M. Jamin, "K π vector form factor constrained by $\tau \to K\pi\nu_\tau$ and K_{l3} decays," JHEP **1009**, 031 (2010).

[77] D. Epifanov *et al.* [Belle Collaboration], "Study of tau- —> K(S) pi- nu(tau) decay at Belle," Phys. Lett. B **654**, 65 (2007).

[78] S. Adhikari and M. Amaryan, "KLF Analysis Report: Meson Spectroscopy Simulation Studies," KLF Note, 2020; https://wiki.jlab.org/klproject/images/2/20/Meson.pdf.

[79] J. R. Peláez and A. Rodas, "Pion-kaon scattering amplitude constrained with forward dispersion relations up to 1.6 GeV," Phys. Rev. D **93**, no. 7, 074025 (2016).

[80] J. Peláez and A. Rodas, "Determination of the lightest strange resonance $K_0^*(700)$ or κ, from a dispersive data analysis," Phys. Rev. Lett. **124**, no.17, 172001 (2020).

[81] J. R. Peláez and A. Rodas, in preparation.

[82] G. Bonvicini *et al.* [CLEO Collaboration], "Dalitz plot analysis of the D+ —> K- pi+ pi+ decay," Phys. Rev. D **78**, 052001 (2008).

[83] D. V. Bugg, "Comments on the sigma and kappa," Phys. Lett. B **572**, 1 (2003); Erratum: [Phys. Lett. B **595**, 556 (2004)]; D. V. Bugg, "An update on the Kappa," Phys. Rev. D **81**, 014002 (2010).

[84] J. R. Peláez, "Light scalars as tetraquarks or two-meson states from large N(c) and unitarized chiral perturbation theory," Mod. Phys. Lett. A **19**, 2879 (2004).

[85] J. R. Peláez, A. Rodas, and J. Ruiz de Elvira, "Strange resonance poles from $K\pi$ scattering below 1.8 GeV," Eur. Phys. J. C **77**, no. 2, 91 (2017).

[86] I. Strakovsky *et al.*, "Conceptual design of beryllium target for the KLF Project," arXiv:2002.04442 [physics.ins–det].

[87] Y. Valdau *et al.*, "Comparison of inclusive K^+ production in proton-proton and proton-neutron collisions," Phys. Rev. C **84**, 055207 (2011).

[88] P. Adlarson *et al.* [WASA-at-COSY Collaboration], "Isoscalar single-pion production in the region of Roper and $d^*(2380)$ resonances," Phys. Lett. B **774**, 599 (2017).

[89] A. Accardi *et al.* "Electron Ion Collider: The Next QCD Frontier - Understanding the glue that binds us all," BNL–98815–2012-JA; JLAB–PHY–12–1652; arXiv:1212.1701 [nucl-ex].

[90] "National Academies of Sciences, Engineering, and Medicine," *An Assessment of U.S.-Based Electron-Ion Collider Science*, (The National Academies Press, Washington, D.C., 2018); https://www.nap.edu/catalog/25171/an-assessment-of-us-based-electron-ion-collider-science .

[91] M. Duer *et al.* [CLAS Collaboration], "Probing high-momentum protons and neutrons in neutron-rich nuclei," Nature **560**, no. 7720, 617 (2018).

[92] B. Schmookler *et al.* [CLAS Collaboration], "Modified structure of protons and neutrons in correlated pairs," Nature **566**, no. 7744, 354 (2019).

[93] W. J. Briscoe, M. Döring, H. Haberzettl, I. I. Strakovsky, and R. L. Workman, Institute of Nuclear Studies of The George Washington University Database; http://gwdac.phys.gwu.edu.

[94] G. Agakishiev *et al.* [Hades Collaboration], "Baryon resonance production and dielectron decays in proton-proton collisions at 3.5 GeV", Eur. Phys. J. **A50**, 82, (2014).

[95] S. Adhikari *et al.* [GlueX Collaboration], "The GlueX Beamline and Detector," [arXiv:2005.14272 [physics.ins-det]].

[96] D. Androic *et al.* [G0 Collaboration], "The G0 Experiment: Apparatus for Parity-Violating Electron Scattering Measurements at Forward and Backward Angles," Nucl. Instrum. Meth. A **646**, 59 (2011).

[97] J. Grames, private communication, April 2018.

[98] R. Kazimi, private communication, April 2018.

[99] T. Satogata, "KLF Final Beam Focusing," Jefferson Lab internal technical note TN-20-017, May 2020, http://toddsatogata.net/Papers/2020-05-07-KLF-Final-Focus.pdf .

[100] S. Adhikari *et al.* [GlueX Collaboration], "Beam asymmetry $\mathbf{\Sigma}$ for the photoproduction of η and η' mesons at $\mathbf{E}_\gamma = 8.8$GeV," Phys. Rev. C **100**, no. 5, 052201 (2019),

[101] A. Ali *et al.* [GlueX Collaboration], "First measurement of near-threshold J/ψ exclusive photoproduction off the proton," Phys. Rev. Lett. **123**, no. 7, 072001 (2019),

[102] D. Day *et al.*, "A conceptual design study of a Compact Photon Source (CPS) for Jefferson Lab," Nucl. Instrum. Meth. A **957**, 163429 (2020).

[103] C. J. Werner *et al.*, "MCNP6.2 Release Notes," Los Alamos National Laboratory, Report LA–UR–18–20808 (2018).

[104] P. Degtyarenko and B. Wojtsekhowski, "Compact Photon Source Conceptual Design," in: *Workshop on Physics with Neutral Kaon Beam at JLab:* mini-Proceedings, arXiv:1604.02141 [hep–ph], p. 223.

[105] A. D. Brody *et al.*, "Production of K0(2) mesons and neutrons by 10-GeV and 16-GeV electrons on beryllium," Phys. Rev. Lett. **22**, 966 (1969).

[106] M. G. Albrow *et al.*, "Photoproduction of k0 mesons from protons and from complex nuclei," Nucl. Phys. B **23**, 509 (1970).

[107] N. Petoussi-Henss, W. E. Bolch, K. F. Eckerman, A. Endo, N. Hertel, J. Hunt, M. Pelliccioni, H. Schlattl, and M. Zankl, *ICRP, 2010. Conversion Coefficients for Radiological Protection Quantities for External Radiation Exposures*, ICRP 116 Publication, Editor C. H. Clement, Ann. ICRP, **40**, (2-5) (2010).

[108] R. G. Williams III, C. J. Gesh, and R. T. Pagh, *Compendium of Material Composition Data for Radiation Transport Modeling*, PNNL–15870, 2006.

[109] I. Larin, in: *Workshop on Physics with Neutral Kaon Beam at JLab*, mini-Proceedings, arXiv:1604.02141 [hep–ph] (February, 2016), p. 198.

[110] We used a modified version of the Pythia [111] package for the GlueX Collaboration at JLab Hall D, http://home.thep.lu.se/torbjorn/Pythia.html .

[111] T. Sjöstrand *et al.*, "An Introduction to PYTHIA 8.2," Comput. Phys. Commun. **191**, 159 (2015).

[112] F. Barbosa, C. Hutton, A. Sitnikov, A. Somov, S. Somov, and I. Tolstukhin, "Pair spectrometer hodoscope for Hall D at Jefferson Lab," Nucl. Instrum. Meth. A **795**, 376 (2015).

[113] G. W. Brandenburg *et al.*, "Production of K0(l) mesons and neutrons from electrons on Beryllium above 10-GeV," Phys. Rev. D **7**, 708 (1973).

[114] M. Bashkanov, D. P. Watts, N. Zachariou, E. Chudakov, M. Amaryan, J. Ritman, J. Stevens, and I. Strakovsky, "KL Flux Monitor," Preprint GlueX-doc-3603, 2019.

[115] A. Somov, "Neutron background estimates in the tagger hal," Preprint GlueX–doc–1646, 2011.

[116] Y. Qiang, C. Zorn, F. Barbosa, and E. Smith, "Radiation hardness tests of SiPMs for the JLab Hall D Barrel Calorimeter," Nucl. Instrum. Meth. A **698**, 234 (2013).

[117] E. Pooser *et al.*, "The GlueX Start Counter Detector," Nucl. Instrum. Meth. A **927**, 330 (2019).

[118] E. Pooser, "The GlueX start counter and beam asymmetry sigma in single pi0 photoproduction," FIU, Ph.D. Thesis, 2016.

[119] P. Degtiarenko, A. Fass, G. Kharashvili, and A. Somov, "Calculation of radiation damage to Silicon Photomultipliers in GlueX Experiment," Preprint JLAB–TN–11–005, GlueX–doc–1660, 2011.

[120] T. D. Beattie *et al.*, "Construction and performance of the Barrel Electromagnetic Calorimeter for the GlueX Experiment," Nucl. Instrum. Meth. A **896**, 24 (2018).

[121] L. Keller, private communication, 2015.

[122] J. Allison *et al.*, "Recent developments in Geant4," Nucl. Instrum. Meth. A **835**, 186 (2016).

[123] C. Keith, "Targets for a Neutral Kaon Beam," in: *Workshop on Physics with Neutral Kaon Beam at JLab: mini-Proceedings*, arXiv:1604.02141 [hep–ph] (February, 2016), p. 223.

[124] D. Meekins, TGT-CALC-401-007: *Hall D Cryogenic Target: General calculations for relief of the LH_2 target*.

[125] J. J. Dudek and R. G. Edwards, "Hybrid Baryons in QCD," Phys. Rev. D **85**, 054016 (2012).

[126] R. Bellwied, S. Borsanyi, Z. Fodor, S. D. Katz, and C. Ratti, "Is there a flavor hierarchy in the deconfinement transition of QCD?," Phys. Rev. Lett. **111**, 202302 (2013).

[127] S. Borsanyi *et al.* [Wuppertal-Budapest Collaboration], "Is there still any T_c mystery in lattice QCD? Results with physical masses in the continuum limit III," JHEP **1009**, 073 (2010).

[128] A. Bazavov *et al.* [HotQCD Collaboration], "Equation of state in (2+1)-flavor QCD," Phys. Rev. D **90**, 094503 (2014).

[129] A. Bazavov *et al.* [HotQCD Collaboration], "Chiral crossover in QCD at zero and non-zero chemical potentials," Phys. Lett. B **795**, 15 (2019).

[130] S. Borsanyi *et al.*, "The QCD crossover at finite chemical potential from lattice simulations," arXiv:2002.02821 [hep-lat].

[131] M. Floris, "Hadron yields and the phase diagram of strongly interacting matter," Nucl. Phys. A **931**, 103 (2014).

[132] L. Adamczyk *et al.* [STAR Collaboration], "Energy dependence of moments of net-proton multiplicity distributions at RHIC," Phys. Rev. Lett. **112**, 032302 (2014).

[133] L. Adamczyk *et al.* [STAR Collaboration], "Beam energy dependence of moments of the net-charge multiplicity distributions in Au+Au collisions at RHIC," Phys. Rev. Lett. **113**, 092301 (2014).

[134] P. Alba, W. Alberico, R. Bellwied, M. Bluhm, V. Mantovani Sarti, M. Nahrgang, and C. Ratti, "Freeze-out conditions from net-proton and net-charge fluctuations at RHIC," Phys. Lett. B **738**, 305 (2014).

[135] J. Adam *et al.* [ALICE Collaboration], "Enhanced production of multi-strange hadrons in high-multiplicity proton-proton collisions," Nature Phys. **13**, 535 (2017).

[136] R. Dashen, S. K. Ma, and H. J. Bernstein, "S Matrix formulation of statistical mechanics," Phys. Rev. **187**, 345 (1969).

[137] R. Venugopalan and M. Prakash, "Thermal properties of interacting hadrons," Nucl. Phys. A **546**, 718 (1992).

[138] F. Karsch, K. Redlich, and A. Tawfik, "Thermodynamics at nonzero baryon number density: A Comparison of lattice and hadron resonance gas model calculations," Phys. Lett. B **571**, 67 (2003).

[139] A. Tawfik, "QCD phase diagram: A Comparison of lattice and hadron resonance gas model calculations," Phys. Rev. D **71**, 054502 (2005).

[140] R. Hagedorn, "Ultimate temperature and the structure of elementary particles," Prog. Sci. Culture **1**, 395 (1976).

[141] S. Capstick and N. Isgur, "Baryons in a Relativized Quark Model with Chromodynamics," Phys. Rev. D **34**, 2809 (1986).

[142] D. Ebert, R. N. Faustov, and V. O. Galkin, "Mass spectra and Regge trajectories of light mesons in the relativistic quark model," Phys. Rev. D **79**, 114029 (2009).

[143] A. Majumder and B. Muller, "Hadron Mass Spectrum from Lattice QCD," Phys. Rev. Lett. **105**, 252002 (2010).

[144] A. Bazavov *et al.*, "Additional strange hadrons from QCD thermodynamics and strangeness freezeout in heavy ion collisions," Phys. Rev. Lett. **113**, no. 7, 072001 (2014).

[145] P. Alba *et al.*, "Constraining the hadronic spectrum through QCD thermodynamics on the lattice," Phys. Rev. D **96**, no. 3, 034517 (2017).

[146] M. M. Giannini and E. Santopinto, "The hypercentral Constituent Quark Model and its application to baryon properties," Chin. J. Phys. **53**, 020301 (2015).

[147] P. Huovinen and P. Petreczky, "Hadron gas with repulsive mean field," PoS Confinement **2018**, 145 (2018).

[148] C. Amsler *et al.* [Particle Data Group], "Review of Particle Physics," Phys. Lett. B **667**, 1 (2008).

[149] E. Santopinto and J. Ferretti, "Strange and nonstrange baryon spectra in the relativistic interacting quark-diquark model with a Gsey and Radicati-inspired exchange interaction," Phys. Rev. C **92**, no. 2, 025202 (2015).

[150] A. Bazavov *et al.*, "Skewness, kurtosis and the 5th and 6th order cumulants of net baryon-number distributions from lattice QCD confront high-statistics STAR data," arXiv:2001.08530 [hep-lat].

[151] R. Machleidt and I. Slaus, "The nucleon-nucleon interaction" J. Phys. G. **27**, R69 (2001).

[152] I. Vidaña, "Hyperons and neutron stars" Nucl. Phys. A **914**, 367 (2013).

[153] I. Vidaña, "Hyperons in Neutron Stars" J. Phys. **668**, 012031 (2016).

[154] R. A. Hulse and J. H. Taylor, "Discovery of a pulsar in a binary system" Astrophys. J. Lett **195**, L51 (1975).

[155] P. B. Demorest *et al*, "A two-solar-mass neutron star measured using Shapiro delay," Nature **467**, 1081 (2010).

[156] P. B. Demorest *et al*, "A Massive Pulsar in a Compact Relativistic Binary," Science **340**, 6131 (2013).

[157] I. Vidaña, "Hyperons: the strange ingredients of the nuclear equation of state," Proc. Roy. Soc. Lond. A **474**, 0145 (2018).

[158] S. R. Beane *et al.*, "Light nuclei and hypernuclei from quantum chromodynamics in the limit of SU(3) flavor symmetry" Phys. Rev. D **87**, 034506 (2013).

[159] *Kaon Production on the Deuteron Using Polarised Photons*, Spokespersons: P. Nadel-Turonski, Y. Ilieva, B.L. Berman, and D.G. Ireland, [CLAS Collaboration], JLab Proposal PR106–103, Newport News, VA, USA, 2006.

[160] "Study of the hyperon-nucleon interaction via final-state interactions in exclusive reactions," N. Zachariou [CLAS Collaboration], SciPost Phys. Proc. **3**, 026 (2020).

[161] The Durham HEP Reaction Data Databases (UK): http://durpdg.dur.ac.uk/hepdata/reac.html

[162] M. Albrow, "Photoproduction of K^0: Early history," in: *Workshop on Physics with Neutral Kaon Beam at JLab: mini-Proceedings*, arXiv:1604.02141 [hep–ph] (February, 2016), p. 5.

[163] S. D. Drell and M. Jacob, "Photoproduction Of Neutral K Mesons," Phys. Rev. **138**, B1313 (1965).

[164] G. Höhler and H. Schopper, *Numerical Data And Functional Relationships In Science And Technology. Group I: Nuclear And Particle Physics. Vol. 9: Elastic And Charge Exchange Scattering Of Elementary Particles. B: Pion Nucleon Scattering. Pt. 2: Methods And Results Of Phenomenological Analyses* (Landolt-Börnstein. New Series, I/9B2) (Springer, Berlin, Germany, 1983) 601 P.

[165] R. A. Arndt, W. J. Briscoe, I. I. Strakovsky, and R. L. Workman, "Extended partial-wave analysis of πN scattering data," Phys. Rev. C **74**, 045205 (2006).

[166] Z. W. Liu, J. M. M. Hall, D. B. Leinweber, A. W. Thomas, and J. J. Wu, "Structure of the $\mathbf{\Lambda(1405)}$ from Hamiltonian effective field theory," Phys. Rev. D **95**, no. 1, 014506 (2017).

[167] J. A. Oller and U.-G. Meißner, "Chiral dynamics in the presence of bound states: Kaon nucleon interactions revisited," Phys. Lett. B **500**, 263 (2001).

[168] A. Cieplý, M. Mai, U.-G. Meißner, and J. Smejkal, "On the pole content of coupled channels chiral approaches used for the $\bar{K}N$ system," Nucl. Phys. A **954**, 17 (2016).

[169] A. V. Anisovich, A. V. Sarantsev, V. A. Nikonov, V. Burkert, R. A. Schumacher, U. Thoma and E. Klempt, "Hyperon I: Study of the $\Lambda(1405)$," arXiv:1905.05456 [nucl-ex].

[170] W. Kamleh, J. M. M. Hall, D. B. Leinweber, B. J. Menadue, B. J. Owen, A. W. Thomas, and R. D. Young, "The Lambda (1405) is a $\overline{K}$N molecule," PoS CD **15**, 037 (2016).

[171] R. Molina and M. Döring, "Pole structure of the $\Lambda(1405)$ in a recent QCD simulation," Phys. Rev. D **94**, no. 5, 056010 (2016); Addendum: [Phys. Rev. D **94**, no. 7, 079901 (2016)].

[172] N. N. Scoccola, H. Nadeau, M. A. Nowak, and M. Rho, "The Hyperons as Skyrmions With Vector Mesons," Phys. Lett. B **201**, 425 (1988); Erratum: [Phys. Lett. B **220**, 658 (1989)].

[173] C. G. Callan, Jr., K. Hornbostel, and I. R. Klebanov, "Baryon masses in the bound state approach to strangeness in the Skyrme Model," Phys. Lett. B **202**, 269 (1988).

[174] K. F. Liu, "Baryons and Chiral Symmetry," Int. J. Mod. Phys. E **26**, no. 01n02, 1740016 (2017).

[175] L. Y. Glozman and D. O. Riska, "The Spectrum of the nucleons and the strange hyperons and chiral dynamics," Phys. Rept. **268**, 263 (1996).

[176] K. F. Liu, Y. Chen, M. Gong, R. Sufian, M. Sun, and A. Li, "The Roper Puzzle," PoS LATTICE **2013**, 507 (2014).

[177] M. Sun *et al.*,"Roper State from Overlap Fermions," Phys.Rev. D **101** 5, 054511 (2020).

[178] M. Sumihama *et al.* [Belle Collaboration], "Observation of $\Xi(1620)^0$ and evidence for $\Xi(1690)^0$ in $\Xi_c^+ \to \Xi^-\pi^+\pi^+$ decays," Phys. Rev. Lett. **122**, no. 7, 072501 (2019).

[179] J. K. Hassall *et al.*, "Production of S = -2 and -3 Baryon States in 6.5-GeV/cK^-P Interactions," Nucl. Phys. B **189**, 397 (1981).

[180] J. J. Dudek *et al.* [Hadron Spectrum Collaboration], "Resonances in coupled $\pi K - \eta K$ scattering from quantum chromodynamics," Phys. Rev. Lett. **113**, no. 18, 182001 (2014).

[181] N. Isgur and M. B. Wise, "Spectroscopy with heavy quark symmetry," Phys. Rev. Lett. **66**, 1130 (1991).

[182] R. Aaij *et al.* [LHCb Collaboration], "Observation of the doubly charmed baryon Ξ_{cc}^{++}," Phys. Rev. Lett. **119**, no. 11, 112001 (2017).

[183] R. Aaij *et al.* [LHCb Collaboration], "First Observation of the Doubly Charmed Baryon Decay $\Xi_{cc}^{++} \to \Xi_c^+\pi^+$," Phys. Rev. Lett. **121**, no. 16, 162002 (2018).

[184] R. Aaij *et al.* [LHCb Collaboration], "Observation of a new Ξ_b^- resonance," Phys. Rev. Lett. **121**, no. 7, 072002 (2018).

[185] R. Aaij *et al.* [LHCb Collaboration], "Observation of five new narrow Ω_c^0 states decaying to $\Xi_c^+K^-$," Phys. Rev. Lett. **118**, no. 18, 182001 (2017).

[186] H. Zhang, J. Tulpan, M. Shrestha, and D. M. Manley, "Partial-wave analysis of $\bar{K}N$ scattering reactions," Phys. Rev. C **88**, no. 3, 035204 (2013).

[187] H. Zhang, J. Tulpan, M. Shrestha, and D. M. Manley, "Multichannel parametrization of $\bar{K}N$ scattering amplitudes and extraction of resonance parameters," Phys. Rev. C **88**, no. 3, 035205 (2013).

[188] D. M. Manley, "$K_L^0 p$ Scattering to Two-Body Final States," in: *Workshop on Physics with Neutral Kaon Beam at JLab: mini-Proceedings*, arXiv:1604.02141 [hep–ph] (February, 2016), p. 42.

[189] H. Kamano, S. X. Nakamura, T.-S. H. Lee, and T. Sato, "Dynamical coupled-channels model of K·p reactions: Determination of partial-wave amplitudes," Phys. Rev. C **90**, no. 6, 065204 (2014).

[190] H. Kamano, S. X. Nakamura, T.-S. H. Lee, and T. Sato, "Dynamical coupled-channels model of $K^- p$ reactions. II. Extraction of Λ^* and Σ^* hyperon resonances," Phys. Rev. C **92**, no. 2, 025205 (2015); Erratum: [Phys. Rev. C **95**, no. 4, 049903 (2017)].

[191] B. C. Jackson, Y. Oh, H. Haberzettl, and K. Nakayama, "$\bar{K} + N \to K + \Xi$ reaction and $S = -1$ hyperon resonances," Phys. Rev. C **91**, no. 6, 065208 (2015).

[192] Z. H. Guo and J. A. Oller, "Meson-baryon reactions with strangeness -1 within a chiral framework," Phys. Rev. C **87**, no. 3, 035202 (2013).

[193] A. Feijoo, V. Magas, and A. Ramos, "$S = -1$ meson-baryon interaction and the role of isospin filtering processes," Phys. Rev. C **99** (2019) no.3, 035211.

[194] A. Cieplý and J. Smejkal, "Chirally motivated $\bar{K}N$ amplitudes for in-medium applications," Nucl. Phys. A **881**, 115 (2012).

[195] H. Osmanović *et al.*, "Fixed-t analyticity as a constraint in single-energy partial-wave analyses of meson photoproduction reactions," Phys. Rev. C **97**, no. 1, 015207 (2018).

[196] Y. Wunderlich, A. Švarc, R. L. Workman, L. Tiator, and R. Beck, "Toward an understanding of discrete ambiguities in truncated partial-wave analyses," Phys. Rev. C **96**, no. 6, 065202 (2017).

[197] A. Švarc, Y. Wunderlich, H. Osmanović, M. Hadžimehmedović, R. Omerović, J. Stahov, V. Kashevarov, K. Nikonov, M. Ostrick, L. Tiator, and R. Workman, Phys. Rev. C **97**, no. 5, 054611 (2018).

[198] G. Höhler, "Determination of πN resonance pole parameters," πN Newslett. **9**, 1 (1993).

[199] N. G. Kelkar and M. Nowakowski, "Analysis of averaged multichannel delay times," Phys. Rev. A **78**, 012709 (2008); and references therein.

[200] G. F. Chew and S. Mandelstam, "Theory of low-energy pion pion interactions," Phys. Rev. **119**, 467 (1960).

[201] S. Ceci, J. Stahov, A. Švarc, S. Watson, and B. Zauner, "Resolution of the multichannel anomaly in the extraction of S-matrix resonance-pole parameters," Phys. Rev. D **77**, 116007 (2008).

[202] P. Masjuan, J. Ruiz de Elvira, and J. J. Sanz-Cillero, "Precise determination of resonance pole parameters through Padapproximants," Phys. Rev. D **90**, no. 9, 097901 (2014).

[203] A. Švarc, M. Hadžimehmedović, H. Osmanović, J. Stahov, L. Tiator, and R. L. Workman, "Introducing the Pietarinen expansion method into the single-channel pole extraction problem," Phys. Rev. C **88**, no. 3, 035206 (2013).

[204] A. Švarc, M. Hadžimehmedović, R. Omerović, H. Osmanović, and J. Stahov, "Poles of Karlsruhe-Helsinki KH80 and KA84 solutions extracted by using the Laurent-Pietarinen method," Phys. Rev. C **89**, no. 4, 045205 (2014).

[205] A. Švarc, M. Hadžimehmedović, H. Osmanović, J. Stahov, L. Tiator, and R. L. Workman, "Pole positions and residues from pion photoproduction using the Laurent-Pietarinen expansion method," Phys. Rev. C **89**, no. 6, 065208 (2014).

[206] A. Švarc, M. Hadžimehmedović, H. Osmanović, J. Stahov, and R. L. Workman, "Pole structure from energy-dependent and single-energy fits to GWU-SAID piN elastic scattering data," Phys. Rev. C **91**, no. 1, 015207 (2015).

[207] A. Švarc, M. Hadžimehmedović, H. Osmanović, J. Stahov, L. Tiator, and R. L. Workman, "Generalization of the model-independent Laurent-Pietarinen single-channel pole-extraction formalism to multiple channels," Phys. Lett. B **755**, 452 (2016).

[208] M. Hazewinkel: *Encyclopaedia of Mathematics* (Springer, 31. 8. 1990) Vol. **6**, p. 251.

[209] S. Ciulli and J. Fischer, Nucl. Phys. **24**, 465 (1961).

[210] I. Ciulli, S. Ciulli, and J. Fisher, Nuovo Cimento **23**, 1129 (1962).

[211] E. Pietarinen, "Dispersion relations and experimental data," Nuovo Cim. A **12**, 522 (1972).

[212] E. Pietarinen, "Fixed Momentum Transfer Analysis of Pion Nucleon Scattering," Nucl. Phys. B **107**, 21 (1976).

[213] R. L. Workman, M. W. Paris, W. J. Briscoe, and I. I. Strakovsky, "Unified Chew-Mandelstam SAID analysis of pion photoproduction data," Phys. Rev. C **86**, 015202 (2012).

[214] M. Lüscher, "Two particle states on a torus and their relation to the scattering matrix," Nucl. Phys. B **354**, 531 (1991).

[215] K. Rummukainen and S. A. Gottlieb, "Resonance scattering phase shifts on a nonrest frame lattice," Nucl. Phys. B **450**, 397 (1995).

[216] KLF Collaboration wiki page
https://wiki.jlab.org/klproject/index.php/KL_Collaboration_Meetings.

[217] S. Aoki *et al.* [CP-PACS Collaboration], "Lattice QCD Calculation of the rho Meson Decay Width," Phys. Rev. D **76**, 094506 (2007).

[218] X. Feng, K. Jansen, and D. B. Renner, "Resonance Parameters of the rho-Meson from Lattice QCD," Phys. Rev. D **83**, 094505 (2011).

[219] J. J. Dudek *et al.* [Hadron Spectrum Collaboration], "Energy dependence of the ρ resonance in $\pi\pi$ elastic scattering from lattice QCD," Phys. Rev. D **87**, no. 3, 034505 (2013); Erratum: [Phys. Rev. D **90**, no. 9, 099902 (2014)].

[220] D. Guo, A. Alexandru, R. Molina, and M. Döring, "Rho resonance parameters from lattice QCD," Phys. Rev. D **94**, no. 3, 034501 (2016).

[221] C. Alexandrou *et al.*, "P-wave $\pi\pi$ scattering and the ρ resonance from lattice QCD," Phys. Rev. D **96**, no. 3, 034525 (2017).

[222] J. Bulava, B. Fahy, B. Hz, K. J. Juge, C. Morningstar, and C. H. Wong, "$I = 1$ and $I = 2$ $\pi - \pi$ scattering phase shifts from $N_{\rm f} = 2 + 1$ lattice QCD," Nucl. Phys. B **910**, 842 (2016).

[223] C. B. Lang, D. Mohler, S. Prelovsek, and M. Vidmar, "Coupled channel analysis of the rho meson decay in lattice QCD," Phys. Rev. D **84**, no. 5, 054503 (2011); Erratum: [Phys. Rev. D **89**, no. 5, 059903 (2014)].

[224] R. Brett, J. Bulava, J. Fallica, A. Hanlon, B. Hz, and C. Morningstar, "Determination of s- and p-wave $I = 1/2$ $K\pi$ scattering amplitudes in $N_{\rm f} = 2 + 1$ lattice QCD," Nucl. Phys. B **932**, 29 (2018).

[225] P. Guo, J. Dudek, R. Edwards, and A. P. Szczepaniak, "Coupled-channel scattering on a torus," Phys. Rev. D **88**, no. 1, 014501 (2013).

[226] R. A. Briceno and Z. Davoudi, "Moving multichannel systems in a finite volume with application to proton-proton fusion," Phys. Rev. D **88**, no. 9, 094507 (2013).

[227] U.-G. Meißner, G. Rios, and A. Rusetsky, "Spectrum of three-body bound states in a finite volume," Phys. Rev. Lett. **114**, no. 9, 091602 (2015); Erratum: [Phys. Rev. Lett. **117**, no. 6, 069902 (2016)].

[228] C. Liu, X. Feng, and S. He, "Two particle states in a box and the S-matrix in multi-channel scattering," Int. J. Mod. Phys. A **21**, 847 (2006).

[229] M. Lage, U.-G. Meißner, and A. Rusetsky, "A Method to measure the antikaon-nucleon scattering length in lattice QCD," Phys. Lett. B **681**, 439 (2009).

[230] C. Morningstar, J. Bulava, B. Singha, R. Brett, J. Fallica, A. Hanlon, and B. Hz, "Estimating the two-particle K-matrix for multiple partial waves and decay channels from finite-volume energies," Nucl. Phys. B **924**, 477 (2017).

[231] M. Döring, U. G. Meißner, E. Oset, and A. Rusetsky, "Unitarized Chiral Perturbation Theory in a finite volume: Scalar meson sector," Eur. Phys. J. A **47**, 139 (2011).

[232] M. Döring and U. G. Meißner, "Finite volume effects in pion-kaon scattering and reconstruction of the κ(800) resonance," JHEP **1201**, 009 (2012).

[233] M. Döring, U. G. Meißner, E. Oset, and A. Rusetsky, "Scalar mesons moving in a finite volume and the role of partial wave mixing," Eur. Phys. J. A **48**, 114 (2012).

[234] D. J. Wilson, R. A. Briceno, J. J. Dudek, R. G. Edwards, and C. E. Thomas, "Coupled $\pi\pi, K\bar{K}$ scattering in P-wave and the ρ resonance from lattice QCD," Phys. Rev. D **92**, no. 9, 094502 (2015).

[235] R. A. Briceno, J. J. Dudek, R. G. Edwards, and D. J. Wilson, "Isoscalar $\pi\pi, K\overline{K}, \eta\eta$ scattering and the σ, f_0, f_2 mesons from QCD," Phys. Rev. D **97**, no. 5, 054513 (2018).

[236] R. A. Briceno, J. J. Dudek, R. G. Edwards, and D. J. Wilson, "Isoscalar $\pi\pi$ scattering and the σ meson resonance from QCD," Phys. Rev. Lett. **118**, no. 2, 022002 (2017).

[237] R. G. Edwards, J. J. Dudek, D. G. Richards, and S. J. Wallace, "Excited state baryon spectroscopy from lattice QCD," Phys. Rev. D **84**, 074508 (2011).

[238] G. P. Engel *et al.* [BGR Collaboration], "QCD with Two Light Dynamical Chirally Improved Quarks: Baryons," Phys. Rev. D **87**, no. 7, 074504 (2013).

[239] C. W. Andersen, J. Bulava, B. Hz, and C. Morningstar, "Elastic $I = 3/2p$-wave nucleon-pion scattering amplitude and the $\Delta(1232)$ resonance from N_f=2+1 lattice QCD," Phys. Rev. D **97**, no. 1, 014506 (2018).

[240] R. Brower, N. Christ, C. DeTar, R. Edwards, and P. Mackenzie, "Lattice QCD Application Development within the US DOE Exascale Computing Project," EPJ Web Conf. **175**, 09010 (2018).

[241] S. Godfrey and J. Napolitano, "Light meson spectroscopy," Rev. Mod. Phys. **71**, 1411 (1999).

[242] S. Narison, "Scalar mesons in QCD," Nucl. Phys. Proc. Suppl. **96**, 244 (2001).

[243] R. J. Crewther and L. C. Tunstall, "$\Delta I = 1/2$ rule for kaon decays derived from QCD infrared fixed point," Phys. Rev. D **91**, no. 3, 034016 (2015).

[244] V. Bernard, N. Kaiser, and U. G. Meißner, "Chiral perturbation theory in the presence of resonances: Application to pi pi and pi K scattering," Nucl. Phys. B **364**, 283 (1991).

[245] J. R. Peláez, "From controversy to precision on the sigma meson: a review on the status of the non-ordinary $f_0(500)$ resonance," Phys. Rept. **658**, 1 (2016).

[246] R. L. Jaffe, "Multi-Quark Hadrons. 1. The Phenomenology of (2 Quark 2 anti-Quark) Mesons," Phys. Rev. D **15**, 267 (1977).

[247] T. Barnes, "Two Photon Decays Support the (K anti-K) Molecule Picture of the S*(975) and Delta(980)," Phys. Lett. **165B**, 434 (1985).

[248] E. van Beveren, T. A. Rijken, K. Metzger, C. Dullemond, G. Rupp, and J. E. Ribeiro, "A Low-Lying Scalar Meson Nonet in a Unitarized Meson Model," Z. Phys. C **30**, 615 (1986).

[249] J. A. Oller, E. Oset, and J. R. Peláez, "Nonperturbative approach to effective chiral Lagrangians and meson interactions," Phys. Rev. Lett. **80**, 3452 (1998); J. A. Oller, E. Oset, and J. R. Peláez, "Meson meson interaction in a nonperturbative chiral approach," Phys. Rev. D **59**, 074001 (1999); Erratum: [Phys. Rev. D **60**, 099906 (1999)]; Erratum: [Phys. Rev. D **75**, 099903 (2007)].

[250] D. Black, A. H. Fariborz, F. Sannino, and J. Schechter, "Evidence for a scalar kappa(900) resonance in pi K scattering," Phys. Rev. D **58**, 054012 (1998); D. Black, A. H. Fariborz, F. Sannino and J. Schechter, "Putative light scalar nonet," Phys. Rev. D **59**, 074026 (1999).

[251] J. A. Oller and E. Oset, "N/D description of two meson amplitudes and chiral symmetry," Phys. Rev. D **60**, 074023 (1999).

[252] F. E. Close and N. A. Tornqvist, "Scalar mesons above and below 1-GeV," J. Phys. G **28**, R249 (2002).

[253] J. R. Peláez, "On the Nature of light scalar mesons from their large N(c) behavior," Phys. Rev. Lett. **92**, 102001 (2004).

[254] R. Jaffe and F. Wilczek, "A Perspective on pentaquarks," Eur. Phys. J. C **33**, S38 (2004).

[255] P. Büttiker, S. Descotes-Genon, and B. Moussallam, "A new analysis of pi K scattering from Roy and Steiner type equations," Eur. Phys. J. C **33**, 409 (2004).

[256] J. M. Flynn and J. Nieves, "Elastic s-wave B pi, D pi, D K and K pi scattering from lattice calculations of scalar form-factors in semileptonic decays," Phys. Rev. D **75**, 074024 (2007).

[257] J. R. Batley *et al.* [NA48-2 Collaboration], "Precise tests of low energy QCD from K(e4)decay properties," Eur. Phys. J. C **70**, 635-657 (2010).

[258] S. M. Roy, "Exact integral equation for pion pion scattering involving only physical region partial waves," Phys. Lett. **36B**, 353 (1971).

[259] F. Steiner, "Partial wave crossing relations for meson-baryon scattering," Fortsch. Phys. **19**, 115 (1971).

[260] D. Aston *et al.*, "The Strange Meson Resonances Observed in the Reaction $K^- p \to \bar{K} 0 \pi^+ \pi^- n$ at 11-GeV/c," Nucl. Phys. B **292**, 693 (1987).

[261] B. R. Martin, D. Morgan, and G. Shaw, *Pion Pion Interactions in Particle Physics* (Academic press, London, 1976).

[262] C. B. Lang, "The πK Scattering and Related Processes," Fortsch. Phys. **26**, 509 (1978).

[263] P. del Amo Sanchez *et al.* [BaBar Collaboration], "Analysis of the $D^+ \to K^- \pi^+ e^+ \nu_e$ decay channel," Phys. Rev. D **83**, 072001 (2011).

[264] M. Antonelli *et al.* [FlaviaNet Working Group on Kaon Decays], "An Evaluation of $|V_{us}|$ and precise tests of the Standard Model from world data on leptonic and semileptonic kaon decays," Eur. Phys. J. C **69**, 399 (2010).

[265] F. Niecknig and B. Kubis, "Dispersion-theoretical analysis of the $D^+ \to K^- \pi^+ \pi^+$ Dalitz plot," JHEP **1510**, 142 (2015).

[266] B. Adeva *et al.* [DIRAC Collaboration], "Measurement of the πK atom lifetime and the πK scattering length," Phys. Rev. D **96**, 052002 (2017).

[267] S. Prelovsek, L. Leskovec, C. B. Lang, and D. Mohler, "K π scattering and the K* decay width from lattice QCD," Phys. Rev. D **88**, no. 5, 054508 (2013).

[268] H. Ohnishi, F. Sakuma and T. Takahashi, "Hadron Physics at J-PARC," arXiv:1912.02380 [nucl-ex].

[269] H. Fujioka *et al.*, "Extension of the J-PARC Hadron Experimental Facility - summary report," arXiv:1706.07916 [nucl-ex].

[270] *Summary of the Report from the Working Group for The External Expert Panel on the Radioactive Material Leak Accident at the Hadron Experimental Facility of J-PARC*; https://j-parc.jp/en/topics/HDAccident20130827_.pdf

[271] H. Noumi *et al.*, *Charmed baryon spectroscopy experiment at J-PARC*, J-PARC Proposal E50, 2012.

[272] M. Naruki, private communication, 2015.

[273] A. J. Bevan *et al.* [BaBar and Belle Collaborations], "The Physics of the B Factories," Eur. Phys. J. C **74**, 3026 (2014).

[274] R. Mizuk *et al.* [Belle Collaboration], "Observation of an isotriplet of excited charmed baryons decaying to Lambda+(c) pi," Phys. Rev. Lett. **94**, 122002 (2005).

[275] T. Lesiak *et al.* [Belle Collaboration], "Measurement of masses and branching ratios of Xi+(c) and Xi0(c) baryons," Phys. Lett. B **605**, 237 (2005) Erratum: [Phys. Lett. B **617**, 198 (2005)].

[276] T. Lesiak *et al.* [Belle Collaboration], "Measurement of masses of the Xi(c)(2645) and Xi(c)(2815) baryons and observation of Xi(c)(2980)$\to$ Xi(c)(2645)pi," Phys. Lett. B **665**, 9 (2008).

[277] J. Yelton *et al.* [Belle Collaboration], "Study of Excited Ξ_c States Decaying into Ξ_c^0 and Ξ_c^+ Baryons," Phys. Rev. D **94**, no. 5, 052011 (2016).

[278] S. H. Lee *et al.* [Belle Collaboration], "Measurements of the masses and widths of the $\Sigma_c(2455)^{0/++}$ and $\Sigma_c(2520)^{0/++}$ baryons," Phys. Rev. D **89**, no. 9, 091102 (2014).

[279] K. Abe *et al.* [Belle Collaboration], "Observation of Cabibbo suppressed and W exchange Lambda+(c) baryon decays," Phys. Lett. B **524**, 33 (2002).

[280] Y. Kato *et al.* [Belle Collaboration], "Search for doubly charmed baryons and study of charmed strange baryons at Belle," Phys. Rev. D **89**, no. 5, 052003 (2014).

[281] S. B. Yang *et al.* [Belle Collaboration], "First Observation of Doubly Cabibbo-Suppressed Decay of a Charmed Baryon: $\Lambda_c^+ \to pK^+\pi^-$," Phys. Rev. Lett. **117**, no. 1, 011801 (2016).

[282] Y. Kato *et al.* [Belle Collaboration], "Studies of charmed strange baryons in the ΛD final state at Belle," Phys. Rev. D **94**, no. 3, 032002 (2016).

[283] J. Yelton *et al.* [Belle Collaboration], "Observation of Excited Ω_c Charmed Baryons in e^+e^- Collisions," Phys. Rev. D **97**, no. 5, 051102 (2018).

[284] Y. B. Li *et al.* [Belle Collaboration], "First Measurements of Absolute Branching Fractions of the Ξ_c^0 Baryon at Belle," Phys. Rev. Lett. **122**, no. 8, 082001 (2019).

[285] Y. B. Li *et al.* [Belle Collaboration], "First measurements of absolute branching fractions of the Ξ_c^+ baryon at Belle," Phys. Rev. D **100**, no. 3, 031101 (2019).

[286] E. Kou *et al.* [Belle-II Collaboration], "The Belle II Physics Book," PTEP **2019**, no. 12, 123C01 (2019).

[287] Y. Q. Chen *et al.* [Belle Collaboration], "Dalitz analysis of $D^0 \to K^-\pi^+\eta$ decays at Belle," arXiv:2003.07759 [hep-ex].

[288] M. Bayar, W. H. Liang, and E. Oset, "B^0 and B_s^0 decays into J/ψ plus a scalar or vector meson," Phys. Rev. D **90**, no. 11, 114004 (2014).

[289] J. P. Lees *et al.* [BaBar Collaboration], "Dalitz plot analysis of $\eta_c \to K^+K^-\eta$ and $\eta_c \to K^+K^-\pi^0$ in two-photon interactions," Phys. Rev. D **89**, no. 11, 112004 (2014).

[290] E. M. Aitala *et al.* [E791 Collaboration], "Model independent measurement of S-wave K-pi+ systems using D+ —> K pi pi decays from Fermilab E791," Phys. Rev. D **73**, 032004 (2006). [Erratum: [Phys. Rev. D **74**, 059901 (2006)]].

[291] J. P. Lees *et al.* [BaBar Collaboration], "Measurement of the I=1/2 $K\pi$ $\mathcal{S}$-wave amplitude from Dalitz plot analyses of $\eta_c \to K\bar{K}\pi$ in two-photon interactions," Phys. Rev. D **93**, 012005 (2016).

[292] M. F. M. Lutz *et al.* [PANDA Collaboration], "Physics Performance Report for PANDA: Strong Interaction Studies with Antiprotons," arXiv:0903.3905 [hep-ex].

[293] J. Ritman, invited talk at *Excited Hyperons in QCD Thermodynamics at Freeze-Out* Workshop, see Ref. [13].

[294] C. Adolph *et al.* [COMPASS Collaboration], "Resonance Production and $\pi\pi$ S-wave in $\pi^- + p \to \pi^-\pi^-\pi^+ + p_{recoil}$ at 190 GeV$/c$," Phys. Rev. D **95**, no. 3, 032004 (2017).

[295] S. Wallner [COMPASS Collaboration], "Strange-Meson Spectroscopy at COMPASS," arXiv:1911.13079 [hep-ex] (2019).

[296] B. Adams *et al.* [COMPASS++/AMBER Collaboration], "Letter of Intent: A New QCD facility at the M2 beam line of the CERN SPS (COMPASS++/AMBER)," arXiv:1808.00848 [hep-ex] (2018).

[297] C. Adolph *al.* [COMPASS Collaboration], "Measurement of the charged-pion polarizability," Phys. Rev. Lett. 114, 062002 (2015)

[298] B. Adams *et al.* [COMPASS++/AMBER Collaboration], "Proposal for Measurements at the M2 beam line of the CERN SPS Phase-1: 2022-2024," CERN-SPSC-2019-022 (2019).

[299] R. Aaij *et al.* [LHCb Collaboration], "Observation of $J/\psi p$ Resonances Consistent with Pentaquark States in $\Lambda_b^0 \to J/\psi K^- p$ Decays," Phys. Rev. Lett. **115**, 072001 (2015).

[300] R. Aaij *et al.* [LHCb], "Observation of the resonant character of the $Z(4430)^-$ state," Phys. Rev. Lett. **112**, no.22, 222002 (2014).

[301] R. Aaij *et al.* [LHCb], "Search for the doubly charmed baryon Ξ_{cc}^+," JHEP **12**, 090 (2013).

[302] R. Aaij *et al.* [LHCb], "First observation of excited Ω_b^- states," Phys. Rev. Lett. **124**, no.8, 082002 (2020).

[303] R. Aaij *et al.* [LHCb], "Near-threshold $D\bar{D}$ spectroscopy and observation of a new charmonium state," JHEP **07**, 035 (2019).

[304] R. Aaij *et al.* [LHCb], "Study of D_{sJ} decays to $D^+K_S^0$ and D^0K^+ final states in pp collisions," JHEP **10**, 151 (2012).

[305] R. Aaij *et al.* [LHCb], "Observation of overlapping spin-1 and spin-3 $\bar{D}^0K^-$ resonances at mass $2.86\mathrm{GeV}/c^2$," Phys. Rev. Lett. **113**, 162001 (2014).

[306] R. Aaij *et al.* [LHCb], "Dalitz plot analysis of $B^0 \to \overline{D}^0\pi^+\pi^-$ decays," Phys. Rev. D **92**, no.3, 032002 (2015).

[307] R. Aaij *et al.* [LHCb], "Observation of the decay $B_s^0 \to \overline{D}^0K^+K^-$," Phys. Rev. D **98**, no.7, 072006 (2018).

[308] J. Goity, P. Huovinen, J. Ritman, and A, Tang, in: Workshop on *Excited Hyperons in QCD Thermodynamics at Freeze-Out: mini-Proceedings*, arXiv:1701.07346 [hep–ph], (November, 2016) p. 158.

[309] A. W. Steiner, M. Prakash, J. M. Lattimer, and P. J. Ellis, "Isospin asymmetry in nuclei and neutron stars," Phys. Rept. **411**, 325 (2005).

[310] C. J. Horowitz and J. Piekarewicz, "Neutron star structure and the neutron radius of Pb-208," Phys. Rev. Lett. **86**, 5647 (2001).

[311] J. Xu, L. W. Chen, B. A. Li, and H. R. Ma, "Nuclear constraints on properties of neutron star crusts," Astrophys. J. **697**, 1549 (2009).

[312] A. W. Steiner, J. M. Lattimer, and E. F. Brown, "The Equation of State from Observed Masses and Radii of Neutron Stars," Astrophys. J. **722**, 33 (2010).

[313] B. G. Todd-Rutel and J. Piekarewicz, "Neutron-Rich Nuclei and Neutron Stars: A New Accurately Calibrated Interaction for the Study of Neutron-Rich Matter," Phys. Rev. Lett. **95**, 122501 (2005).

[314] D. H. Wen, B. A. Li, and L. W. Chen, "Super-soft symmetry energy encountering non-Newtonian gravity in neutron stars," Phys. Rev. Lett. **103**, 211102 (2009).

[315] S. J. Pollock and M. C. Welliver, "Effects of neutron spatial distributions on atomic parity nonconservation in cesium," Phys. Lett. B **464**, 177 (1999).

[316] M. B. Tsang *et al.*, "Constraints on the symmetry energy and neutron skins from experiments and theory," Phys. Rev. C **86**, 015803 (2012).

[317] K. Hebeler, J. M. Lattimer, C. J. Pethick, and A. Schwenk, "Constraints on neutron star radii based on chiral effective field theory interactions," Phys. Rev. Lett. **105**, 161102 (2010).

[318] M. Centelles, X. Roca-Maza, X. Vinas, and M. Warda, "Nuclear symmetry energy probed by neutron skin thickness of nuclei," Phys. Rev. Lett. **102**, 122502 (2009).

[319] A. Carbone, G. Colo, A. Bracco, L. G. Cao, P. F. Bortignon, F. Camera, and O. Wieland, "Constraints on the symmetry energy and on neutron skins from the pygmy resonances in 68Ni and 132Sn," Phys. Rev. C **81**, 041301 (2010).

[320] L. W. Chen, C. M. Ko, B. A. Li, and J. Xu, "Density slope of the nuclear symmetry energy from the neutron skin thickness of heavy nuclei," Phys. Rev. C **82**, 024321 (2010).

[321] A. Tamii *et al.*, "Complete electric dipole response and the neutron skin in 208Pb," Phys. Rev. Lett. **107**, 062502 (2011).

[322] B. A. Li, L. W. Chen, and C. M. Ko, "Recent Progress and New Challenges in Isospin Physics with Heavy-Ion Reactions," Phys. Rept. **464**, 113 (2008).

[323] M. B. Tsang, Y. Zhang, P. Danielewicz, M. Famiano, Z. Li, W. G. Lynch, and A. W. Steiner, "Constraints on the density dependence of the symmetry energy," Phys. Rev. Lett. **102**, 122701 (2009).

[324] N. Shishov, "Decay of K^0 to $K^+e^-\bar{\nu}_e$," Yad. Fiz. **82** (2019) no.1, 85-86 [Phys. Atom. Nucl. **82** (2019) no.1, 77-78].